Al-Mustansiriyah Journal of Science

ISSN 1814 - 635X

Vol. 19, No. 1, 2008

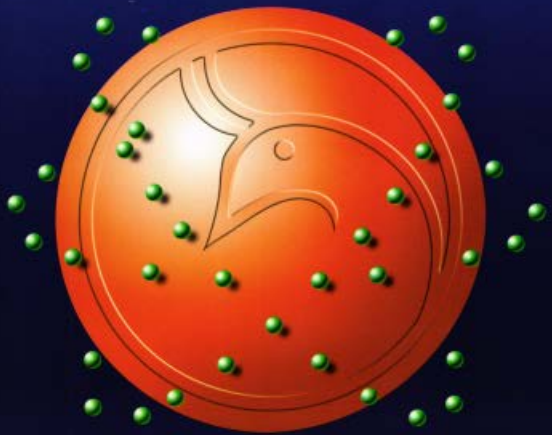

Issued by College of Science - Mustansiriyah University

AL- MUSTANSIRYA JOURNAL OF SCIENCE

INSTRUCTION FOR AUTHORS

1. The journal accepts manuscripts in Arabic and English languages. Which had not been published before.
2. Author (s) has to introduce an application requesting publication of his manuscript in the journal. Four copies (one original) of the manuscript should be submitted. Should be printed by on the computer by lasser printer and re produced on A4 white paper in three coppice with flopy disc should be also submitted.
3. The title of the manuscript together with the name and address of the author (s) should typed on a separate sheet in both Arabic and English. Only manuscript,s title to be typed again with the manuscript.
4. For manuscripts written in English, full name (S) of author (s) and only first letters of the words (except prepositions and auxiliaries) forming title of the manuscript should be written in capital letters. Author (s) address (es) to be written in small letters.
5. Both Arabic and English abstracts are required for each manuscript. They should be typed on two separate sheets (not more then 250 words each).
6. References should be denoted by a number between two bracket on the same level of the line and directly at the end of the sentence. A list of references should be given on a separate sheet of paper, following the intemational style for names and abbreviations of journals.
7. Whenever possible, research papers should follow this pattem: INTRODUCTION, EXPERIMENTAL (MATERIALS AND METHODS), RESULTS, DISCUSSION and REFERENCES. All written in capital letters at the middle of the page. Without numbers or underneath lines.
8. The following pattern should be followed upon writing the references on the reference sheet: Sumame (s), intials of author (s), title of the paper, name or abbreviation of the journal, volume, number, pages and (Year). For books give

the author(s) name(s), the title, edition, pages, publisher, place of publication and (Year).

9. A publication fees in the amount of ID. 20 thousend is charged upon a Reciepet of the paper and 20 thousend upon the acceptance for publication for their ID. 40 thousend should be paid for the editorial board.

CONTENTS

Interleukin-1α Level among Iraqi patients with Acute Leukemia

Batool A. Al-Haidary [1], Firyal N. Aziz [2], Samira N. Al-Naiem [3] & Yasmin M.G. Zangana [4]

[1,4] Clinical Immunology / College of Medical & Health Technology.

[2] Medical Microbiology /College of Medical & Health Technology.

[3] Technical Institute / Baghdad

Received 2/4/2007 – Accpted 29/7/2007

Key words:- Leukemia, AML, ALL, IL-1α.

االخلاصة

إن إبيضاض الدم هو مرض خبيث (سرطان) لنخاع العظم و الدم. يتميز هذا المرض بتراكم غير مسيطر عليه لخلايا الدم. ينقسم ابيضاض الدم الى أربع مجاميع : ابيضاض نقوي و ابيضاض لمفاوي ، كلاهما يمكن أن يكون حادا أو مزمنا".

تم تقدير مستوى (IL-1α) في أربعين عينة مصلية لمرضى ابيضاض الدم الحاد التي ضمت 22 عينة لأبيضاض الدم النقوي AML و 18 عينة لأبيضاض الدم اللمفاوي ALL بإستخدام مقايسة الأنظيم المرتبط الممتز المناعية ELISA ، مقارنة بـ 25 عينة لأفراد يبدون أصحاء كسيطرة.

أظهرت هذه الدراسة إن هناك إرتفاعا" عالي المعنوية في مستوى هذا السايتوكين مقارنة بعينات اسيطرة ($P< 0.001$) ولكلا من مجموعتي الـ AML و ALL . فضلا" عن ذلك ليس هناك فارق معنوي بين مستوى (IL-1α) قبل وبعد المعالجة ($P> 0.05$) . يستنتج من ذلك إن هناك تأثيراً لأبيضاض الدم على مستوى (IL-1α) و خصوصاً ضمن حالات ابيضاض الدم النقوي و التي يبدأ فيها بالهبوط بعد المعالجة رغم كونه تغيراً غير معنوياً .

ABSTARCT

Leukemia is a malignant disease (cancer) of the bone marrow and blood. It is characterized by the uncontrolled accumulation of blood cells. Leukemia is divided into four categories: Myelogenous or Lymphocytic, each of which can be acute or chronic.

Forty Iraqi Acute Leukemic patients' samples included 22 Acute Myelogenous Leukemia (AML) and 18 Acute Lymphoblastic Leukemia (ALL) have been estimated for IL-1α using ELISA technique in comparison with 25 apparently healthy controls.

This study reveals that there is a highly significant elevation in the level of this cytokine among ALL patients' samples in comparison with control group ($P< 0.001$) for both AML and ALL group. Moreover there is no significant difference in IL-1α level before and after treatment ($P> 0.05$). In conclusion there is an effect for acute leukemia on IL-1α level particularly among AML cases in which it began to decline after treatment though it is non-significantly.

INTRODUCTION

The first solid description of a case of leukemia in a medical literature dated 1827, [1]. In 1845, a series of patients who died with enlarged spleens and changes in the "colors and consistencies of their blood". It was reported that "Leucocythemia" described this pathological condition [2].

Acute myelogenous leukemia (AML) is a fast-growing cancer of the blood and bone marrow. In AML, the bone marrow makes many unformed cells

called blasts. Blasts normally develop into white blood cells that fight infection. However, the blasts are abnormal in AML. They do not develop and cannot fight infections. The bone marrow may also make abnormal red blood cells and platelets [1]. It was noticed that the incidence rates for all types of leukemia are higher among males than among females. Acute Myelocytic Leukemia is the most common AL affecting adults, and its incidence increases within age [2].

It was declared that (ALL) is a malignant disorder resulting from the clonal proliferation of lymphoid precursors with arrested maturation [3]. It was denoted that ALL is the most common cancer of childhood. The incidence of ALL among (1-4) year old children is more than 10 times greater than the rate for young adults ages 20-24 [3].

The incidence of AML increases with aging [4]. The median age at diagnosis of ALL is 12 years [5]. Furthermore, it was observed that in all ages, the incidence is higher among males than females [6,7].

Although the cause of AL in human is unknown, several studies have tried to identify leukemia etiology for its development, but definite conclusions cannot be drawn [8].

The main symptoms of leukemia are anemia which results in short breathing and looking pale; bleeding due to low number of platelets and bone with joints pain [7].

Acute Leukemia is diagnosed when blood and bone marrow samples show a large number of leukemia cells [7, 8]. Interleukin-1 (IL-1) is a cytokine with diverse immunologic, physiologic and hematopoietic effects, produced mainly by macrophages and monocytes. There are two existed forms of IL-1 (ά and β). They bind to the same receptors and have similar biologic activities [9]. Interleukin-1 appears to be primarily involved in the inflammation, having direct effects on endothelial cells as well as on both B and T cells [10]. It was observed to have a number of effects on the

hematopoietic system, inducing the stimulation of bone marrow stromal cells to produce IL-6 in addition to a range of colony stimulating factors [11].

This study is a trail to estimate the level of IL-1 α in the sera of leukemic patients in comparison with healthy control group since it is myelo-protective and accelerate Neutrophils and Platelets recovery after chemotherapy [12].

MATERIALS AND METHODS

This study was carried out in Baghdad Medical Hospital. It was conducted during the period from September /2006 to January /2007. Forty Iraqi patients with Acute Leukemia involved in this study. Their ages ranged between (10-70) years. They were sequentially selected from cases admitted to the hospital at first presentation. They were diagnosed under the supervision of consultant committee based upon the patient's medical history, physical examination and laboratory tests which include some Hematological and serological parameters. These samples have been undergone complete blood picture (CBP), IL-1α estimation and the results were compared with those for 25 apparently healthy individuals with age ranged from (10-60) years as healthy control group. This group includes 15 males and 10 females [13, 14].

Statistical Analysis:

All results have been analyzed statistically using Bionomial test, Kruskal Wallis test and ANOVA test (F-test) for multivariate comparison (LSD) [15].

RESULTS AND DISSCUSION

I. Demographical Picture for Acute Leukemic Patients:

Some of demographical parameters had been listed in Table 1. This table also showed the distribution of AL according to the age groups. It is clear that the majority of patients are with ages ranged between 10-30 years (55%) while those at the age above 51 years form the minority among patients (15%)
with very highly significant differences between age groups ($P< 0.001$). Furthermore, it is obviously that the frequency of AL decreases by aging as clearly shown in Table 1.

Table-1: Demographical picture of Acute Leukemia patients

Studied Groups	Subtypes of AL	Number	Frequency	P value
Acute Leukemia	AML	22	55	0.527
	ALL	18	45	
Age Groups (Years)	10-30	22	55	0.001
	31-50	12	30	
	51-70	6	15	
Gender	Male	17	42.5	0.343
	Female	23	57.5	
Total		40	100	

The distribution of patients according to gender reveals that there is no significant difference between both sexes (P =0.343), though the frequency of females is higher (57.5%), with a female: male ratio of 1.4:1.

Patients' distribution according to the age groups and regarding the subtype of Leukemia either ALL or AML are listed in table 2. It is clear from this table that there is no effect of age on the frequency of ALL or AML (P = 0.797).

Table- 2: Distribution of Acute Leukemia subtypes according to age groups.

Acute Leukemia	Age Groups (Years)			Total	P value
	10-30	31-50	51-70		
AML	12 (54.5)*	6 (27.3)	4 (18.2)	22 (100)	0.797
ALL	10 (55.6)	6 (33.3)	2 (11.1)	18 (100)	
Total	22 (55)	12 (30)	6 (15)	40 (100)	

* = No. between brackets represents the frequency

II. Interleukin-1α Level among Patients' Sera:

Interleukin-1α has been estimated in the sera of patients in comparison with apparent healthy control, table 3 shows highly significant arising in IL-1α level among the patients' sera in comparison with control group (P = 0.001); and there is no significant variation between IL-1α titer before and after treatment (P> 0.05) for both patients studied groups (AML & ALL).

Table- 3 : Interleukin-1 α (IL-1 α) pg /ml Level among the studied groups

Studied Groups	Number	Mean ± SD	ANOVA P value
Apparent Healthy Control	25	7.52 ± 1.19	
AML- Before treatment	8	18.50 ± 5.88	0.001
AML- After treatment	14	17.00 ± 5.32	
ALL-Before treatment	4	14.75 ± 1.26	
ALL-After treatment	14	18.43 ± 6.68	
Total	65		
LSD Multicomparison P values' results are: All the studied groups Vs Apparent Healthy control: (P =0.001 for each comparison) All the studied groups Before & After treatment comparisons: (P> 0.05)			

Regarding the incidence of leukemia among the children; the explanation for this result may be associated with high incidence of infections among the children and young youth rather than adults which enhance the possibility for Leukemia development. Moreover the likelihood exposure to so many agents [such as the mutagens] which facilitate the disease development; occurs at this age [10-30] group more than old ages.

Although there is no significant difference between AML and ALL frequency with the different age groups, young ages [i.e. below 30 years] are still representing the majority for both subtypes (P =0.797). On the contrary, studies mentioned that 75% of ALL cases occur in children under age of 16 years [16]. This variation is due to racial, geographical and environmental conditions.

Regarding the age effect, on the contrary of the current study's result, the high frequencies of new cases of AML occur in the United States each year, mostly in older adults. The average age of a person with AML is 65 years. Less than 10% of people with AML are children [17]. While about 3,970 new cases of (ALL) are diagnosed each year in the United States, under the age of 19 years. Children are most likely to develop the disease, but it can occur at any age [18].

These results conflict with the fact that most AML Iraqi patients are less than 30 years. This variation may be related to high exposure of Iraqis to mutagenic factors during the last wars such as the radiated bombs besides the infectious agents and psychological stress which increase the chance for disease development [19]. On the other hand, the above result is regarding ALL to some extent, agreed with this study. However, frequency of ALL among Iraqi children (55.6%) is higher than those observed in other countries as reported in USA that 30% of ALL are children who are < 19 years old [20, 21].

No significant effect for gender on the frequency of ALL or AML as shown in table 1 (P = 0.343). While other studies' conclusions were clashed with this criterion; for some denoted that the majority of patients were the men, while the others observed that nearly frequency of infection was among both males and females [22]. The interpretation for this result is due to the hormonal and physiological variations and perhaps women nowadays take more responsibilities than the men which enhance their exposure to so many carcinogenic agents. In addition, the security circumstances may prohibit most men to go out even to visit hospitals which reduce their samples' collections.

Interleukin-1 (IL-1) is a proinflammatory cytokine that plays a pivotal role in driving the *in vitro* proliferation of leukemic cells through autocrine or paracrine pathways [23]. This is true since arising level of IL-1α in the sera of leukemic patients has been demonstrated as shown in Table 3 in comparison with apparent healthy control group. Furthermore, it was proposed that this cytokine has potent direct and indirect effects on normal and malignant hematopoiesis, and its widespread constitutive expression by neoplastic blood cells may play a fundamental role in driving the leukemic process [2, 24]. This fact also explains the low level of IL-1α among the apparent healthy control group's sera samples [25].

REFERENCES

1. Hoffman R, Benz E, Shattil S, Furie B, Cohen H, *et al.*, " *Haematology: Basic principles and practice.*" 4th [Ed.]: 1071-75; Churchill-Livingstone (2005).
2. Le Maistre CF & Stein AS, "Acute Myelogenous Leukemia (AML)." National Marrow Donor Program at American Cancer Society: What is acute myeloid leukemia?: http://www.cancer.org/docroot/CRI/content/CRI (2006)
3. The Leukemia & Lymphoma Society Fitting Blood cancers. "Leukemia "Leukemia Facts & Statistics." *Leukemia, Lymphoma, Myeloma, Facts 2005-2006,* June (2005).
4. Jemal A, Thomas A, Murray T, Thun M."Cancer Statistics." CA. Cancer J. Clin. 52: 23, (2002).
5. Web MD University "Blood cancer." Web MD University; http://www.studentlounge Web MD/ Lycose, Inteli Health ; Edis 551:71-6 (2001).
6. Med News "Acute Leukemia." http://www.canceranswers.com/ html.

7. Poplack DG. "Clinical manifestation of acute Lymphoblastic leukemia." In: Hoffman R, Benz EJ Jr, Shattil SJ, *et al.*, (eds) "*Hematology Basic principles and practice.*" 2nd [ed], 776-84 (1991).
8. Larson RA. "Oncology", In: Dale DC & Federman DD [Eds] "*Acute Leukemia.*" APC medicine Online. Web MD Inc; NY,(2000).
9. Dinarello CA. "Interleukin-1 and interleukin-1 antagonism." BLOOD 77: 1627-52 (1991).
10. Roitt IM & Delves PJ. "*Roitt's Essential Immunology.*" 10th Ed, 250 Black Well Publishing, USA, (2004).
11. Mule JJ, Marcus SG, Yang JC, et al., "Clinical applications of IL-6 in cancer therapy." Res. Immunol. 143: 777-9 (1992).
12. Futami H, Jansen R, Macphee MJ, et al., "Chemoprotective effects of recombinant human IL-1 alpha in cyclophosphamide-treated normal and tumor-bearing mice: Protection from acute toxicity, hematologic effects, development of late mortality and enhanced therapeutic efficiency." J. Immunol. 145: 4121-30 (1990).
13. Dacie JV & Lewis SM. "*Practical Hematology.*" 8th Ed , 1-351 Churchill-Livingstone, Edinburg (1996).
14. BioSource "Interleukin-1α-ELISA kit; Biosource Europe SA Rue de l'Instrie; 8; B-1400 Nivelles. Belgium; USA.
15. Sorlie DE. "*Medical biostatistics and Epidemiology: Examination and Broad Review.*" 1st Ed, 74-88; Appleton and Lange Com ; Norwalk Connecticut, (1995).
16. Wiernik PH, *et al.*, "*Neoplastic disease of the blood.*", 12-17 Churcill Livingstone; New York; (1991) [Midline].
17. Le Maistre CF & Stein AS "Acute Myelogenous Leukemia Symptoms and Diagnosis" Leukemia and Lymphoma Society:AML:http://www.leukemia-lymphoma.org/all_page?item_id=7049
18. Sandler DP. "Epidemiology & Etiology of acute leukemia." Update leukemia 6: 3-5 (1992).
19. Greenlee RT, Hill-Harmon MB, Murrage T, *et al.*, "Cancer statistics, 2001 [erratum appears in CA cancer]." CA. Cancer J. Clin. 51(2): 15-36 (2001).
20. Seiter K. "Acute Myelogenous Leukemia" American Society of Hematology Last Updated: January 24, (2006). http://www.eMedicine.
21. The Leukemia & Lymphoma Society Fighting Blood Cancers. "Acute lymphocytic Leukemia" Leukemia Education Series (2005) http://www.leukemia-lymphoma.org./allpages.
22. American Cancer Society Report "What is acute Myeloid Leukemia? http://www.cancer.org/docroot/CRI/content/CRI_2_2_.

23. Oppenheim JJ & Ruscetti FW. "Cytokines." In: "*a LANGE medical book: Medical Immunology*." Parslow TG, Stites DP, Terr AI & Imboden JB. (eds); 10th Ed.; PP: 148-167; Lange Medical Books/ McGraw-Hill by Appleton & Lange, USA ; (2001)
24. Estrov Z & Talpaz M. "Role of interleukin-1 beta converting enzyme (ICE) in leukemia." Cytokines Mol. Ther. 2(1):1-11 (1996).
25. Kurzrock R, Kantarjian H, Wetzler M, Estrov Z , *et al.* , "Ubiquitous expression of cytokines in diverse leukemias of lymphoid and myeloid lineage." Exp. Hematol. 21(1): 80-5 (1993).

Study Of Extended-Spectrum ß-lactamases Producing *Enterobacteria* isolated from Cockroaches (*Periplaneta americana*) of Central Medicine City Hospital

Mohammed Faraj Al- Marjani
Department of Biology,College of Science, Al-Mustanairiya university
Received 3/4/2006 – Accpted 16/9/2007

الخلاصة

تم جمع 15 حشرة من الصرصر الأمريكي(*Periplaneta americana*) من مستشفى مدينة الطب/بغداد لدراسة دورها في نقل البكتريا المرضية المقاومة لمضادات الحياة في المستشفيات والمنتجة لأنزيمات البيتالاكتاميز وخاصة انزيمات البيتالاكتاميز واسعة الطيف . جمعت الصراصر بأستخدام قناني زجاجية ، بعدها وضع كل صرصر في أنبوبة أختبار تحوي 5 مل من الملح الفسيولوجي المعقم ومزجت محتويات الأنبوبة بالمازج(vortex) لعمل معلق بكتيري ، بعد زرع المعلق البكتيري على الأوساط الزرعية المناسبة شخصت 32 عزلة بكتيرية مختلفة تعود للعائلة المعوية وكانت اعلى نسبة عزل هي لبكتريا *Klebsiella pneumoniae* أذ تم عزلها بنسبة 25% ثم بكتريا *Shigella spp* بنسبة عزل 18.7% ، ثم بكتريا *Enterobacter aerogenes* وبكتريا *Proteus mirabilis* اذ عزلت بنسبة 15.6% لكل منها ، ثم تأتي بعدها بكتريا *Serratia marcescens* بنسبة عزل 12.5% وبكتريا *E.coli* بنسبة 3.12% .

أختبرت حساسية هذه العزلات لمضادات الحياة المختلفة، وأظهرت النتائج وجود مقاومة عالية لمضادي الأموكسسلين والسيفوركسيم وان جميع العزلات تحمل مقاومة متعددة لمضادات الحياة . بالمقابل كانت جميع العزلات حساسة لمضاد الامبنيم ومعظم العزلات حساسة لمضاد السبروفلوكساسين (78.2%) والأزتريونام (68.8%) .

من جانب أخر أظهرت 18 عزلة (56.25 %) من هذه العزلات قابليتها على انتاج انزيمات البيتالاكتاميز، وكانت خمسة عزلات (15.6%) منتجه لأنزيمات البيتالاكتاميز واسعة الطيف من مجموع 32 عزلة تحت الدراسة . أظهرت نتائج الترحيل الكهربائي في هلام الاكاروز احتواء 59.37 % من العزلات البكتيريه المعزولة من الصرصر الأمريكي على حزم بلازميدية مختلفة الاحجام.

ABSTRACT

Fifteen American Cockroaches (*Periplaneta americana*) were captured to determine the potential role of the cockroaches in carrying Extended-Spectrum ß-lactamases producing pathogens from Central Medicine City hospital. Only cockroaches captured whole and live were utilized for the study. After that each cockroach was placed in a test tube with 5 ml sterile saline solution , and then homogenized. The resulting solution was cultured on the culture media. 32 isolates of *Enterobacteriaceae* were identified , the most frequent were *Klebsiella pneumoniae* (25%), *Shigella spp.*(18.7%), *Enterobacter aerogenes* and *Proteus mirabilis*(each 15.6%) , *Serratia marcescens* (12.5%) and *E. coli* (3.12%) .

Bacterial isolates were tested against (11) antimicrobial agents: Amoxicillin, Cefotaxime ,Imipenem, Ciprofloxacine, Aztreoname , Cefuroxime , Nalidixic acid , Trimethoprim , Tetracycline , Mezlocillin and Gentamicin . Results showed that all the isolates were resistant to Cefuroxime , Amoxycillin , and all the isolates have showen multiple resistance for antibiotics. All isolates (100%) were susceptible to imipenem. The majority of isolates remained susceptible to Ciprofloxacine (78.2%) and Aztreoname (68.8%) .

The results showed also that 18 isolates (56.25 %) had the ability to produce ß -lactamase enzymes , 5 isolates (15.6%) were able to produce Extended-Spectrum ß -lactamases (ESBLs) . DNA analysis (Plasmid profile) showed that 59.37 % of the Bacterial isolates contained plasmid of different molecular weights.

INTRODUTION

Insects play a role as alternate vectors for bacteria (1).Cockroaches are capable of carrying many human pathogens and they may have a role in transmitting some serious nosocomial infections to man and his domestic animals (2) . In one recent study, ESBL-producing *Klebsiella pneumoniae* isolated from cockroaches was indistinguishable from that isolated from patients (3).

Gram-negative organisms such as *Pseudomonas, E. coli, Enterobacter, Klebsiella,* and *Serratia* are nosocomial pathogens that have developed resistance to multiple antibiotics. These organisms have developed ingenious mechanisms of antibiotic resistance. The mechanisms include the production of Extended-spectrum ß-lactamases (ESBLs) with the ability to degrade the third-generation cephalosporins and monobactams, by the alteration of their outer membrane proteins so that the antibiotic cannot enter the organism, and the production of broad spectrum ß-lactamases that can be induced during a course of therapy with third-generation cephalosporins (4).

Extended-spectrum ß-lactamases are a rapidly evolving group of ß-lactamases which share the ability to hydrolyze third-generation cephalosporins and aztreonam , typically, they derive from genes for TEM-1, TEM-2, or SHV-1 by mutations that alter the amino acid configuration around the active site of these ß-lactamases(5) . An increasing number of ESBLs not of TEM or SHV lineage have recently been described , the presence of ESBLs carries tremendous clinical significance(6) . The ESBLs are frequently plasmid encoded, Plasmids responsible for ESBL production frequently carry genes encoding resistance to other drug classes (for example, aminoglycosides). Therefore, antibiotic options in the treatment of ESBL-producing organisms are extremely limited (7). Transfer of genotypically related ESBLs from hospital to hospital within a single city (8), from city to city , and from country to country has been documented (9).

The aims of this study were to determine the potential role of the American cockroach in carrying pathogens in Central Medicine City hospital , and to test the antimicrobial susceptibility of these microorganisms , and study the ability of Cockroaches isolates for ESBLs production.

MATERIALS AND METHODS

1. Isolation of bacteria from Cockroaches : Fifteen Cockroaches (*Periplaneta americana*) were captured in the morning , they were placed in flasks , rinsed with 70% alcohol, transferred to sterilized flasks, and then taken to the laboratory. Only cockroaches captured whole and live were utilized for the study. After that each cockroach was placed in a test tube with 5 ml sterile saline solution (0.8%) and then homogenized. The resulting solution was cultured on the following three medium: MacConkey's agar, Blood agar and nutrient agar. Bacterial isolates were identified according to (10) by using the cultural and biochemical examinations and API 20-E system.
2. Antimicrobial susceptibility: The disks diffusion test was used to determine antimicrobial susceptibility of Bacterial isolates on Mueller-Hinton agar by use of the antibiotics : Imipenem (IPM), Ciprofloxacine (CIP), Aztreoname (ATM), Cefuroxime (CXM), Amoxicillin(AML),Cefotaxime(CTX), Nalidixic acid(NA) , Trimethoprim (W) , Tetracycline (TE) , Mezlocillin (MEZ) and Gentamicin (G).
3. Detection of beta-lactamases : The ability of Bacterial isolates for beta-lactamases production were tested according to (11), by rapid iodometric method as followes: Test Bacterial isolates were removed with a loop from an overnight culture on solid medium and suspended with Penicillin solution , at 1 h. two drops of starch indicator were added to the suspension ,followed by one drop of iodine reagent and were mixed thoroughly . A blue colour developed immediately , persistence of the blue colour for longer than 10 min. constitutes a negative result.
4. Detection of Extended-Spectrum beta-lactamases (ESBLs): The ability of Bacterial isolates for ESBLs production were tested according to (5), by using a clavulanate double –disk diffusion method: synergy between cefotaxime and Clavulanate was detected by placing a disk of amoxicillin / clavulanate (20 µg/10 µg . respectively) and a disk of cefotaxime(30 µg), 30 mm a part (center to center) on an inoculate agar plate . A clear extension of the edge of the cefotaxime inhibition zone toward the disk containing Clavulanate was interpreted as synergy , indicating the presence of an ESBLs
5. plasmid extraction : Plasmid DNA was extracted according to (12) by Alkaline method . Electrophoresis was conducted at 5 V/cm in TBE buffer. plasmid DNA bands were observed under U.V. light (Transilluminator) with wave length of 340 n.m.

RESULTS AND DISSCUSSION

In the present study , 32 isolates of *Enterobacteriaceae* were identified , the most frequent were *Klebsiella pneumoniae* (25%), *Shigella spp.*(18.7%) , *Enterobacter aerogenes* and *Proteus mirabilis* (15.6% for each , *Serratia marcescens* (12.5%) and *E. coli* (3.12%) Table (1).

Cotton *et al* (3) recently experienced an outbreak of nosocomial disease due to extended spectrum beta-lactamase-producing *Klebsiella pneumoniae* in a neonatal unit infested with cockroaches . *Klebsiella pneumoniae* is a common cause of serious nosocomial gram-negative infections, including ventilator-associated pneumonia, urinary tract infection, and bloodstream infection (BSI) . Infections due to *K. pneumoniae* occur in both outbreak settings and settings of endemicity ,Unfortunately, isolates of *K. pneumoniae* are becoming increasingly resistant to antibiotics(13).

Table -1: Enterobacteria isolates from *Periplaneta americana*. L.

Microorganism	Isolates no.	%
Klebsiella pneumoniae	8	25
Shigella spp	6	18.7
Enterobacter aerogenes	5	15.6
Proteus mirabilis	5	15.6
Serratia marcescens	4	12.5
Pseudomonas aeruginosa	3	9.3
E. coli	1	3.12
Total	32	100

A total of 32 Cockroaches isolates were tested against (11) antibiotics.Results showed that all Cockroaches isolates were resistant to Cefuroxime and Amoxycillin , all the isolates have showen multiple resistance for antibiotics . The resistance percentages were as follows: for Tetracycline , 96.8% ;Trimethoprim, 81.2% ; Gentamicin,62.5% ; Mezlocillin and Cefotaxime (each 56.2%) ; and Nalidixic acid ; 46.8% . All isolates (100%) were susceptible to imipenem. The majority of isolates remained susceptible to Ciprofloxacine (78.2 %) and Aztreoname (68.8 %) (Table 2).

Table- 2 : Antibiotic resistance of Enterobacteria isolates .

Antibiotics	Resistance of isolates %							
	Klebsiella pneumoniae	Shigella spp	Entero bacter aerogenes	Proteus mirabilis	Serratia marcescens	Pseud omonas aeruginosa	E. coli	Total
CXM	100	100	100	100	100	100	100	100
AML	100	100	100	100	100	100	100	100
CTX	62.5	66.6	60	40	50	66.6	0	56.2
CIP	25	16.6	20	20	25	33.3	0	21.8
G	75	66.6	40	60	75	33.3	100	62.5
ATM	25	33.3	20	40	25	66.6	0	31.2
NA	62.5	66.6	40	20	25	66.6	0	46.8
W	87.5	66.6	80	80	75	100	100	81.2
TE	100	83.3	100	100	100	100	100	96.8
MEZ	62.5	50	60	40	50	66.6	100	56.2
IMP	0	0	0	0	0	0	0	0

Cefuroxime(CXM),Amoxicillin(AML),Cefotaxime(CTX), Ciprofloxacine(CIP), Gentamicin (G), Aztreoname(ATM), Nalidixic acid(NA) , Trimethoprim(W), Tetracyclin(TE) , Mezlocillin (MEZ)and Imipenem(IPM)

The results showed also that 18 Cockroaches isolates (56.25 %) had the ability to produce ß- lactamase enzyme , 5 isolates (15.6%) were able to produce Extended-Spectrum ß -lactamases (Table 3).

Over the last 20 years, there has been an increased resistance to ß-lactams because of the secretion of extended-spectrum ß-lactamases (ESBLs) mediated by plasmids (14). This type of resistance is now observed in all species of *Enterobacteriaceae* and is currently disseminated throughout the world (15). A common environmental source of ESBL-producing organisms has occasionally been discovered. Examples have included contamination of ultrasonography coupling gel, bronchoscopes , blood pressure cuffs (16), and Cockroaches (3).

Since around 2000—earlier in Poland and Spain and later in France and the UK—dramatic shifts have occurred in the prevalence and types of extended-spectrum ß-lactamases (ESBLs) in Europe. Before this watershed, most producers were nosocomial isolates, often *Klebsiella* spp. or *Enterobacter* spp. from specialist care units, and had mutant TEM or SHV ESBLs. Subsequently, CTX-M ESBLs have become dominant, with much greater penetration into *Escherichia coli*, and with many infections in 'complicated community' patients, usually with underlying disease, recent antibiotic usage, or healthcare contact (17 , 18).

Table -3 : Production of ß - Lactamase by Enterobacteria isolates from Periplaneta americana.

Microorganism	No. of isolates that produced ß -lactamase	%	% from all Enterobacteria isolates
Klebsiella pneumoniae	5	62.5	15.6
Shigella spp	3	50	9.3
Enterobacter aerogenes	2	40	6.25
Proteus mirabilis	3	60	9.3
Serratia marcescens	2	50	6.25
Pseudomonas aeruginosa	2	66.6	6.25
E. coli	1	100	
Total	18		56.25

DNA analysis (Plasmid profile) showed that 59.37 % of the Bacterial isolates contained plasmid of different molecular weights (Figure 1).

A B C D

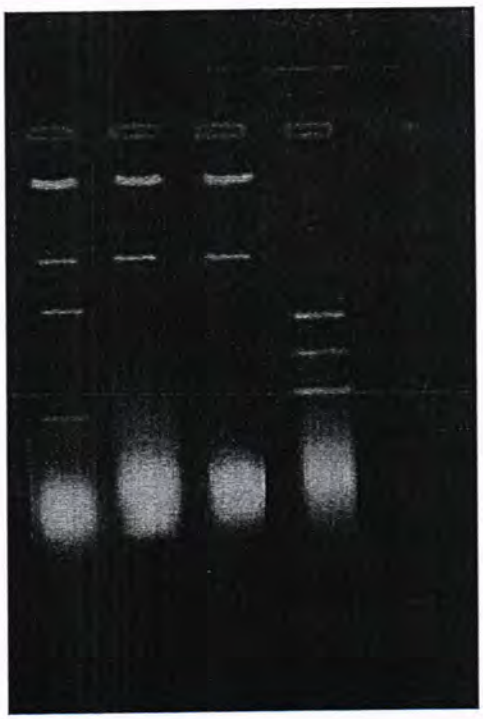

Figure-1: Plasmid profile for Enterobacteria isolates from Periplaneta americana. A- Plasmid band for Proteus mirabilis. B- Plasmid band for Enterobacter aerogenes. C- Plasmid band for Pseudomonas aeruginosa D- Plasmid band for E. coli.

CONCLUSIONS

Cockroaches are an important mechanical carrier of pathogens in the hospital environment.The prevalence of *Enterobacteriaceae* isolated from *Periplaneta americana* cockroaches in the studied hospital reflects the weakness of the measures adopted both for vector control and for antimicrobial use. Also ,the results indicated that isolates of cockroaches are increasing resistant to antibiotics and production of ESBLS enzyme.

REFERANCES

1. Rasmussen, M.A. and Casey, T.A. Environmental & food safety aspects of *E.coli* O157: H_7 infections in cattle. Critical Reviews in Microbiology., 27(2): 57-73, (2001).
2. Naieni,H.K . The potential role of the German cockroach (*Blatella germanica*) in carrying pathogens in two general hospitals, Tehran. Europ.Clinic.Microbiol.& Infect.DisAbstract No. 902,P. 887, (2004).
3. Cotton,M.F. ; Wasserman,W. ; Pieper, C. ;Theron, D.; Tubbergh, G.; Campbell, F. ; Fang ,C. and Barnes , J. Invasive disease due to extended spectrum beta-lactamase-producing *Klebsiella pneumoniae* in a neonatal unit: the possible role of cockroaches. J.Hospital. Infect.44(1):13-17,(2000) .
4. Tan,T. The growing problem of antibiotic resistance: Are we on the verge of a medical disaster? Internet. Copyright © 2007 by Children's Memorial Hospital.
5. Paterson,D.; Robert ,A.and Bonomo,A . Extended-Spectrum ß-Lactamases: a Clinical Update . Clinic. Microbiol. Reviews 18(4) : 657-686 ,(2005).
6. Neuhauser, M. M. ;Weinstein, R.; Rydman, L. H.; Danziger, G.; Karam,D. and Quinn,J.P. Antibiotic resistance among gram-negative bacilli in US intensive care units: implications for fluoroquinolone use. JAMA 289:885-888.(2003).
7. Bonnet, R., J. ; Sampaio, C. ;Chanal, D.; Sirot, C. ;De Champs, J. L.; Viallard, R. ;Labia,R. and Sirot,J. A novel class A extended-spectrum beta-lactamase (BES-1) in *Serratia marcescens* isolated in Brazil . J. of Antimicrob. Chemother.. 44:3061-3068,(2000).
8. Mavroidi, A.; Tzelepi, A. ;Tsakris, V.; Miriagou, D. ;Sofianou,M. and Tzouvelekis,L.S. An integron-associated beta-lactamase (IBC-2) from *Pseudomonas aeruginosa* is a variant of the extended-spectrum beta-lactamase IBC-1. J. of Antimicrob. Chemother. 48:627-630,(2001).
9. Fiett, J. A.; Palucha, B. ;Miaczynska, M.; Stankiewicz, H. ;Przondo-Mordarska, W. ;Hryniewicz,S. and Gniadkowski,M. A novel complex mutant beta-lactamase, TEM-68, identified in a *Klebsiella pneumoniae* isolate from an outbreak of extended-spectrum beta-lactamase-producing klebsiellae. J. of Antimicrob. Chemother. 44:1499-1505 ,(2000).
10. Greenwood, D.; Slack, R.C. and Peutherer, J.F. Medical Microbiology. (Sixteenth ed.). Churchill Livingston,(2002).

11. Collee, J.G.; Fraser, A.G.; Marimon, B.P. and Simmons, A. Macki & MacCartney Practical Medical Microbiology (eds.). Churchill Linvingston (14th) ed. (1996).
12. Hejazi, A.; Keane, C.T. and Falkiner, F.R. The use of RAPD-PCR as a typical method for *Serratia marcescens*.J. Med. Microb., 46: 913,(1997).
13. Anderson, D.J.; Engemann , R.; Harrell, L.J. ; Carmeli, Y.;Reller, B. and Kay,K.S . Predictors of Mortality in Patients with Bloodstream Infection Due to Ceftazidime-Resistant *Klebsiella pneumoniae* . J. Antimicrob. Agent. Chemother . 50(5):1715-1720,(2006).
14. Lincopan, N.; Leis, R.; Vianello, M. A.; Araujo, M. R. E.; Ruiz, A. and Mamizuka, E. M. Enterobacteria producing extended-spectrum {beta}-lactamases and IMP-1 metallo-{beta}-lactamases isolated from Brazilian hospitals.. *J Med Microbiol* 55: 1611-1613 , (2006).
15. Lavigne,J.; Bouziges,N.; Chanal, C.; Mahamat , A. ; Michaux-Charachon,S. and Albert , A. Molecular Epidemiology of *Enterobacteriaceae* Isolates Producing Extended-Spectrum ß-Lactamases in a French Hospital . J . Clinic. Microbio. 42 (8) : 3805-3808,(2004).
16. Bureau-Chalot, F. L.; Drieux, C.; Pierrat-Solans, D. ;Forte, C. ; Champs, and Bajolet,O. Blood pressure cuffs as potential reservoirs of extended-spectrum beta-lactamase VEB-1-producing isolates of *Acinetobacter baumannii.* J. Hosp. Infect. 58:91-92 , (2004).
17. Livermore ,D. ; Canton,R. ; Gniadkowski, M.; Nordmann,P.; Rossolini,G. Guil Arlet,G.; Ayala, J.; Luzzaro,F.; Poirel , F. and Woodford ,N. CTX-M: changing the face of ESBLs in Europe , J. of Antimicrob. Agent. Chemother. 59(2):165-174,(2007).
18. Woodford, N.; Reddy,S. ; Fagan,E.; Hill. R.; Hopkins,K.L. ; Kaufmann,M.E.; Kistler,J.; Palepou,M.I. ; Pike,R. M. ; Ward,E. ; Cheesbrough ,J. and Livermore ,D.M. Wide geographic spread of diverse acquired AmpC ß-lactamases among *Escherichia coli* and *Klebsiella* spp. in the UK and Ireland , J. of Antimicrob.and Chemother . 59(1):102-105 , (2007) .

Effect of Ca/P Ratio on Biotype Hydroxyapatite Characterization

[1]Abdul-Salam Khashan, [2]Their Latif, [3]Ismael Khalil and [4]Sherin Abdul-Muhsin
[1,2,3]*Directorate of Materials Science, Ministry of Science and Technology*
[4]*Al-Mustansiriya University, Ministry of Higher Education and Scientific Research*
Received 15/1/2006 – Accepted 29/7/2007

Key words: Hydroxyapatite (HAP); bioceramics; biocompatibility; Nanoparticles.

الخلاصة

ان متطلبات تحضير مركب الهيدروكسي ابتايت($Ca_{10}(PO_4)_6(OH)_2$ /HAP) الملائم للاستخدامات الطبية قد تم تحضيره بإضافة محلول فوسفات الامونيوم إلى محلول نترات الكالسيوم باستخدام الطريقة الكيمياوية الرطبة وبالمواصفات المعتمدة بيولوجيا (Ca/P 1.67) ، وقد تضمن البحث دراسة وافية حول اهمية الحصول على تلك النسبة.

تجب السيطرة وبمنتهى الدقة على المتغيرات التي تؤثر على تحضير هذه المادة والتي لها تأثير كبير على شكل وحجم البلورة اللذان يلعبان دورا مهما في التركيب الدقيق للمركب الذي يشترط أن يكون خاليا من الأطوار الأخرى المحتملة الحدوث وهذه المتغيرات هي (الدالة الحامضية – درجة حرارة التفاعل- مراحل عملية الإنضاج ، درجة حرارة التلبيد ومعدل سرعة نزول قطرة المحلول الحامضي).

اثبتت الفحوصات الطورية والصور المجهرية للمركب المحضر فعاليته للاستخدام الطبي والبايولوجي.

ABSTRACT

The parameters required for the preparation of stiochiometric hydroxyapatite (HAP/ $Ca_{10}(PO_4)_6(OH)_2$) with biological Ca/P ratio 1.67 was carried out by using wet chemical method which refers to the drop wise addition of $(NH_4)_2HPO_4$ to Ca $(NO_3)_2$ solution.

The effect of intrinsic factors like those that pH, reaction temperature, ageing, digestion time and sintering temperature on the synthesis of HAP powders were studied and then the powder were characterized by analytical and spectral techniques. The method is indicating the formation of crystalline HAP with no major decomposition peaks and absence of impurities by close control of the all process parameters.

INTRODUCTION

Hydroxyapatite $Ca_{10}(PO_4)_6(OH)_2$ (HAP) is the most versatile material used for implantation purposes owing to their similarity with natural bone mineral and its ability to bond to bone. These materials characterized by a certain solubility, which provokes the surrounding bone or tissue to form direct bonding to the implant [1, 2].

The solubility leads to gradual degradation and resorption by the surrounding tissue, which stimulates the bone to grow on the material and through its pores, and in some cases; it believed to cause total transformation of the material into living bone [3]. This bonding is able to transfer shear and tensile stress along the interface that could be an advantage in anchoring the implants and reducing the stress peaks in the bone. The main restriction of these materials lies

in their low strengths so that they can use as bulk materials only for low loaded devices [4].

The dominant requirements connected with the development of HAP coatings on metallic implants are preparation of stiochiometric powder material with required chemical and phase composition established by their chemical identity (Ca/P ratio 1.67) and by close crystallographical affinity with bone tissue and their deposition as coatings without the presence of non-stiochiometric phases of the powder [5,6].

The objective of the present study is to provide a novel and simple process for the preparation of hydroxyapatite powder suitable to use in biomedical applications with exactly Ca/P ratio suitable to use in bio fields.

MATERIAL AND METHODS

Synthesis of Hydroxyapatite (HAP)

Hydroxyapatite is generally synthesised by wet chemical method, which involves the addition of phosphate reagent to a solution of calcium ions in one of two main methods (method I: Ca $(OH)_2 - H_3PO_4$ [7]), and method– II: Ca $(NO_3)_2 - (NH_4)_2HPO_4$, which has been currently administrated below.

A solution of analytical reagent grade calcium nitrate (1M) adjusted to pH 11 with concentrated $NH_4(OH)_2$ in 45 ml of degassed distilled water and diluted to 90 ml. A solution of diammonium hydrogen phosphate, 0.6 M in 75 ml distilled water brought to pH 11 with 37.5 ml of aqueous NH_3 and diluted to 160 ml. The $Ca(NO_3)_2.4H_2O$ solution was vigorously stirred at room temperature and the phosphate solution ($(NH_4)_2HPO_4$) was added drop wise for 2 hours to produce a milky white semi gelatinous precipitate which was then stirred for 20-30 hours.

The changes in the pH of the reaction system during HAP synthesis maintained with aqueous NH_3 at pH 11 using the pH meter. It left for ageing for 24 hours, followed by stirring for 30 minutes, then filtered, washed thoroughly with double distilled water and dried in an air oven at 110 °C for 3 hours. Sintering of the precipitate carried out in a muffle furnace. The samples initially kept at a temperature of 240 °C for 1 hour to remove the traces of ammonium nitrate that could be present and then raised to 900 °C for the same time and cooled in the furnace after sintering.

RESULTS AND DISCUSSION

Wet Chemical Method

Hydroxyapatite is generally synthesised by wet chemical method, which involves the addition of phosphate reagent to a solution of calcium ions and occurs by a mechanism, which is interracially controlled [1,4]. The reactants dissolve incongruently and HAP over grows on these particles and its conversion eventually becomes diffusionally controlled. The rate of formation of the products is dependent on the solution chemistry and reaction temperature. However, stiochiometric HAP may only obtained in small quantities after using time consuming (several months) and tedious processes. It is a great challenge to prepare large amounts of HAP by precipitation with in a few hours or days. Hence, the methods listed below explore the possibilities to over come these drawbacks to synthesis stiochiometric hydroxyapatite (Ca/P ratio 1.67) devoid of other calcium phosphate phases.

Hydroxyapatite with varying Ca/P ratio from 1.28 to 2.01 is synthesised by wet chemical methods under varying experimental conditions. The physiochemical parameters of HAP give in table 1. The number with prefix C indicates the sample identity numbers. The Ca/P molar ratios reported in this table obtained after sintering the powder.

Table- 1 : Influences of the Physicochemical Parameters on HAP Synthesis.

Sample Identity no.	Strength of Solution (conc.)		Ageing Time (hr)	Addition Rate Ml/min	Ca/P molar Ratio
	$Ca(NO_3)_2$	$(NH_4)_2HPO_4$			
C1	1.0	0.6	24	1.10	1.61
C2	1.0	0.6	24	1.80	1.48
C3	1.0	0.6	24	1.30	1.67
C4	1.0	0.6	30	1.30	1.78
C5	2.0	0.6	24	1.30	2.01
C6	1.0	0.6	16	1.30	1.28

Ca/P Stiochiometric Ratio

A change in the stoichiometry of hydroxyapatite (Ca/P 1.67) primarily influences its structure, properties and hence its nature of application in implantation and oral surgery [8, 9]. HAP with Ca/P ratio of 1.67 is non-resorbable while α and β- TCP and other nonstoichiometeric CaP phases are resorbable when implanted in the human body.

$$5\,Ca(OH)_2 + 3H_3PO_4 \text{ ---------- } Ca_5(PO4)_3OH + 9\,H_2O$$

The large amount of water produced leads to a decrease in pH of the reaction system on completion of the reaction. These factors bring complexity in controlling the reaction conditions to prepare the powder of desired characteristics [4].

The Ca/P ratio for the powders prepared using $Ca(NO_3)_2$ under NH_3 alkaline conditions varied from 1.28 to 2.01. During the sintering process, the amorphous products formed initially were converted to crystalline HAP, which is in agreement with the results of Berry and Eanes et al. The decreases in Ca/P ratio in samples is, due to the formation of Ca^{2+} deficient apatite and decrease in pH. The apparently low Ca/P ratios obtained is due to the existence of absorbed phosphate ions on the precipitated solids and at low pH, where $HPO4^{2-}$ ions are more stable than $PO4^{3-}$ ions in the neighborhood of hydroxide ions, the non-stiochiometric HAP is obtained.

When HAP precipitated from a basic aqueous solution, three main solid phases formed, ACP, Octa calcium phosphate and HAP ascending in thermodynamic order and descending on the time scale. This is in agreement with well-published theory of on crystal growth [6], that "growth units (ions) constantly bombarded the crystal surface and are attracted by electrical charges of the ions on the surface. As the water molecule leaves the ion, it passes through an activated state and the activation energy (Gibbs) is several times the thermal energy ($_kT$). Therefore, an adsorption layer form and constantly renewed. The ions hydrated in solution and give of some of their hydration water molecules in order to get closer to the ions already integrated on to the surface. Therefore, the adsorption rate may be controlled by the partial dehydration of the cations or by partial penetration through the hydration layer of the crystal [10]". This may explain why ACP is to precipitate first, because the formation of a solid containing the hydration sphere, like the ions in solution requires much lesser energy than Ea (energy barrier).

The total time required for amorphous to crystalline transformation increases with increasing pH. The stirring rate, slurry concentration and particle size altered the induction time but these factors did not change the transformation half-life. The conversion started sooner in the presence of fast stirring, smaller amorphous particles and/or greater concentration of the amorphous particles. The increased rate of conversion with increased water to solid ratio reported as up to 400:1 further illustrate the necessity for water in this conversion [11].

The theory of the process of conversion of amorphous to crystalline product states that solution consisting of stable and crystalline nucleus alone result in the subsequent growth

proliferation of the material. An induction period where no formation of crystalline material observed is a characteristic feature of such reactions. It is during this period that a critical supersaturating attained subsequent to the formation of the primary nuclei. In the ACP to HAP transformation, the induction period includes additionally the time required for the amorphous calcium phosphate to dissolve and is a function of all factors related to the solubility of ACP. Thus, the induction time is decreased by using smaller ACP particles, higher ACP slurry concentration, aqueous rather than non aqueous solutions. Lower pH and higher temperature all of which decrease the time required for some critical degree of supersaturating to reach [9].

The conversion of amorphous precursor phase to HAP has shown to be autocatalytic, while the rate of conversion at any given temperature depends on the pH of the mediating solution [12, 13]. In hydroxylated amorphous phase, the hydroxide ions provide more charge carriers per unit weight and therefore movement of anions for crystallization will occur more readily [8].

In dilute solutions where only one phase seen, the growth of HAP appears to occur by a ripening process after a brief period during which nucleation and growth probably take place simultaneously. In addition, in this system, it is seem that the number of particles decreases as a function of time suggesting that the smaller more soluble particles dissolve and redeposit on larger particles. Again, this reinforces the view that a ripening process is taking place.

The lack of systematic deviation of Ca/P from the expected ratio for hydroxyapatite of 1.67 indicates that during the course of the experiment only one phase is being formed and that the precipitated phase has the Ca/P ratio expected for HAP.

The rate of addition, pH, and the ripening processes play a critical role in the formation of stiochiometric HAP. It is during the ripening process that the ACP formed initially converted to crystalline HAP [2, 5].

The existence of phosphate species and its effects on stoichiometry

The rates of crystallization initially surge during the first few minutes of the reaction, which might be due to the rapid reconditioning of the seed surface from that of the saturated suspension to the higher supersaturated solution concentration. The decrease in the rate, with the extension of reaction is not due to the available surface area for growth, but it could attribute to a surface maturation phenomenon in which the number of available growth sites decrease to a steady state value under conditions of sustained supersaturation. In general, apatites have a relatively high specific

surface area as compared to many sparingly soluble salts. When normalized with respect to this parameter HAP seen to have a relatively slow growth and a high sensitivity to the presence of molecules, which may adsorb to the surface [15].

When the precipitating conditions improperly maintained in the apatite systems, various factors contribute to induce non-stoichiometry, which summarized by [14]. From the experimental results presented in table 1, the non stoichiometry in the samples are attributed to high addition rates of phosphate solutions or low Ca/P ratios, temperature and also by the presence of mono hydrogen orthophosphate HPO_4^{2-} .

In the pH interval between 7.21 and 12.3, predominate species is HPO_4^{2-}. The range of the stability of the different phosphate species vs. pH is given in figure 1. The pH is necessarily to maintain at 9 to 11, because when the pH is around 10 the predominant species is HPO_4^{2-} , which also be inferred from figure 1. Hence, at pH 10, the rate of formation of stiochiometric HAP is high due to increased amount of OH^- and HPO_4^{2-} species. At higher pH above 10.5, PO_4^{3-} and NH_4 are predominant when compared with other phosphate species while at pH lower than 8, HPO_4^{-2} species is dominant.

The calcium phosphates decrease in solubility in the order $CaHPO_4 .2H_2O$ (brucite) > $CaHPO_4$ (monetite) > $Ca_8H_2PO_4.5H_2O$ (octacalcium phosphate) > β- $Ca_3(PO_4)_2$ (β- tricalcium phosphate) > $Ca_5(PO_4)_3OH$ (hydroxyapatite) [1, 14].

Initially at pH between 9.5 and 10.5, the solution supersaturated with respect to HAP and the precipitation takes place. From figure 1 it can be observed that in the pH range between 9 and 10.5 the predominant species together with HPO_4^{2-}, (can be HCO^{3-} or CO_3^{2-} as traces with starting material) consequently, both of them can precipitate together with HAP.

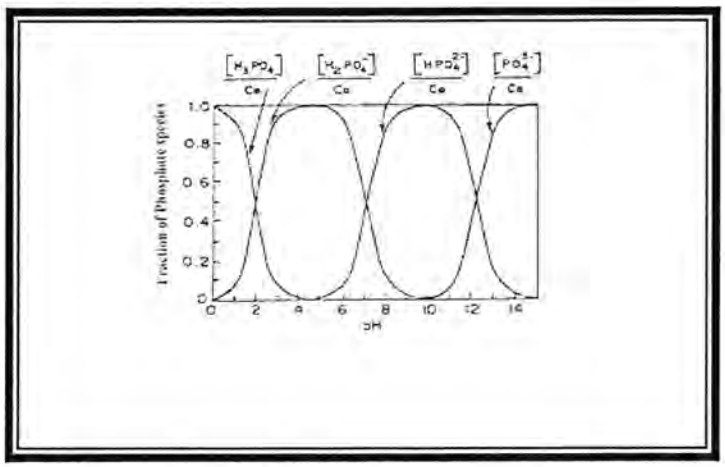

Fig- 1 : Distribution of phosphate species as a function of pH [3].

Characterization of HAP

XRD analysis

X-ray diffraction studies of the powder samples carried out only for the samples, which supplemented by their chemical analysis of near stiochiometric HAP. Figure 2 shows the XRD patterns recorded for stiochiometric HAP sample. The peaks indexed based on the JCPDS file card numbers for the various CaP phases that could exist in HAP (JCPDS file card no. 9-432) [16].

The XRD patterns of HAP sintered at 900 °C given in (fig.2) did not contain any peak other than those of HAP. The CaP ratio measured as 1.6 ± 0.01, which is very close to the Ca/P stiochiometric ratio (1.67) of perfect HAP.

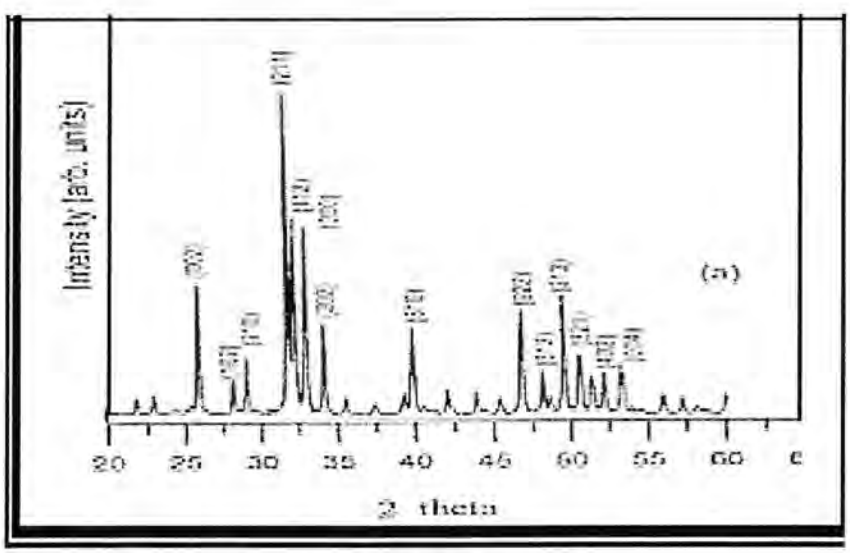

Fig -2: XRD pattern of HAP Prepared

Morphological Studies

The morphology of the HAP powders indicates that it is composed of spheroid and angular agglomerates with wider particle size distributions. The micrograph shows the presence of nearly spherical agglomerates of (1-10 μm) in diameter.

The formation of a regular crystal structure observed that could group in crystal colonies of different morphologies with some entanglement. It is also possible to observe the presence of some sintered polyhedrons (pentagon dodecahedrons) stacks in the micrograph [15, 17].

The HAP powders indicated as a single phase by XRD investigations had a pore free microstructure. Figure 3 showed the micrograph of HAP powder synthesized by wet chemical method.

Fig- 3: SEM Micrographs of HAP Powder Prepared.

CONCLUSIONS

Nanostructure calcium phosphate materials are required for biotype HAP applications to identified as potentially useful materials for a number of biomedical applications including scaffolds for tissue engineering and as carrier for non-viral gene delivery.

The results of present work indicate that the nature of the reagents, pH of solutions and ageing time influences the composition of the final product. The reproducibility of the proces achieved by close control of these parameters.

HAP with Ca/P ratio of (1.67) is non-resorbable while α and β-TCP and other nonstoichiometry CaP phases are resorbable when implanted in the human body.

A change in the stiochiometric of hydroxyapatite Ca/P (1.67) primarily influences its structure, properties and its nature of application in implantation and oral surgery.

The pH of 10 required to maintain for all the system II powders, as the state of HPO_4^{2-} species is pH dependent. A slow rate of addition of phosphate solution was found to be at 1.3 -1.50 ml/min, accompanied

an appropriate ripening procedure is essential to obtain stiochiometric HAP.

During the ageing process, the amorphous phases formed converted to crystalline HAP. Sintering of the precipitates at 900°C causes densification and increases the mechanical strength of the precipitates.

REFEFENCES

1. Nithyanantham T., kandassamy C., Gnanam F.D., "The Effect of Powder Processing on Densification, Microstructure and Mechanical Properties of Hydroxyapatite", *J. Ceram. International.* vol.28, p. 355 (2002).
2. Pramtarova E. P., Presker R., Pham M.T., Maitz M. F. and Stutzmann M., "Hydroxyapatite Growth Induced by Native Extraacellular Matrix Deposition on Solid Surfaces", *J. Erop.Cel. Mater.,* vol. 9, p. 9 (2005).
3. Von Recum A. F., " *Handbook biomater. Evalu. Scient. Tech and clin. Test. of impl. Mater*". 2nd (Ed) (Philadelphia: Taylor & Francis), (1999).
4. Prashant N.K., Charles S., Dong H.L., Ana O.D. and Daiwan C., "Nanostructure Calcium Phosphates for Biomedical Applications" Acta.Biomaterialia, vol. 1, p. 65 (2005).
5. Sridhar T.M, Rajeswari S., Subbaiyan M. and Kamachi U. M., "Sintering Effects on Hydroxyapatite Coated and It's Impedance Behavior"., *FAME, Bangalore*, p. 265 (2001).
6. Robert B. H. and Richard W., "Formation and transformation of amorphous calcium phosphates on Ti alloy surfaces during atmospheric plasma spraying and their subsequent in vitro performance", *J. Bio. Mater.*, vol.27, p. 823 (2006).
7. K. Abdulsalam, L. Thair, K. Ismaeel and A. Sherin, "Influences of the Physiochemical Parameters on Novel Synthesis of Hydroxyapatite for Biomedical Applications" *Irq. J. Sci &Tech.*vol.3, no. 1, (2006).
8. Gross K. A., Gross V. and Berndt C. C., "Biomedical Application of Apatites", *J. Am. Ceram. Soc.* vol. 81, p.106 (1998).
9. Gross K. A. and Berndt C. C., "Biomedical Application of Apatites", *J. Mineralogical Society of America*, vol. 48, pp: 634-672 (2002).
10. Park Joon B. and Lakes Roderic S., "Biomaterials Introduction" 2ed (Eds), Plenum Press, New York, USA (1992)
11. Brandusa G. Gabriela J. and Georgeta C., "Structural Investigation of Electrodeposited Hydroxyapatite on Titanium Supports", Romanian *J. of phys.*, vol. 51, no. 1-2, pp: 173-180 (2006).
12. Arumugam T.K., "*Invitro* and *In vivo* Electrochemical Corrosion Studies on Modified Stainless Steel Materials for Orthopaedic Implant Applications", ph D Thes., Univ.of Madras, Chenna. (1998).
13. Jae M.C., Young M.K., Sona K., Hyoun E.K. and Cheol S.H. "Formation and Characterization of Hydroxyapatite Coating Layer on Ti – Based Metal Implanted by Electron-Beam Deposition" *J. Mater .Res.*, vol. 14,no. 7, p.2980 (1999).

14. Mudali U.K., Sridhar T.M., Baldev R., J., "Corrosion of Bio Implants", *Sadhana* vol.28, Parts 3 & 4, pp: 601-637, June /August (2003), Printed in India.
15. Karils G.A. & Christopher C., "Biomedical Application of Apatites", *J. mineralogical Society of America*, vol.48, pp: 17-22 (2002).
16. Sorensen O. T. "*In Non stiochiometric Oxides*", O. T. Sorensen (Ed.) Academ. Pres, New York, p. 2 (1981).
17. Znang B., Fukne Y.,Wang Y. & Shipu Li, "morphology & formation mechanism of hydroxyapatite whiskers from moderately acid solution" . *J. Mat. Res*, vol. 6, no. 1, p. 8 (2002).

Effect of Fibers Distribution on the Mechanical Properties of Reinforced Laminated Composites

[1]Muhammed Abdul-Nebi AL-Nesearawi and [2]Atheer Alaa AL-Zubaidy*
[1]Department of Physics, College of Education Ibn Al-Haithem, University of Baghdad.
[2]Polymer Research Unit, College of Science, Al-Mustansiriyah University.

Received 28/4/2007 – Accpted 16/9/2007

الخلاصة

درست المواد المركبة الطبقية المكونة من خشب-خشب و الراتينج hP-F المعزز بألياف الزجاج بتغيير اتجاهات الألياف□ قيست الخواص الميكانيكية مثل (مقاومة الصدمة, مقاومة الانضغاط, مقاومة الشد, مقاومة القص, مقاومة الانحناء,و معامل المرونة) للمواد المركبة الطبقية□

و ظهر أن الخواص الميكانيكية للمواد المركبة الطبقية المعززة بألياف الزجاج أفضل مما عليها للمواد المركبة الطبقية غير معزز بالألياف□ فلقد لوحظ أن المقاومة الكلية للمواد المركبة الطبقية تزداد مع التوزيع المناسب للألياف و بالتحديد طريقة الحصيرة و التي تشير إلى أن ترتيب الألياف المعززة يجب أن لا تكون عشوائية□

ABSTRACT

Laminated composite consisting of wood- wood and glass fibers reinforced Ph-F resin was investigated by varying fibers directions. Mechanical properties such as (impact strength, compression strength, tensile strength, shear strength, bending strength, and elasticity modulus) of laminated composite have been measured. Glass fibers reinforced laminated composite exhibited better mechanical properties than fibers anreinforced composite. A increase in the total strength of laminated composite was observed with a suitable fibers distribution, namely mat way, indicating the reinforcing fibers arrangement should not be arbitrary.

INTRODUCTION

Layered composites are found in many familiar applications. Plywood is a laminated composite of thin layers of wood and a suitable thermosetting resin. The layers of wood used provides the bulk of the strength, while the resin acts as a semi-rigid binder[1]. As a result laminates formed from bonding layers of wood by organic adhesive exhibits properties distinctively different from these of the individual ply (lamina) used to make the composite[2].

Most of the modern adhesives are composed of (base, solvent, hardener, and filler) which have their own specific functions. Base is the material from which the adhesive derives its name, like epoxy, polyester, phenol, polyurethane, and urea resins. It is usually solid and serves as the bake-bone of the adhesive. Solvent is used to dissolve the base and additive to provide a liquid adhesive. Hardener is compound which reacts chemically with the base after adding it in stochiometric proportions to the base for curing the adhesive during bonding. It provides an increased curing rate and an acceptable

viscosity. The resin set was cured by heat or at room temperature. Filler is solid powder or particulate additive, organic or inorganic, for reinforcement with low weight ratio, such as silica flour, oxides, and sulfates [3,4].

Adhesion is the interaction between two different substrates across an interface may involve either physical or chemical bonding. Chemical bonding consists of direct interlinking between molecules of two substrates, e.g. the adhesive and the substrates, by covalent or ionic bonds. The physical bonding may result from mechanical interlocking or from the forces of physical adsorption between adhesive molecules and substrate molecules, or by the penetration of adhesive molecules into substrate by diffusion. Thus the mechanism of adhesive action is quite different according to type of reaction[5,6].

Fiber reinforced materials form the biggest and most group of composite materials. The advantage of fiber reinforcement is two-fold: (i) enhance the mechanical properties such as strength, stiffness and heat deflection temperature (ii) increase the toughness of the matrix (the product), so that more energy is require to initiate and propagate fracture[7]. In a fiber reinforced materials, the stress is carried almost entirely by the fibers and the matrix is used to(1) bind the fibers together (by cohesion and adhesion),(2)transmit the stress from one fiber to the other(distributes load evenly among fibers),(3)provide resistance for composite to crack propagation,(4) protect the fibers from environment,(5) keep reinforcing fibers in desired orientation[8] . However, we must know the factors considered in the design of fibers reinforced composites. They are (a) aspect ratio(fiber length per diameter). Where the fiber should has high ratio to promote the toughness of the matrix,(b) volume fraction,(c)type of fiber, metallic, glass, carbon and graphite, ceramic, polymer, and whisker fibers are used to produce variety of composites having wide ranges of properties.(d)critical length(L_c),where for chopped fiber reinforced composite the critical length of fiber play role in the strength of composite.(e)the way of inforcement of composite by fibers which, according to arrangement of fibers in matrix, may be classified as (1)continuous fibers along the matrix length or width, (2) orthogonal fibers, (3) multiply fibers, (4) chopped fibers (discontinuous), (5) mat (in which the fibers distributed equally along the matrix longitudinally and transversely to give the form of mat or net) [9,10]. In this paper seek to investigate the effect of adding glass fibers on the mechanical properties such as impact strength, compression strength, tensile

strength, shear strength, bending strength, and elasticity modulus of laminated composite and select the desirable arrangement.

EXPERIMENTAL

Laminated composite reinforced by glass fibers consists of wood, fibers, and resin. The last was prepared in polymer searches unit, college of science ,university of Al-Mustansiriyah through many steps. The first was started with putting the solvent (ethanol) in flask to dissolving Ph-R by using water bath (70°C)under control temperature. Then adding Epon, talk , H.MTA,C-8quin and continuous mixing for 30min at (70°C).We choose the best amounts that improves the adhesion for wood. The reaction was stirred and heated at 120°C for 30min until the solution becomes turbid and then the mixture was distilled under vacuum till a clear viscous compound was obtained. The Reinforcing glass fibers with 20wt% was manually distributed on adhesive by previous four ways (length, width, orthogonal, and mat).Finally the pieces of wood of varies dimensions were prepared. The prepared (30 samples) were treated with bonding system and heating under pressure to obtain the final solid product .

Charpy impact instrument was used for impact test ,where the samples were prepared with dimensions 10x10x55mm according to (ISO-179). Hydraulic piston type Leybold Harris No.36110 was used to measure the compressive strength of samples at room temperature . ASTM-D695 method was used for preparation of the samples with the length doubled its width in the ratio 2:1 and the thickness was equal to its width. Bending test of rectangular samples with dimensions of (10x135mm)was carried out according to ASTM-D790 test. Tensile strength , modulus of elasticity ,and shear strength was determined by Zweigle instrument according to ASTM-D648 test. They carried out in physics laboratory, college of science, technology university.

RESULTS AND DISCUSSION

The mechanical properties results of the standard and reinforced laminated composites which measured experimentally are summarized in table(1). The glass fibers reinforced laminated composites exhibited better the mechanical properties than the anreinforced composites. Comparing the mechanical properties of the glass fibers (standard) anreinforced and reinforced laminated composites is shown in figures (1,2,3,4,5,and 6). They ensure that the presence of the reinforcing fibers strengthen the composite. Also they

show the effect of fibers arrangement in matrix on the mechanical properties. Based on these studies we conjecture that distribution of reinforcing fibers with mat way improving the mechanical properties of glass fiber reinforced composites. Figs.(1-6) show the plots of impact strength, compression strength, tensile strength, shear strength, bending strength, and elasticity modulus of the glass fibers reinforced and standard composites versus fibers orientation. Where we here are using for facility the symbols (s, L, w, o, m), which mean; standard, length, width, orthogonal, and mat respectively. We observe from Fig.(1) that impact strength increases as a function of fibers distribution. It can be seen from Fig.(2) according to table(1) the increases compression strength with fibers distribution, namely mat. The effect of mat fibers distribution can be also observed through increasing the elasticity modulus as shown in table(1) and Fig.(3). The same behavior was observed for both tensile and shear strength with the variation in fibers distribution as shown in Fig.(4) and Fig.(5) respectively. Moreover we observed decreasing of deflection and then bending of composite due to the reinforcing fibers, specifically mat way as illustrated from Fig.(6) based on table(1) .

Table-1: Mechanical properties of standard and reinforced composites.

Fibers distribution	impact (kJ/m^2)	Compression (Mpa)	Elasticity (Mpa)	Tensile (Mpa)	Shear (Mpa)	Bending (cm)
s	7.318	13.99	16.72	8.12	6.09	0.90
L	8.000	14.47	17.25	10.70	8.03	0.85
w	8.909	16.31	21.32	13.99	10.49	0.80
o	10.200	17.43	21.92	15.64	12.88	0.71
m	10.909	19.39	22.37	18.83	14.12	0.50

CONCLUSIONS

From the experimental results one can conclude that the presence of the reinforcing fibers strengthen the composite. Since glass fibers reinforced laminated composites exhibited better mechanical properties with mat way , so fibers arrangement should not be arbitrary.

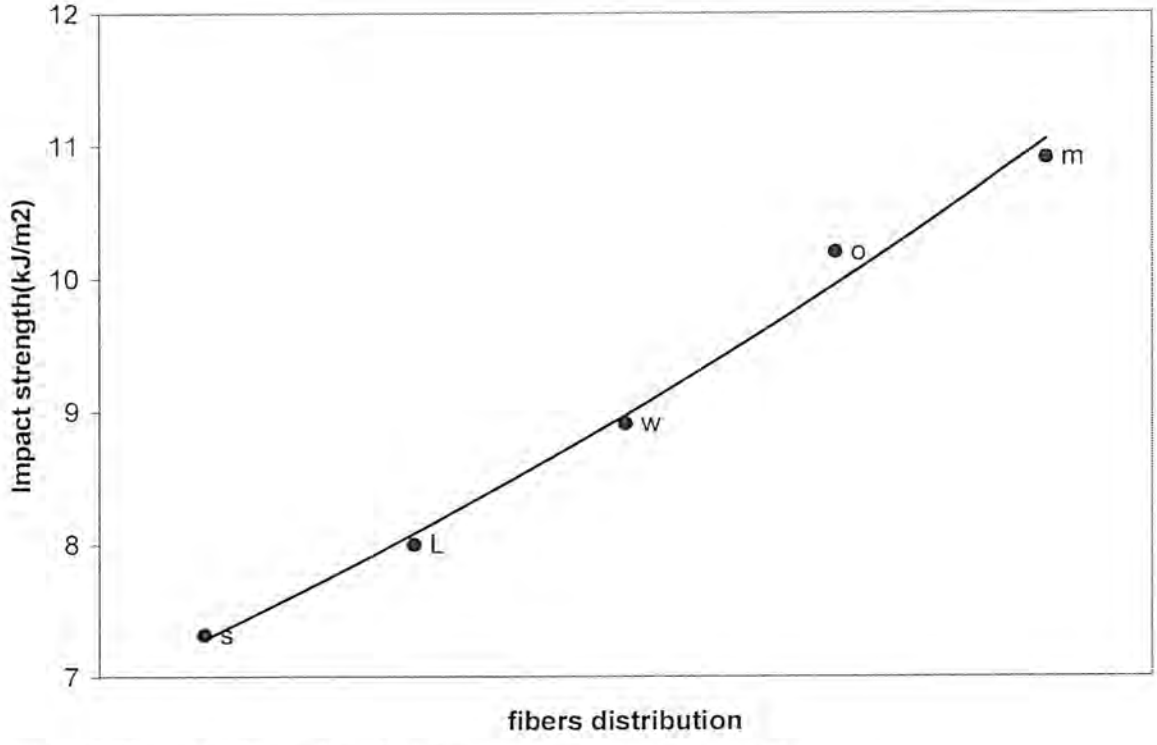

Fig.-1:Effect of fibers distribution on the impact strength.

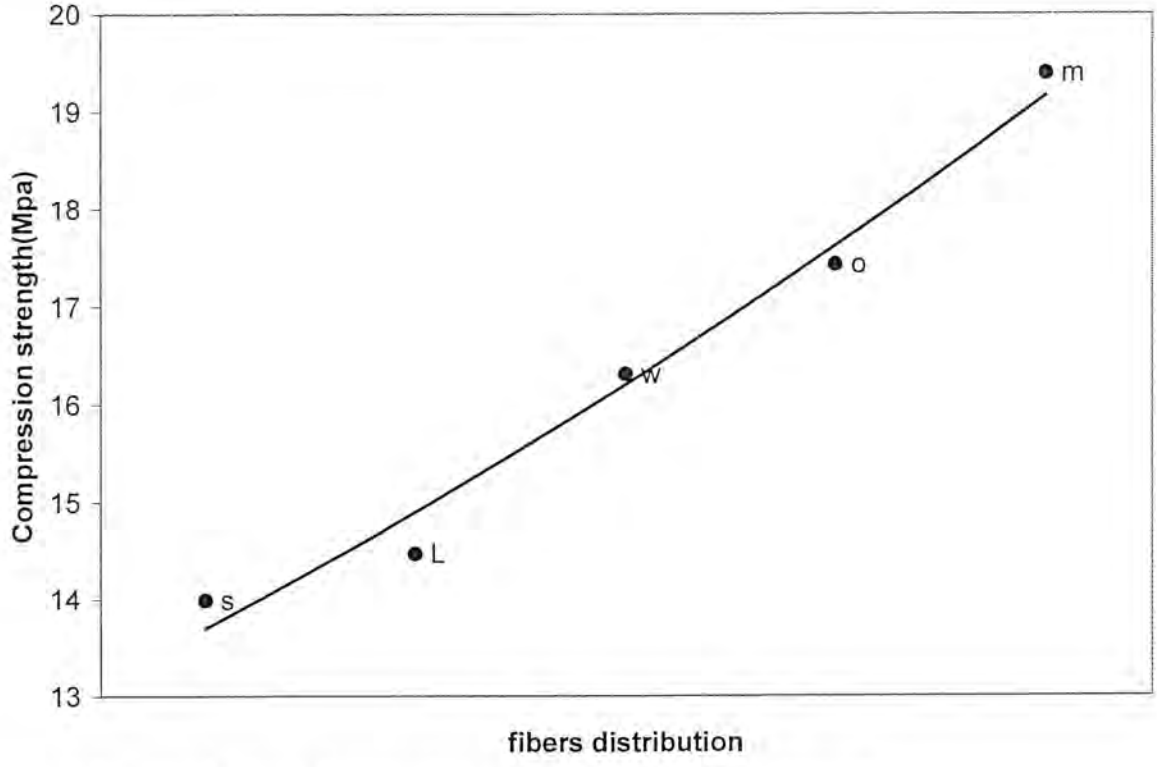

Fig.-2:Effect of fibers distribution on the compression strength.

REFERENCES

1. Eckold G.,"Design and Manufacture of Composite Structure",3rd ed,pp.126-128, McGraw-Hill Inc., England,(2000).
2. Bolton W., "Engineering Materials Technology", 3rd ed.,pp.72-74, John Wiley, U.S.A,(1998).
3. Paker R.S and Taylor J., "Adhesion and Adhesives", 2nd ed,pp.60-63, Pergamon press, London ,(1966)
4. Bikerman J.J, "The Science of Adhesive Joint", 2nd ed, pp.23-26, Academic press, New York, (1967)
5. Kaelble H., "Physical Chemistry of Adhesion", 2nd ed,pp.56-59, Wiley Interscience, New York , (1971)
6. Skeist I.,"Hand Book of Adhesive",3rd ed ,pp.41-46, (1990),Krieger, New York, (1990)
7. Pisharath S. and Wong S.C., "Effect of LCP Addition on the Properties of Hybrid Composites", J.Mater.Process. Tech., vol. 113, 167-171,(2001).
8. Gupta R.B., "Materials Science and Processes",4thed., pp:529-534, (1979), Satya Prakashan,India.
9. Pande S.J and Sharma D.K., "Fracture Toughness of Short Glass Fiber Hybrid Composites" Fib.Sci.Tech.,vol.21,pp:307-317,(1984).
10. Craig M.C. and Daniel F.C., "Dynamic Fracture Toughness of Cellulose Fiber Reinforced Polypropyleme", J.Elast.Plas. ,vol.31, :367-372,(1999) .

Para-Banach Space for the Sequence Space ℓ_p, $0<p<1$

Jawad Kadhim Khalaf Al-Delfi
Department of Mathematics, College of Science, Al-Mustansiriyah University

Received 17/7/2006 – Accpted 6/6/2007)

الخلاصة

جواد كاظم الدلفي قدم مفهوم فضاء بناخ الى حد ما واثبت أن فضاء المتتابعات ℓ_p, $0<p<1$ هو فضاء بناخ الى حد ما كما مبين في المصدر[1]. في هذا البحث تم إدخال مفهوم فضاء فوق بناخ للفضاء ℓ_p, $0<p<1$. هذا المفهوم يعتمد على توسيع مهم لمفهوم فضاء فوق معياري كما معرف في المصدر [2]. حيث ندرس فضاء المتتابعات ℓ_p, $0<p<1$ ونبرهن هذا الفضاء هو فضاء فوق معياري ولكن ليس فضاء معياري. ثم ندرس تقارب المتتابعات في فضاء فوق معياري لنقدم مفهوم فضاء بناخ فوق معياري .كذلك نثبت كل فضاء بناخ هو فضاء فوق بناخ والعكس غير صحيح .

ABSTRACT

In [1] , the concept of a quasi - Banach space for the sequence space $0<p<1$ was introduced by Jawad . K.Al -Delfi. In this paper , we introduce the notion of a para-Banach space for the sequence space ℓ_p, $0<p<1$. This concept is based on the important extension of a para-normed space concept as defined in [2]. We consider the sequence space ℓ_p, $0<p<1$ and prove this space is a para-normed space , but it is not a normed space. We study convergence of the sequences in a para-normed space and introduce the concept of a para- Banach space .We also show that every Banach space is a para-Banach space , but the converse is not true.

Key words: Sequence space ℓ_p, $0<p<1$, para-normed space, para-metric space, para-Banach space.

INTRODUCTION

One of the important notions in functional analysis is the concept of Banach space as defined in [3,4,5] which was introduced by Polish mathematician Stefan Banach in 1922 .

The purpose of this paper is to present the notion of a para-Banach space for sequence space ℓ_p where $0<p<1$. This paper is organised as follows. Section 2 includes the definition of the sequence space ℓ_p, $0<p<1$ and show that it is not a normed space. In section 3, we introduce two concepts which are para-normed space and para-metric space and give some interesting results related to these concepts. In the last section, we study the convergent sequence and Cauchy sequence in a para-normed space ℓ_p, $0<p<1$ in order to show that it is a para-Banach space.

Sequence space ℓ_p, $0<p<1$

In this section, we recall the definition of sequence space ℓ_p, $0<p<1$ and show that this space is not normed space .

Definition 2.1 [6]: The sequence space ℓ_p, $0<p<1$ is the space of all sequences $x=\{x_i\}$ in R or C such that $\sum_{i=1}^{\infty}|x_i|^p<\infty$.

Remark 2.2: The sequence space ℓ_p, $0<p<1$ with the function

$$\|x\|_p=\left(\sum_{i=1}^{\infty}|x_i|^p\right)^{1/p}$$

is not a normed space, because the condition (3) of the norm definition as in [4] is not satisfied. To explain this remark, we consider the following example:

Example 2.3: Let $p=1/3$, and suppose x and y are two sequences, where

$$x=\{x_i\}=\{1,0,0,0,\ldots\} \text{ and } y=\{y_i\}=\{0,1,0,0,\ldots\}.$$

Then we have:

$$\|x+y\|_{1/3}=\left(\sum_{i=1}^{\infty}|x_i+y_i|^{1/3}\right)^3=8$$

and

$$\|x\|_{1/3}+\|y\|_{1/3}=\left(\sum_{i=1}^{\infty}|x_i|^{1/3}\right)^3+\left(\sum_{i=1}^{\infty}|y_i|^{1/3}\right)^3=2$$

It is clear that:

$$\|x+y\|_{1/3}>\|x\|_{1/3}+\|y\|_{1/3}$$

Thus, the space ℓ_p, $0<p<1$ is not a normed space.

We need the following known lemma whose proof can be found in [7] .

Lemma 2.4 [7]: Let $\{x_i\}$ be any (real or complex) sequence and $0<p<1$ Then,

$$\left|\sum_{i=1}^{\infty}x_i\right|^p\le\sum_{i=1}^{\infty}|x_i|^p$$

Para-normed space for the space ℓ_p, $0<p<1$

In this section, we introduce the concepts of para-normed space and para-metric space , and extend the concept of para-normed space to the case of sequence space ℓ_p, $0<p<1$.

Definition 3.1 [2]: Let X be a vector space over a field F. A para-norm on X is a function ${}_\rho\|.\|:X\longrightarrow R_+$ such that:-

(1) ${}_\rho\|x\|=0$ if and only if $x=0$

(2) ${}_\rho\|\lambda x\|=|\lambda|_\rho\|x\|$ for each $x\in X$, $\lambda\in F$

(3) $_{\rho}\| x+y \|^{q} \leq {}_{\rho}\| x \|^{q} + {}_{\rho}\| y \|^{q}$ **for each** $x, y \in X$ **, and for some** $0 < q \leq 1$

The pair $(X, {}_{\rho}\|.\|)$ **is called a para-normed space. We shall use the symbol** ${}_{\rho}X$ **to denote a para-normed space.**

Now we introduce the following concept :

Definition 3.2: A function d_{ρ}**, which associates with any two elements x , y of a non-empty set X a real number** $d_{\rho}(x,y)$ **, is called a para-metric on X , if it possesses the following properties:**

(1) $d_{\rho}(x,y) \geq 0$ **,** $d_{\rho}(x,y) = 0$ **if and only if x = y**

(2) $d_{\rho}(x,y) = d_{\rho}(y,x)$

(3) $(d_{\rho}(x,y))^{q} \leq (d_{\rho}(x,z))^{q} + (d_{\rho}(z,y))^{q}$ **for some** $0 < q \leq 1$

The pair (X, d_{ρ}) **is a para-metric space.**

In the following result, we extend the notion of para-metric space to the space ℓ_p, $0 < p < 1$

Proposition 3.3: The sequence space ℓ_p, $0 < p < 1$ **with:**

$$_{\rho}\| x \|_{p} = \left(\sum_{i=1}^{\infty} | x_i |^{p} \right)^{1/p}$$ **is a para-normed space.**

Proof: **We must satisfy the three conditions of the para-norm**

(1) Since $| x_i | \geq 0$ **for each i then** $_{\rho}\| x \|_{p} = \left(\sum_{i=1}^{\infty} | x_i |^{p} \right)^{1/p} \geq 0$ **for each** $x \in \ell_p$

and

$_{\rho}\| x \|_{p} = 0$ **if and only if** $x_i = 0$ **for each i if and only if** $x = 0$

(2) Now, we have:

$$_{\rho}\| \lambda x \|_{p} = \left(\sum_{i=1}^{\infty} | \lambda x_i |^{p} \right)^{1/p} = \left(\sum_{i=1}^{\infty} | \lambda |^{p} | x_i |^{p} \right)^{1/p}$$

$$= | \lambda |_{\rho} \| x \|_{p} \quad \text{for each } x \in \ell_p, \ \lambda \in F$$

(3) Let $x, y \in \ell_p$**, where** $x = \{x_i\}$ **and** $y = \{y_i\}$**. Then by using lemma 2.4, we have:**

$$_{\rho}\| x+y \|_{p}^{p} = \sum_{i=1}^{\infty} | x_i + y_i |^{p} \leq \sum_{i=1}^{\infty} (| x_i |^{p} + | y_i |^{p})$$

$$= \sum_{i=1}^{\infty} | x_i |^{p} + \sum_{i=1}^{\infty} | y_i |^{p}$$

$$= {}_{\rho}\| x \|_{p}^{p} + {}_{\rho}\| y \|_{p}^{p}$$

Hence the space ℓ_p, $0 < p < 1$ **is a para-normed space.**

The following remark explain the relationship between normed spaces and para-normed spaces.

Remark 3.4: According to definitions of the para-norm and the norm . A normed space $\ell_p, 1\le p<\infty$, with the norm :

$$\|x\|_p=\left(\sum_{i=1}^{\infty}|x_i|^p\right)^{1/p}$$

is a para-normed space . Conversely, in general, is not true and is true only if p=1, as it is shown in the following example:

Example 3.5: The space $\ell_p, 0<p<1$ is a para-normed space , but it is not normed space in accordance with proposition 3.3 and remark 2.2 .

In the following remark , we give the relation between para-normed spaces and para-matric spaces.

Remark 3.6: From the definitions 3.1 and 3.2, every para-normed space ${}_\rho X$ is a para-metric space with respect to the para-metric function: $d_\rho(x,y)={}_\rho\|x-y\|$ for each $x,y\in {}_\rho X$,but the converse may not be true, as it is shown in the following example:

Example 3.7: Let X be the space of all complex sequences $\{x_i\}$ with the following para-metric function:

$$d_\rho(x,y)=\sum_{i=1}^{\infty}\frac{|x_i-y_i|}{2^i\left(1+|x_i-y_i|\right)}\ ;$$

where $x=(x_1,x_2,.....x_n,...)$, $y=(y_1,y_2,.....y_n,.....)$

Then (X,d_ρ) is a para-metric space, but it is not a para-normed space [5].

In the following remark , we have another relation between matric spaces and para-matric spaces

Remark 3.8: In accordance with definitions of the para – metric space and the metric space as in [3], $\ell_p, 1\le p<\infty$ with the function :-

$$d_\rho(x,y)={}_\rho\|x-y\|=\sum_{i=1}^{\infty}|x_i-y_i|^p \quad \text{for each } x,y\in\ell_p,\ 1\le p<\infty$$

is a para-metric space .The converse is not true and true only if p=1, for example the space ℓ_p, $0<p<1$ with $d_\rho(x,y)=\sum_{i=1}^{\infty}|x_i-y_i|^p$ for each $x,y\in\ell_p$, $0<p<1$ is para-metric space , but it is not metric space.

4 . Para-Banach space for the space ℓ_p, $0<p<1$

In this section, we present the notion of a Para-Banach space for the space ℓ_p, $0<P<1$. Then, we introduce the convergent sequence and Cauchy sequence in the para-normed space.

Definition 4.1: Let ${}_\rho X$ be a para-normed space.

(1) A sequence $\{x_n\}$ in ${}_\rho X$ is called para-convergent to a point $x\in {}_\rho X$ if and only

if $\rho\| x_n - x \| \to 0$ as $n \to \infty$

(2) A sequence $\{x_n\}$ in ${}_qX$ is a para-Cauchy sequence if and only if

$\rho\| x_n - x_m \| \to 0$ as $n,m \to \infty$

Definition 4.2: A sequence $\{x_n\}$ in a para-normed space ${}_\rho X$ is called para-bounded if and only if there exists a positive real number M such that $\rho\| x_n \| \le M$ for all $n \in N$.

The proof of the following theorem is similar to the one of the theorem itself in a normed space that can found in [5]

Theorem 4.3: Let ${}_\rho X$ be a para-normed space, then

(1) Every para-convergent sequence is a para-Cauchy sequence, but the converse need not be true

(2) Every para-Cauchy sequence is para-bounded.

(3) A para-convergent sequence has a unique limit.

(4) A para-Cauchy sequence is a para-convergent if and only if it has a para-convergent subsequence.

Now , we introduce the following definitions

Definition 4.4: Let $\{x_n\}$ be a sequence in a para-normed space ${}_\rho X$.

(1) A series $\sum_{n=1}^{\infty} x_n$ is called a para-convergent to $s \in X$ if and only if

$\rho\| S_n - s \| \to 0 \quad (n \to \infty)$, where

$S_n = \sum_{k=1}^{n} x_k$ and s is the limit of a sequence $\{S_n\}$. Otherwise, it is para-divergent.

(1) A series $\sum_{n=1}^{\infty} x_n$ is called absolutely para-convergent if and only if

$$\sum_{n=1}^{\infty} \rho\| x_n \| < \infty$$

Definition 4.5: A para-normed space, in which every para-Cauchy sequence is para-convergent, is called a complete para-normed space or a para-Banach space.

The following theorem gives a nice series characterization of a para-Banach space.

Theorem 4.6: A para-normed space ${}_\rho X$ is complete if and only if every absolutely para-convergent series in ${}_\rho X$ is also para-convergent in ${}_\rho X$.

Proof: Let ${}_\rho X$ be a complete and $\sum_{n=1}^{\infty} {}_\rho\| x_n \| < \infty$. Then for $n > m$ we have:

${}_\rho\| S_n - S_m \|^q = {}_\rho\| x_{m+1} + \cdots + x_n \|^q \le \left({}_\rho\| x_{m+1} \|^q + \cdots + {}_\rho\| x_n \|^q \right)$, for some $0 < q \le 1$.

This implies that ${}_\rho\| S_n - S_m \| \to 0$ $(m \to \infty)$. Hence, $\{S_n\}$ is a Cauchy sequence in ${}_\rho X$ and so para-convergent, since ${}_\rho X$ is complete. Thus $\sum_{n=1}^{\infty} x_n$ is a para-convergent series.

Conversely, suppose that every absolutely para-convergent series be Para-convergent, and let $\{x_n\}$ be any a para-Cauchy sequence in ${}_\rho X$. Then we may determine natural numbers $n_1, n_2, \ldots$ with $n_1 < n_2 < \ldots$ such that:

${}_\rho\| x_{n_{k+1}} - x_{n_k} \| < 2^{-k}$ for all $k \in N$, hence $\sum_{k=1}^{\infty} {}_\rho\| x_{n_{k+1}} - x_{n_k} \| < \infty$

Our assumption implies that $\sum_{k=1}^{\infty} (x_{n_{k+1}} - x_{n_k})$ converges to an element of ${}_\rho X$, where the partial sums of this series is equal to $x_{n_{k+1}} - x_{n_1}$. Thus we see that $\{x_{n_k}\}$ is a para-convergent in ${}_\rho X$. Therefore, the para-Cauchy sequence $\{x_n\}$ has a Para-convergent subsequence $\{x_{n_k}\}$. So by theorem 4.3 (4), we have $\{x_n\}$ is para-convergent in ${}_\rho X$. Hence, ${}_\rho X$ is complete.

Now ,we are ready to state the final result about the space ℓ_p, $0<p<1$

Theorem 4.7: The sequence space ℓ_p, $0<p<1$ is a para-Banach space.

Proof: According to the proposition 3.3, the space ℓ_p, $0<p<1$ is a para-normed space. It remains to prove that ℓ_p, $0<p<1$, is complete. Let $\{x_n\}$ be a para-Cauchy sequence in ℓ_p, $0<p<1$ with $x_n = \left(x_1^{(n)}, x_2^{(n)}, \ldots\right)$. For each fixed k, $\left\{x_k^{(n)}\right\}$ is a para-Cauchy sequence, indeed

$$|x_k^{(n)} - x_k^{(m)}| \le \left(\sum_{i=1}^{\infty} |x_i^{(n)} - x_i^{(m)}|^p \right)^{1/p} = {}_\rho\| x_n - x_m \|_p \quad \text{for all } n, m \ge N$$

Hence there exists $\lim_{n\to\infty} x_k^{(n)}$, call it x_k. We now prove that the sequence $\{x_k\}$ belongs to the space ℓ_p. From the theorem 4.3 (2), we have

$_{\rho}\| x_n \|_p \le M$ where $M > 0$, and so for any k, $\left(\sum_{i=1}^{k} x_i^{(n)} |^p\right)^{1/p} \le {}_{\rho}\|x_n\|_p \le M$. Now if $n \to \infty$, we obtain: $\left(\sum_{i=1}^{k} x_i |^p\right)^{1/p} \le M$.

Since k is arbitrary, this shows that $\{ x_k \} \in \ell_p$, $0 < p < 1$, and $_{\rho}\|x_k\| \le M$. Let $x = \{x_k\}$. It remains to prove that $_{\rho}\| x_n - x \|_p \to 0$. Since $\{ x_n \}$ is a para-Cauchy sequence, for every $\varepsilon > 0$ there exists a positive integer N such that $_{\rho}\| x_n - x_m \|_p < \varepsilon$ for all $n, m \ge N$. Therefore, for any k,

$$\left(\sum_{i=1}^{k} | x_i^{(n)} - x_i^{(m)} |^p\right)^{1/p} \le {}_{\rho}\| x_n - x_m \|_p < \varepsilon \quad \text{for all } n, m \ge N$$

Keeping k and n fixed, let $m \to \infty$. This gives:

$$\left(\sum_{i=1}^{k} | x_i^{(n)} - x_i |^p\right)^{1/p} < \varepsilon \qquad \text{for all } n \ge N$$

Since this is true for all k, we can let $k \to \infty$ and we obtain the result that $_{\rho}\| x_n - x \|_p < \varepsilon$ for all $n \ge N$

Thus the space ℓ_p, $0 < p < 1$, is complete, and hence it is a Para-Banach space.

Remark 4.8: It is clear that , every Banach space is a para-Banach space. But the converse may not be true, as it is shown in the example3.5, where the sequence space ℓ_p, $0 < p < 1$ is a para-Banach space , but, it is not a Banach space .

CONCLUSION

In this paper, we have defind the sequence space ℓ_p, $0 < p < 1$, and have shawn that , it is not a normed space. Then, the concept of a para-normed space is extended for this space. Many results are presented and examined concerning this concept. We have studied Para-convergent and Para-Cauchy sequence. Thus, the notion of a para-Banach space is introduced for the space ℓ_p, $0 < p < 1$,. Finally, we have shown that there exists space which is not Banach space, but may be a para-Banach space.

REFERENCES

1. Jawad.K.Al-Delfi .," On an Infinite Dimensional Leslie Matrix in the Sequence Space ℓ_p, $0 < p < 1$, M.Sc. Thesis ,College of science, University of Al-Mustansiriyah ,(2005)
2. Bastero J., Bernue's J. and Pin˜a A., "An Extension of Mailman's Reverse Burn- Minkowski Inequality", *GAFA Journal* , 5, P. 572 – 581, (1995).
3. Curtain R. F. and Pritchard A. J., "Functional Analysis in Modern Applied Mathematics", 1 st Ed , *Academic Press*, Inc., London, P:107-112 , (1977) .
4. Kreyszig E.," Introductory Functional Analysis with Applications", 1 st Ed, John Wiley and Sons, Inc.,P:49-70, (1978).
5. Siddiqi A. H., "Functional Analysis with Applications",1 st Ed, *Tata McGraw-Hill Publishing Company* , Ltd, New Delhi, India, P.1-58, (1986).
6. Aliprantis C. and Burkinshaw O., "Principles of Real Analysis",3 rd Ed, *Elsevier North Holland*, Inc., P.206-214 ,(1998).
7. Maddox I. J., "Elements of Functional Analysis" ,*2 nd Ed, Cambridge University Press*, New Delhi, India,P.20-23, (1988).

On Compactification of an Orbit Space of Finite Group Action

Amal Ibrahim AlAttar and Bassam Jabbar Al-Asadi
Department of Mathematics, College of Science, Al-Mustanisiryah University

Received 5 /2 /2007 – Accepted 31 / 10 /2007

Keywords and phrases: compactification, Ston-Cech compactification, one point (Alexandroff) compactification.

الخلاصة

لقد قمنا بدراسة رص Stone-Cech أو ما يسمى رص $\beta(\beta X)$ لفضاء تخنوفي X وقد ساعدنا توسيع فعل الزمرة G على X إلى βX ولقد برهنا أن الرص ل Stone-Cech لفضاء المسارات لفعل الزمرة التبولوجية المبعثرة المنتهية G لفضاء الجداء هو فضاء المسارات لرص Stone-Cech لفضاء الجداء لفعل الزمرة G هذا يعني $\beta(\prod X_\alpha/G) = \beta\prod X_\alpha/G$ ومع شروط إضافية حصلنا على

$$\prod \beta X_\alpha/G = \beta(\prod X_\alpha/G)$$

وكذلك قمنا ببرهان نتيجة مشابهة في حالة رص النقطة $(\prod X_\alpha)^*$ للفضاء X أي أن

$$(\prod X_\alpha/G)^* = (\beta\prod X_\alpha)^*/G$$

ABSTRACT

In this work, we studies another construction to the β-compactification (Stone-Cech) of a Tychnoff space X which helps us to extend the action on X to βX and we prove that:

The Stone-Cech (resp., one point) compactification of the orbit space by G, where G is a finite discrete group of product $\prod X_\alpha/G$ is the orbit of the Stone-Cech (resp., one point) compactification of the product of the G-spaces that is $\beta(\prod X_\alpha/G) = \beta\prod X_\alpha/G$ (resp., $(\prod X_\alpha/G)^* = (\beta\prod X_\alpha)^*/G$) and with extra conditions we get that $\prod \beta X_\alpha/G = \beta(\prod X_\alpha/G)$.

INTRODUCTION

The compactification of spaces is one of the most important branches of topology.

In 1913 Caratheodory first formally considered the problem of extending a space. Work on compactification being with Tietze, Alexandroff and Urysohn, whom introduced the one-point compactification, in 1924. it continued with Tychonoff who proved that : Every Tychonoff space can be embedded in a compact Hausdurff space, in 1930.

In 1937 Cech and M.H Stone gave their names to the compactification constructed by Tychonoff by proving it is maximality.
In 1959 Glicksberg introduced results of Stone-Cech.

PRELIMINARIES

Definition 2.0[1]: A topological space X is said to be completely regular iff whenever A is a closed subset of X and $x \in X$ such that $x \notin A$, there is continuous function $f: X \to I$, such that $f(x) = 0$ and $f(A) = 1$, where $I = [0,1]$ as a subspace of IR with the relative usual topology. A completely regular T_1-space is called Tychnoff space.

Definition 2.1[1]: A space X is called pseudo-compact iff every continuous real-valued function on X is bounded.

Definition 2.3[1][2]: A zero- set of space X is a subset of the form $f^{-1}(0)$, where f is a continuous function from X into I. The family of all zero sets of X is denoted by $Z(X)$.

Remark 2.4: (i) Any zero-set of a space X is closed.
(ii) If $f: X \to Y$ is a continuous function and Z is zero-set of Y then $f^{-1}(Z)$ is a zero-set of X.

Proof: (i) Let Z be a zero-set of X, then there is a continuous function $f: X \to I$ such that $f^{-1}(0) = Z$ since $\{0\}$ is closed and f is continuous then Z is closed.
(ii) Since Z is a zero-set of Y , then there is a continuous function $g: Y \to I$ such that $Z = g^{-1}(0) \Rightarrow f(Z) = f^{-1}(g^{-1}(0)) = (g \circ f)^{-1}(0)$ and $g \circ f: X \to I$ is a continuous function, therefore $f^{-1}(Z) = (gf)^{-1}(0)$ is zero-set of X.

Proposition 2.5: (i) A space X is completely regular space iff the family $Z(X)$ is base for the closed sets in X.
(ii) Let X be a space, then $Z(X)$ is closed under finite union and countable intersection.

Proof: see [1]

Definition 2.6[1]: Let $\wp$ be a family of subsets of a topological space X such that if P_1 and P_2 are elements from $\wp$, then $P_1 \cap P_2$ and $P_1 \cup P_2$ belong to $\wp$. A $\wp$-filter on X is a non-empty family $\Im$ of non-empty elements of $\wp$ with properties:

(i) if $P_1, P_2 \in \Im$, then $P_1 \cap P_2 \in \Im$.
(ii) $P_1 \in \Im$ and $P_1 \subseteq P_2 \in \Im$, then $P_2 \in \Im$.

Definition 2.7[3]:1- A $\wp$-filter $\Im$ converge to $x \in X$ iff each neighborhood of x contains an element of $\Im$, and a $\wp$-filter $\Im$ has x as

a cluster point iff $x \in \bigcap\{\overline{P} : P \in \wp\}$. Moreover a $\wp$-ultrafilte is a maximal $\wp$-filter.

2- A $\wp$-filter $\Im$ is called prime iff whenever $F_1 \cup F_2 \in \Im$, then either $F_1 \in \Im$ or $F_2 \in \Im$.

Proposition 2.8: For a $\wp$-filter $\Im$ the following are equivalent:

(i) $\Im$ is a $\wp$-filter.

(ii) Whenever $P \in \wp$ and $P \cap F \neq \phi$ for each $F \in \Im$, then $P \in \Im$.

Proposition 2.9: Every $\wp$- ultrafilte is prime and every $\wp$-filter is contained in $\wp$- ultrafilte.

Proof: See [3].

Definition 2.10[3]: A compactification of a space X is an ordered pair (k,h) where k a compact space is and h is an embedding of X as a dense subset of k.

Definition 2.11[3]: Two compactification (k_1,h_1) and (k_2,h_2) of a space X are called equivalent iff there is a homeomorphism f from k_1 onto k_2 such that $f \circ h_1 = h_2$, that is the diagram commutes

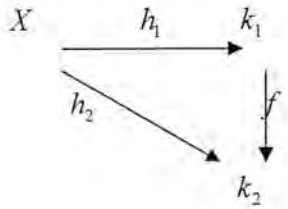

Definition 2.12[3]: Let (k,h) be a compactification of a space X, then (k,h) is said to have the extension property for compactification of X if for every continuous function f from X in to a compact Hausdorff space Y the composite function $f \circ h^{-1}$ has a continuous extension, which maps k into Y that is the diagram

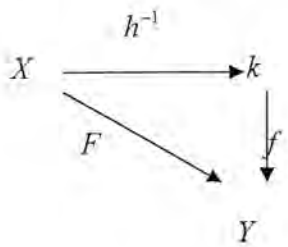

Commutes.

Proposition 2.13: If f is a continuous function of a subspace A of a space X into Hausdorff space Y and if the set A is dense in X, then there exists at most one continuous extension of f to X.

Proposition 2.14: Let (k_1,h_1) and (k_2,h_2) be Hausdorff compactifications of a space X and let both have the extension property for compactification of X, then (k_1,h_1) is equivalent to (k_2,h_2).

Proof: See [3].

Proposition 2.15: Let (X,τ) be a topological space and ω is a point not in X. Let $X^* = X \cup \{\omega\}$, and let $Q = \{U \cup \{\omega\} : U \in \tau \ \& \ X \setminus U \text{ is compact}\}$, then $\tau^* = \tau \cup Q$ is a topology on X^* and (X,τ) is a subspace of (X^*,τ^*).

Proof: See [1].

Proposition 2.16: Let X be a locally compact, Hausdorff space such that $X^* = X \cup \{\omega\}$, $x \notin X$ then (X^*,τ^*) is compact Hausdorff space and $\overline{X} = X^*$ (where τ^* is as defined in proposition (2.15)).

Proof: See [1].

Definition 2.17[3]: Let (X,τ) be a Tychonoff space and I be the closed unite interval $[0,1] \subseteq$ IR, and let $C(X,I)$ be the family of all continuous functions from X into I. Let h be a function from X into $\prod I_\lambda$ where I_λ a copy of is I indexed by $\lambda \in C(X,I)$ defined as follows $h(x)$ is an element of $\prod I_\lambda$ whose f-th coordinate is $f(x)$ where $f \in C(X,I)$ That is $h(x) = f(x)_f$. The image of h is a subset of the compact space $\prod I_\lambda$ and $\overline{h(X)}$ is denoted by βX.

Proposition 2.18: Let X be a Tychonoff space, then βX is Hausdorff compact space.

Proof: see [3].

Proposition 2.19:A function h from X onto the subspace $h(X)$ of the space $\prod I_\lambda$ is a homeomorphism.

Proof: see [3].

Proposition 2.20: Let X be a Tychonoff space, then βX is Hausdorff compactification of X.

Proof: It is clear by propositions (2.18) and (2.19).

Proposition 2.21: βX has the extension property.

Proof: see [1].

Note: βX which is defined in definition (2.17) is called the Stone – Cech compactification or β- compactification. It is largest compactification of X.

Proposition 2.22: Let Z be a zero-set of X,and let $S(Z)=\{\Im \in BX : Z \in \Im\}$. Now, if Z_1, Z_2 are zero-sets of X, then :

(i) $S(Z_1)\bigcup S(Z_2)=S(Z_1 \bigcup Z_2)$

(ii) $S(Z_1)\bigcap S(Z_2)=S(Z_1 \bigcap Z_2)$.

Proof: It is clear.

Note: The family of all z-ultrafilter is denoted by BX where z-ultrafilter is an ultrafilter consists of zero sets.

Proposition 2.23: Let B be the family of all sets of the form $S(Z)$, where Z is zero set of the space X, then B is a base for the closed subsets of BX.

Proof: see [1].

Proposition 2.24: Let Z_1, Z_2 and Z be zero-sets of X, then

(i) If $Z_1 \subseteq X \setminus Z_2$ then $S(Z_1) \subseteq BX \setminus S(Z_2)$

(ii)If $Z_1 \subseteq Z_2$ then $S(Z_1) \subseteq S(Z_2)$

(iii) $S(X \setminus Z)=BX \setminus S(Z)$

Proof: It is clear by definition.

Proposition 2.25: Let X be a Tychonoff space and h be a function from X into BX which assigns to each x in X the ultrafilter $\Im_x$ of all zero-sets containing x (that is $\Im_x$ principal z-ultrafilter), then h is a homeomorphism from X onto $h(X)$.

Proposition 2.26: Let X be a Tychonoff space and h denote the homeomorphism in proposition (2.25), then

1- $h(X)$ is dense in BX with the topology define in proposition (2.23).

2- BX is a compact Hausdorff space.

3- $S(X)=Cl_{BX}h(X)$, for any zero-set of X

4- $Cl_{B\prod X_\alpha} Z=S(Z)$.

Proof: see [1].

Proposition 2.27: Let X be a Tychonoff space, then $\beta X = BX$.

Proof: see [3].

Proposition 2.28: Let $\{X_\alpha\}_{\alpha \in \wedge}$ be a family of Tychnoff spaces, then $\beta\prod X_\alpha = B\prod X_\alpha$

Proof: by proposition (2.26) and proposition (2.27).

Proposition 2.29: Let $\{X_\alpha\}_{\alpha \in \wedge}$ a family of Tychnoff spaces, and suppose the set $\prod_{\alpha \neq \alpha_\circ} X_\alpha$ is infinite for every $\alpha_\circ$, then a necessary and sufficient condition that $\beta\prod X_\alpha = \prod \beta X_\alpha$ is that $\prod X_\alpha$ be pseudo-compact.

Proof: see [4].

Proposition 2.30: If X is Hausdorff G-space with G compact then X/G is compact.

Proof: see [1].

ACTION ON COMPACTIFICATION

Proposition 3.1: Let $\{X_\alpha\}_{\alpha\in\wedge}$ be a family of Tychnoff spaces and let ϑ_α be the action of G on X_α for each $\alpha\in\wedge$. The product action $\vartheta=\prod\vartheta_\alpha$ of G on product space $X=\prod X_\alpha$ is defined by $\vartheta: G\times X\to X$ such that $P_\alpha(\vartheta(g,x))=(\vartheta_\alpha(g,P_\alpha(x)))$ for each $\alpha\in\wedge$ where x is any element of $X, g\in G$ and $P_\alpha: X\to X_\alpha$ is the natural projection map.

Proof: see [5].

Note: Let $\{X_\alpha\}_{\alpha\in\wedge}$ be a family of G-spaces .For each $g\in G$ a homeomorphism $T_g:\prod X_\alpha\to\prod X_\alpha$ is defend by $T_g(g)=\vartheta(g,x)=g\cdot x$ and $(T_g)^{-1}=T_{g^{-1}}$. For subset A of $\prod X_\alpha$ define $T_g(A)=\{g\cdot a: a\in A\}$ by gA and for a family $\Re$ of subsets of $\prod X_\alpha$ denote $T_g(\Re)=\{g\cdot A: A\in\Re\}$ by $g\Re$.

Proposition 3.2: Let $\prod X_\alpha$ be a G-space. If $\Im$ is z-ultrafilter on X $(\Im\in B\prod X_\alpha)$, then so is $g\cdot\Im$ for each $g\in G$.

Proof: since $g\cdot\Im=\{g\cdot Z: Z\in\Im\}$ and $g\cdot Z=\{g\cdot x: x\in Z\subseteq\prod X_\alpha\}$, then $g\cdot\Im$ is defined. Now let Z be a zero-set of $\prod X_\alpha$, since T_g is homeomorphism that is $T^{-1}{}_g$

Is continuous and $(T_g{}^{-1})^{-1}(Z)=(T_{g^{-1}})^{-1}(Z)=T_{(g^{-1})^{-1}}(Z)=T_g(Z)=gZ$ is a zero-set. And by the same way $g^{-1}Z$ is zero-set. Now let $Z_1, Z_2\in\Im$, then $gZ_1, gZ_2\in g\Im$ and $gZ_1\cap gZ_2=T_g(Z_1)\cap T_g(Z_2)=T_g(Z_1\cap Z_2)$ (T_g is one-one)

$=g(Z_1\cap Z_2)$ and since $Z_1, Z_2\in\Im$ then $Z_1\cap Z_2\in\Im$ ($\Im$ is filter)

Hence $g(Z_1\cap Z_2)\in g\Im$. Let $Z\in\Im$, then $gZ\in g\Im$, and let Z_1 be any zero-set of $\prod X_\alpha$ such that $gZ\subseteq Z_1$ to prove that $Z_1\in g\Im$.

Since $gZ\subseteq Z_1$, then $Z\subseteq g^{-1}Z_1$ and since $g^{-1}Z_1$ is zero-set and $Z\in\Im$, then $g^{-1}Z_1\in\Im$

($\Im$ is filter), then $g(g^{-1}Z_1)\in g\Im$ by definition of action $(gg^{-1})Z_1\in g\Im$, hence $Z_1\in g\Im$, and $g\Im$ is z-filter .

Now, suppose $\Im'$ is z-filter on $\prod X_\alpha$ such that $g\Im\subseteq\Im'$, then $\Im\subseteq g^{-1}\Im'$ by above $g^{-1}\Im'$ is a filter but $\Im$ is an ultrafilter, hence $\Im=g^{-1}\Im'$ and $g\Im=\Im'$ therefore $g\Im$ is z-ultrafilter.

Note3.3: Let $\prod X_\alpha$ **be a** G **–space, for each** $g \in G, gx \in \prod X_\alpha$ **where** $x \in \prod X_\alpha$, **and for each** $g \in G$ $g\Im_x$ **is principal z-ultrafilter on** $\prod X_\alpha$ **where** $\Im_x$ **is principal z-ultrafilter on** $\prod X_\alpha$ $(g\Im_x \in B\prod X_\alpha)$, **then** $g\Im_x$ **corresponds a point in** $\prod X_\alpha$ **which is** gx.

Proposition 3.4: Let $\prod X_\alpha$ **be a** G**-space and** Z **be a zero-set of** $\prod X_\alpha$, **then** $g \cdot Cl_{B\prod X_\alpha} Z = Cl_{B\prod X\alpha} gZ$ **for all** $g \in G$.

Proof: By proposition (2.26) $Cl_{B\prod X_\alpha} Z = S(Z)$ **,then** $g \cdot Cl_{B\prod X_\alpha} Z = g \cdot S(Z)$

$= g \cdot \{\Im \in B\prod X_\alpha : Z \in \Im\}$ **and since** $g\Im = \{gZ : Z \in \Im\}$, **then**

$g \cdot \{\Im \in B\prod X_\alpha : Z \in \Im\}$

$= \{\Im \in B\prod X_\alpha : gZ \in \Im\} = S(gZ) = Cl_{B\prod X_\beta} gZ$.

Theorem3.5: Let $\prod X_\alpha$ **be a** G**-space with the product action, where** G **is finite discrete group. Define** $B\vartheta : G \times B\prod X_\alpha \to B\prod X_\alpha$ **by** $B\vartheta(g, \Im) = g\Im, g \in G$ **and** $\Im \in B\prod X_\alpha$, **then** $B\vartheta$ **is an extension of the action** ϑ **on** $\prod X_\alpha$ **to** $B\prod X_\alpha$.

Proof: To prove $B\vartheta$ **is continuous function.**

Let Z **be zero-set of** $\prod X_\alpha$, **then**

$(B\vartheta)^{-1}(Cl_{B\prod X_\alpha} Z) = \bigcup_{g\in G}(\{g\} \times g^{-1} Cl_{B\prod X_\alpha} Z) = \bigcup_{g\in G}(\{g\} \times Cl_{B\prod X_\alpha} g^{-1} Z)$ **(proposition (3.4))**

Since G **is finite and the finite union of closed sets is closed, thus** $B\vartheta$ **is continuous function. Now to prove restriction of the function** $B\vartheta$ **on** $\prod X_\alpha$ **equal to** ϑ.

By proposition (3.2) $g\Im \in B\prod X_\alpha$ **and** $B\vartheta(g, x) = g\Im_x$, **while** $\vartheta(g, x) = gx$ **by note (3.3)**

$g\Im_x$ **corresponds** gx, **then** $B\vartheta(g, x) = \vartheta(g, x)$ **for all** $x \in \prod X_\alpha$ **and** $g \in G$, **then** $B\vartheta$ **is an extension of the action** ϑ **on** $\prod X_\alpha$ **to** $B\prod X_\alpha$.

Theorem3.6: Let $\prod X_\alpha$ **be a** G**-space with the product action, where** G **is finite discrete group and let** $(\prod X_\alpha)^*$ **be the one-point compactification of** $\prod X_\alpha$, **then** $\vartheta^* : G \times (\prod X_\alpha)^* \to (\prod X_\alpha)^*$ **defined by :**

$\vartheta^*(g, x) = \begin{cases} gx & if x \in x, g \in G \\ \omega & if x = \omega, g \in G \end{cases}$ **is the extension of the action** ϑ **on** $\prod X_\alpha$ **to** $(\prod X_\alpha)^*$.

Proof: Let C **be a closed subset of** $(\prod X_\alpha)^*$, **then** $C = (\prod X_\alpha) \setminus U$ **where** U **is an open subset of** $\prod X_\alpha$ **or** $C = (\prod X_\alpha)^* \setminus U \cup \{\omega\}$ **where** U' **is an open subset of** $\prod X_\alpha$, **then**

$C=(\prod X_\alpha \cup\{\omega\})\setminus U=(\prod X_\alpha \setminus U)\cup\{\omega\}$ **since** $\omega\notin U$ **or**

$C=(\prod X_\alpha \cup\{\omega\})\setminus(U'\cup\{\omega\})=\prod X_\omega \setminus U'$, **then**

$\vartheta^{*^{-1}}(C)=\bigcup_{g\in G}(\{g\}\times g^{-1}(C)=\bigcup_{g\in G}(\{g\}\times g^{-1}((\prod X_\alpha \setminus U)\cup\{\omega\}))$

$\vartheta^{*^{-1}}(C)=\bigcup_{g\in G}(\{g\}\times g^{-1}((\prod X_\alpha \setminus U)\cup\{\omega\}))$ **or**

$\vartheta^{*^{-1}}(C)=\bigcup_{g\in G}(\{g\}\times g^{-1}(C)=\bigcup_{g\in G}(\{g\}\times g^{-1}((\prod X_\alpha \setminus U')$, **then the product of two closed set is closed and since** G **is finite and the finite union of closed set is closed , then** ϑ **is a continues function.**

Theorem 3.7: Let $\{X_\alpha\}_{\alpha\in\Lambda}$ **be a family of Tychonoff** G**-spaces with discrete group, then the Stone-Cech compactification of the orbit space by** G **of a product** $\prod X_\alpha/G$ **is the orbit of Stone-Cech compactification of the product of the** G**-space, that is** $\beta\prod X_\alpha/G=\beta\prod X_\alpha/G$.

Proof: In order to prove this theorem we show that Stone extension βi **of inclusion function** $i:\prod X_\alpha/G\to\beta\prod X_\alpha/G$ **is homeomorphism.**

Clear that $i\circ P_\prod = P\circ i_\prod$ **, where** $P_\prod:\prod X_\alpha\to\prod X_\alpha/G$, $P:\beta\prod X_\alpha\to\beta\prod X_\alpha/G$ **are quotient function and** $i:\prod X_\alpha\to\beta\prod X_\alpha$ **is the inclusion function**

$$\begin{array}{ccc}\prod X_\alpha & \xrightarrow{i_\prod} & \beta\prod X_\alpha \\ \downarrow{\scriptstyle P_\prod} & & \downarrow{\scriptstyle P} \\ \prod X_\alpha/G & \xrightarrow[\beta i]{} & \beta\prod X_\alpha/G\end{array}$$

It follows that $\beta(i\circ P_\prod)=\beta(P\circ i_\prod)$, **then** $(\beta i)\circ\beta P_\prod = P\circ I_{\beta\prod}$ **(see[6])**

That is

$$\begin{array}{ccc}\beta\prod X_\alpha & \xrightarrow{I_{\beta\prod}} & \beta\prod X_\alpha \\ \downarrow{\scriptstyle \beta P_\prod} & & \downarrow{\scriptstyle P} \\ & & \end{array}$$

$\beta(\prod X_\alpha/G) \xrightarrow{\beta i} \beta\prod X_\alpha/G$ **Commutes.**

Now for $x_1, x_2 \in \beta(\prod X_\alpha/G)$ **, choose** $y_1 \in (\beta P_\prod)^{-1}(x_1)$ **and** $y_2 \in (\beta P_\prod)^{-1}(x_2)$**, then** $(\beta i)(x_1) = (\beta i)(x_2)$ **implies that** $Gy_1 = Gy_2$ **therefore** $y_1 = gy$ **for some** $g \in G$ **, then** $(\beta P_\prod)(y_1) = (\beta P_\prod)(gy_2)$ **and since** $\beta P_\prod$ **is equiveriant, then** $(\beta P_\prod)(y_1) = g(\beta P_\prod)(y_2)$**, since the action on** $\beta\prod X_\alpha/G$ **is trivial, then** $(\beta P_\prod)(y_1) = (\beta P_\prod)(y_2)$**, hence** $x_1 = x_2$**, therefore** βi **is one to one.**

Now to prove βi **is on to, let** $Gx \in \beta\prod X_\alpha/G$ **, then** $(\beta i) \circ (\beta P_\prod)(x) = (\beta P) \circ I_{\beta\prod}(x) = (\beta P)(x) = Gx$**. Hence** βi **is on to.**

Now by proposition (2.18) $\prod X_\alpha/G$ **is dense subspace of the space** $\beta\prod X_\alpha/G$ **and by proposition (2.26)** $\beta\prod X_\alpha$ **is compact and since** $P : \beta\prod X_\alpha \to \beta\prod X_\alpha/G$ **is continuous function, then** $\beta\prod X_\alpha/G$ **is compact (a continuous image of a compact space is compact) and since** G **is finite, then by proposition (2.30)** $\beta\prod X_\alpha/G$ **is Hausdorff , then by proposition (2.21) there is a unique continuous extension of** i **which is** βi**. Now** βi **is one to one continuous function of compact space onto Hausdorff space, then** βi **is a homeomorphism.**

Theorem3.8: Let $\{X_\alpha\}_{\alpha\in\wedge}$ **be a family of Tychonoff, pseudo-compact** G**–spaces and all but one** X_α **is locally compact, then** $\beta(\prod X_\alpha/G) = \prod \beta X_\alpha/G$ **, where** $\prod_{\alpha\neq\alpha_\circ} X_\alpha$ **is infinite for all** $\alpha_\circ$ **and** G **is finite discrete group.**

Proof: Since $\{X_\alpha\}_{\alpha\in\wedge}$ **is a family of Tychonoff, pseudo-compact** G**– spaces and all but one** X_α **is locally compact then** $\prod X_\alpha$ **is pseudo-compact and by proposition (2.29)** $\beta\prod X_\alpha = \prod \beta X_\alpha$**, therefore** $\beta\prod X_\alpha/G = \prod \beta X_\alpha/G$ **and by theorem (3.7)** $\beta\prod X_\alpha/G = \beta(\prod X_\alpha/G)$ **hence** $\beta(\prod X_\alpha/G) = \beta\prod X_\alpha/G = \prod \beta X_\alpha/G$ **, then** $\beta(\prod X_\alpha/G) = \prod \beta X_\alpha/G$**.**

Theorem3.9: If $\prod X_\alpha$ is a G –space with G is finite discrete group, then the one point (Alexandroff) compactification of orbit space $\prod X_\alpha / G$ is the orbit space of the one point (Alexandroff) compactification of $\prod X_\alpha$ that is $(\prod X_\alpha / G)^* = (\prod \beta X_\alpha)^* / G$.

Proof: Define ` by

$f([x]) = \begin{cases} [x] & if \quad x \in \prod X_\alpha \\ [\omega] & if\ x = \omega \end{cases}$ **, then it is clear that f is a homeomorphism.**

REFERENCES

1. Porter, J.R. and Woods, R.G.; Extensions and Absolutes of Hausdorff Space, Springer-Veriag New York (1988).
2. Navalgi, G.B.; Definition Bank in General Topology, 54G (1991).
3. Willard, S.; General Topology, Addison-Wesley Inc. Mass (1970).
4. Irving, G.; Stone-Cech Compactifications of Product, Trans. Amer. Math. Soc., 90 p.369-382(1959).
5. Jeburi, S.S, " On Adjunction Space of Proper G-spaces", MSc. thesis Col. Of Science, Al-Mustansiriya Univ. (2001).
6. Al-Attar, A.I " Functorial Relation Ships Between the Category of Topological Space and the Category of Banach Spaces", MSc. thesis Col. Of Science, Baghdad Univ. (1973).

A Proposed Strategy for Segmenting the Video Clips into Shots and Selecting the Master Frame

Soukaena Hassan Hashem
University of Technology, Baghdad, Iraq

Received 7/7/2007 – Accepted 16/9/2007

Keywords: Master frame, video clips, clustering, genetic algorithm, and retrieval and mining system

الخلاصة

لبناء فهرسة قواعد البيانات الخاصة باسترجاع وتعدين الفيديو كليب من اكبر التحديات التي ستواجهها هذه الانظمة هي عملية تحديد مقاطع الفيديو ثم اختيار افضل لقطة صورية تمثل المقطع لكل الفيديو كليب.
هذا البحث يقترح طريقة لتقطيع الفيديو كليب الى لقطات صورية مباشرة ثم تطبيق خوارزمية العنقدة لجمع كل اللقطات الصورية المتشابهه ضمن مقطع واحد (عنقود واحد) وبهذا المقطع سوف لن يكون فقط سلسلة من اللقطات الصورية المتتابعة بل ممكن ان تحتوي على لقطات صورية من اماكن مختلفة من الفيديو كليب. هذا سوف يقلص عدد المقاطع ويجعلها اكثر اعتمادا وامثل. بعدها سيتم اختيار اللقطة الاكثر ملائمة لتمثيل كل مقطع من خلال اقتراح خوارزمية باستخدام الخوارزميات الجينية كوسيلة للاختيار من خلال تمثيل كل لقطة كنقطة.

ABSTRACT

To build indexes databases for retrieval and mining video clips. The most challenge will be the detection of shots and extraction of the master frames of each shot from video clips.

This research proposed a method to segment the video clips directly to frames, then applying clustering technique to collect the so much similar frames into shots (clusters), so the shot will not be sequential frames only but may have frames from other places of video clip, that to optimize and reduce the no. of shots. Then that research will propose a strategy to select the master frame in each shot using genetic algorithms, that by represent each frame as a point.

INTRODUCTION

Currently text-based search engines are commercially available, and they are predominant in the *World Wide Web* for search and retrieval of information. However, demand for search and mining multimedia data based on its content description is growing. Search and retrieval of contents is no longer restricted to traditional database retrieval applications. As an example, it is often required to find a video clip of a certain event in a television studio. In the future the content customers will demand to search and retrieve video clips based on content description in different forms. It is not difficult to imagine that one may want to mine and download the images or video clips containing the presence of Mother Teresa from the Internet or search and retrieve them from a video archival system. It

is even possible to demand for retrieval of a video which contains a tune of a particular song. In order to meet the demands for retrieval of audio-visual contents, there is a need for efficient solution to search, identify and filter various types of audio-visual content of interest to the user using non-text based technologies [1-5]

RELATED WORKS

Rretrieve and mine the video clips depending on MPEG, concentrate only with the metadata which has at most the general information of the feature and keywords of sound in the related video clip, the MPEG (Moving Picture Expert Group) standard committee, under the auspices of the International Standard Organization, is engaged in a work item to define a standard for multimedia audio-visual content description interface. JPEG2000 is the new standard for still picture compression and has been developed in such a way that metadata information can be stored in the file header for access and retrieval by users as well. There is a mode in JPEG2000 standard which particularly focuses on compressing moving pictures or video and its content description. All these developments will influence effective mining of video data in the near future, [6].

Traditionally, in general, the retrieval and mining system video clips temporarily segmented into video shots. A shot is a piece of a video motion (a sequential group of frames or pictures) where the video content from one frame to the adjacent frames does not change abruptly. One of these frames in a shot is considered to be a master frame. This master frame is considered to be a representative for the picture content in that shot (the selection of master frame differs from one system to another may be randomly for example). Sequence of master frames can define the sequence of events happening in the video clip. This is very useful to identify the type and content of the video, see figure (1), [7, 8].

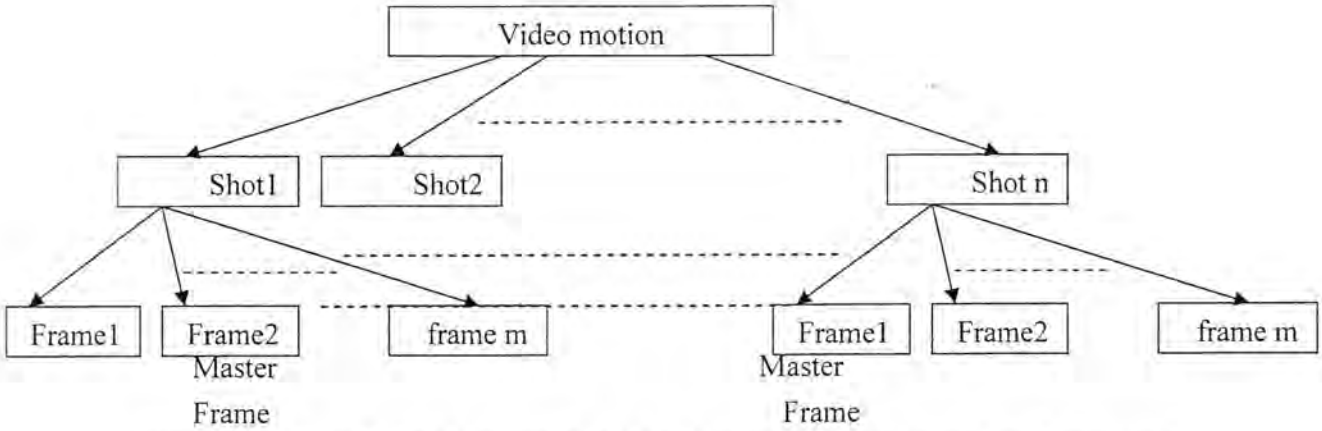

Figure -1: the main architecture for video Segmentation to shot, then frames and detecting the master frame for each shot.

THE PROPOSED SYSTEM

In this research we will propose to segment the video clips to frames directly so the video clip will has huge no. of frames each frame is a picture (image), see figure (2).

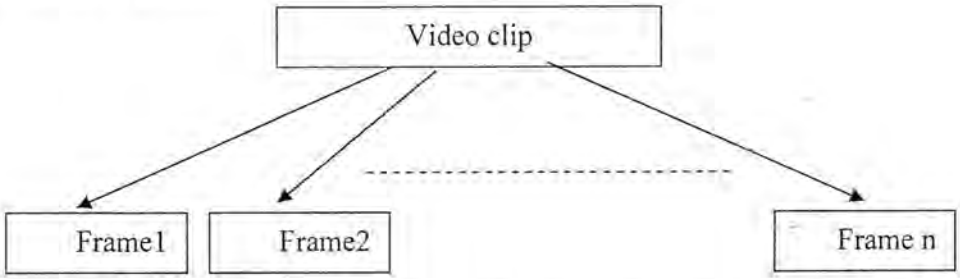

Figure -2: the proposed architecture for video Segmentation to frames directly without segmenting the clips to shot the frames.

After segmentation process we suggest to take each frame, image, and extract its feature vector, the images in an image database are indexed-based on extracted inherent visual contents (or features) such as:

1. **no. of objects: to detect the number of objects in each image we use edge detection filters (for more details see [9]).**
2. **then extract the features for each object such as position (x, y-coordinates), which mean calculate coordinates of the center for the specific object using normal image pixels coordinate from left to right and top down.**

3. Color (color histogram, color coherence vector, color moment , and linguistic color tag), for a specific image (m x n) we use the following equations for extracting all color features:

$$\mu_c = \frac{1}{MN}\sum_{i=1}^{M}\sum_{j=1}^{N} p_{ij}^{c},$$

$$\sigma_c = \left[\frac{1}{MN}\sum_{i=1}^{M}\sum_{j=1}^{N}(p_{ij}^{c} - \mu_c)^2\right]^{\frac{1}{2}},$$

$$\theta_c = \left[\frac{1}{MN}\sum_{i=1}^{M}\sum_{j=1}^{N}(p_{ij}^{c} - \mu_c)^3\right]^{\frac{1}{3}},$$

where $p^{\wedge}$ is value of the cth color component of the color pixel in the ith row and *jth* column of the image. As a result, M, N are dimension of Image, I and j are the counter of dimension is the standard deviation we need to extract only nine parameters (three moments for each of the three color planes) to characterize the color image.[2]

4. texture, for a specific image (m x n) we use the following equations for extracting all texture features:

$$Energy = \sum_{i}\sum_{j} C^2(i,j),$$

$$Contrast = \sum_{i}\sum_{j}(i-j)^2 C(i,j),$$

$$Homogeneity = \sum_{i}\sum_{j}\frac{C(i,j)}{1+|i-j|}.$$

5. Object shape and topology. for a specific image (m x n) we use the following equations for extracting all texture features: The *Euler number* is defined as the difference between number of *connected components* and number of *holes* in a binary image. Hence if an image has *C* connected components and *H* number of holes, the *Euler number E* of the image can be defined as [2]

$E = C\text{-}H.$

The feature vector actually acts as the *signature* of the image, figure (3) represent the main architecture to build indexes database for all frames, images, of the video clips. Table (1) represent the indexes database for each video clip and corresponding all frames of that clip.[2]

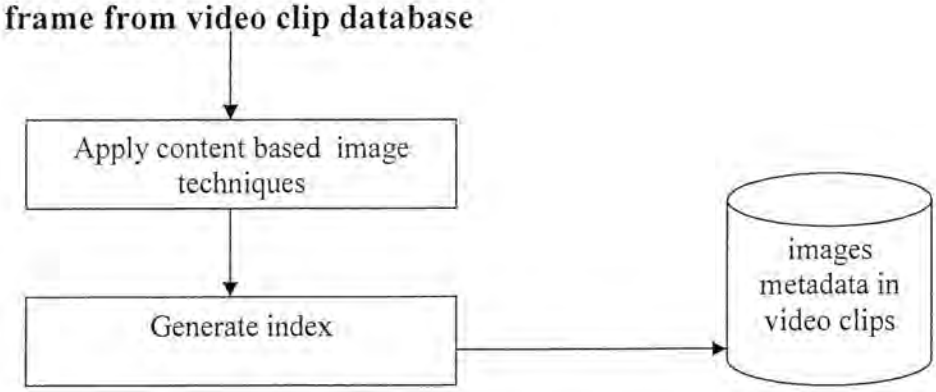

Figure -3 : the main architecture to build indexes database for the frames of the video clips.

Table -1: the indexes dbase for video clips and corresponding frames of that clip.

frame ID	No. of objects	Object ID	Features of objects x y histo mom coher tag texture shape topology
I1	4	O1	50 40 116.84 122.84 117.84 116.86 0.87 0.58 0.61
		O1	
		O2	
I2		O3	
I3			

THE PROPOSED CLUSTERING ALGORITHM

The steps of similarity algorithm are searching by no. of object in frames databases and the proprieties. The Euclidian distance $(\sum(x - yi))$ is used to take the minimum distance between the frame and all the frames of one cluster.

Input: Take frame from frames database and set it to first created cluster.

Output: put each frame to the cluster (shot) similar to it, see figure (4).

Step1: checking the no. of object and object properties in the taken frame with each frame in each cluster, shot, then record the degree of similarity with each cluster.

Step 2: put the frame in the shot which has a minimum degree of differential with it is frames.

Step 3: take the next frame and go to step 1.

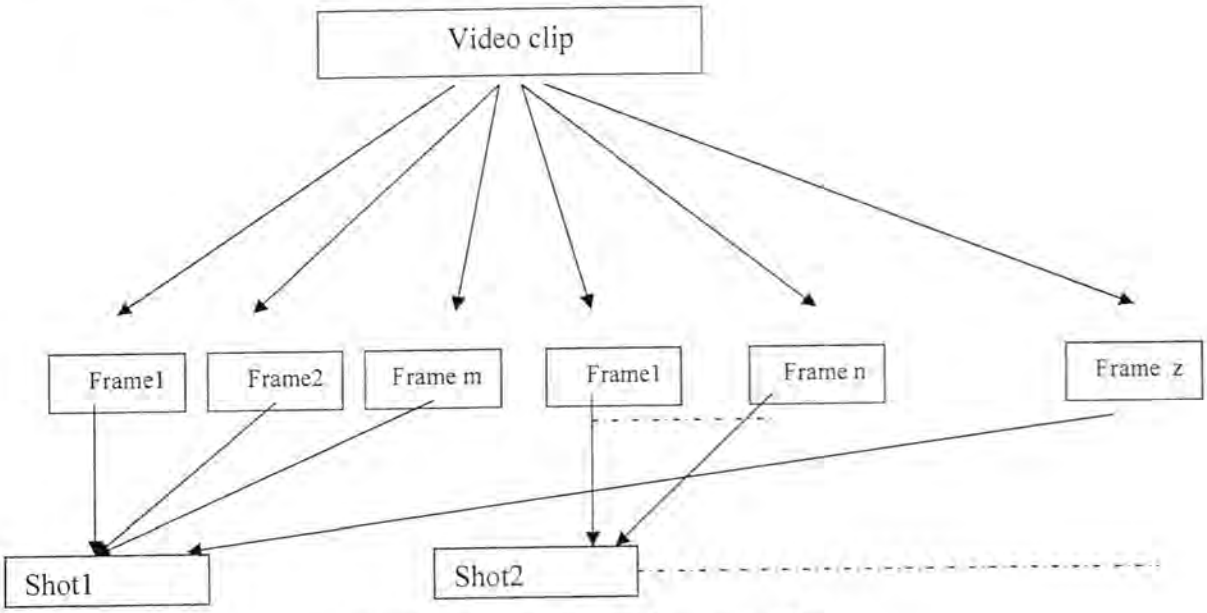

Figure -4: distributing frames to shots

THE PROPOSED GENETIC ALGORITHM

To apply a genetic algorithm for problem selecting master frame from shot, this research propose to define or to select the following components, for more explanation see the flowchart (figure 5):

Note: o represent symbol of object and oi represent the object o has the ith order.

1. **A genetic representation or encoding schema for potential solutions to the problem, here each frame will be presented as a point each point consist from the following (*no. of objects, (o1, (position (x, y coordinates), color (color histogram, color coherence vector, color moment , linguistic color tag), texture, object shape and topology), o2(.....), on(.....)).* For example the frame n in shot m has the following point representation (3, *(o1, (position (450,300), color (*118.84 122.84 117.84 116.86 *),***

0.80 , 0.68 *and* 0.71*), (o2, (position (450,400), color (*116.84 123.84 117.84 116.86 *),* 0.66 , 0.58 *and* 0.61*), (o3, (position (550,300), color (*116.84 122.84 117.84 117.86 *),* 0.99 , 0.58 *and* 0.61*)).*

2. A way to create an initial population of potential solutions, the initial population already created with clustering algorithm which established the shots. So this mean the initial population of each shot, will be all its frames represented by points.
3. An evaluation function that plays the role of the problem environment (best frame), rating solutions in terms of their "fitness". Here the proposed evaluation function for each frame is $f(point) = (no.\ of\ object + \sum (features\ of\ each\ objects))$.
4. Genetic operators that alter the composition of offspring. *One-point crossover* is the most basic crossover operator, where a crossover point on the genetic code is selected at random, and two parent frames are interchanged at this point.
5. Crossover exploits existing frame potentials, but if the population does not contain all the encoded information needed to find the best frame, no amount of frames mixing can produce a satisfactory solution. For this reason, a mutation operator capable of spontaneously generating new frame is included. The most common way of implementing mutation is to flip a bit with a probability equal to a very low, given mutation rate (MR). A mutation operator can prevent any single bit from converging to a value through the entire population and, more important, it can prevent the population from converging and stagnating at any local optima.
6. Values for the various parameters that the genetic algorithm uses population size, rate of applied operators, etc..In our particular problem we use the following parameters of the genetic algorithm: Population size, *pop-size* = 400 (the parameter was already used), Probability of crossover, PC = 1, Probability of mutation, PM = 0.001 (the parameter will be used in a mutation operation).
7. Continue with genetic processing until obtain the optimized frame to be the master frame

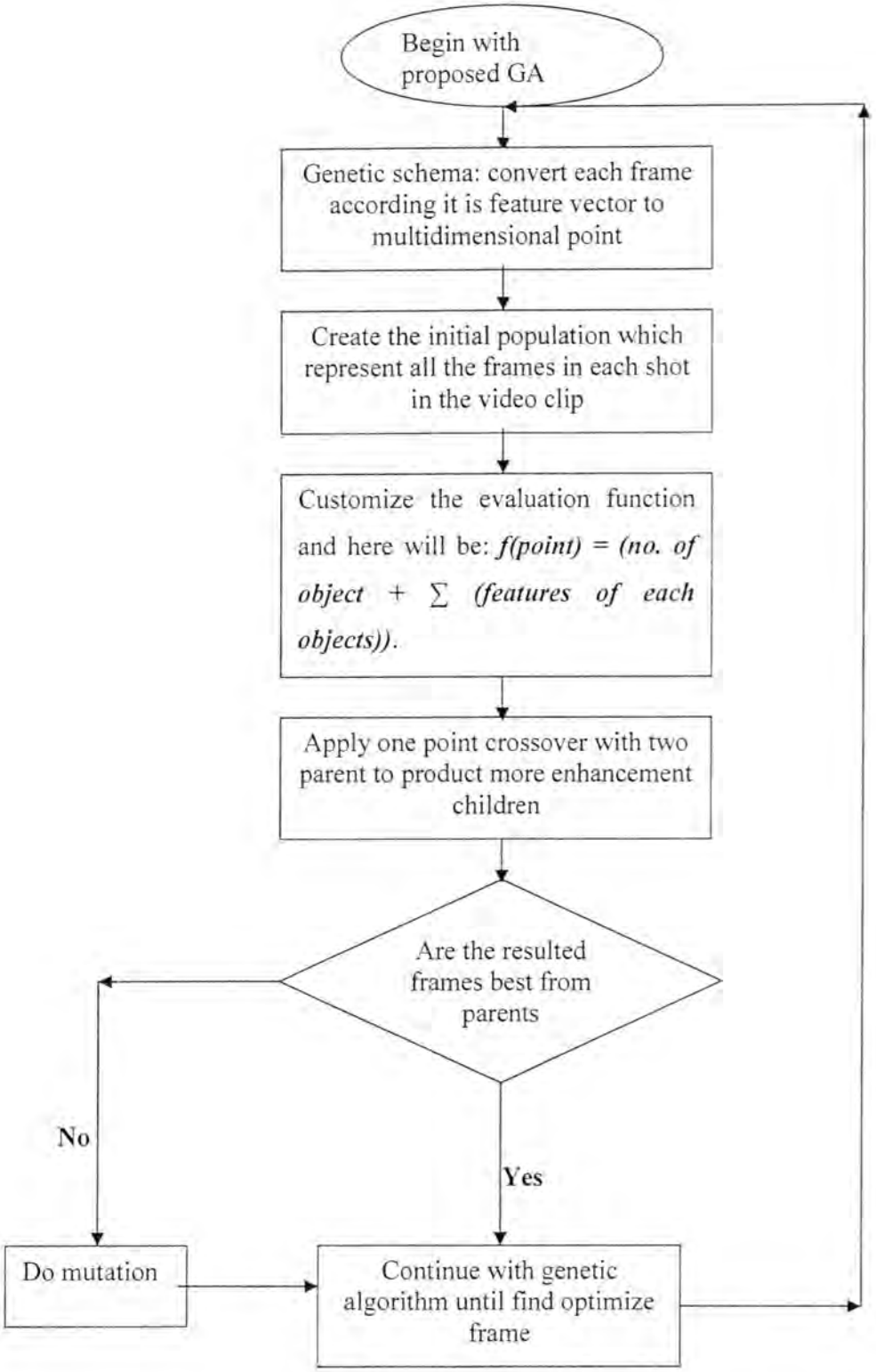

Figure-5 : the general flowchart for selecting best frame using genetic algorithms.

THE IMPLEMENTATION OF THE PROPOSED SYSTEM

The implementation of the proposed system will take each video clip will be introduced by the administrators and then analyze the video clip into collection of sequenced frame as in figure (6).

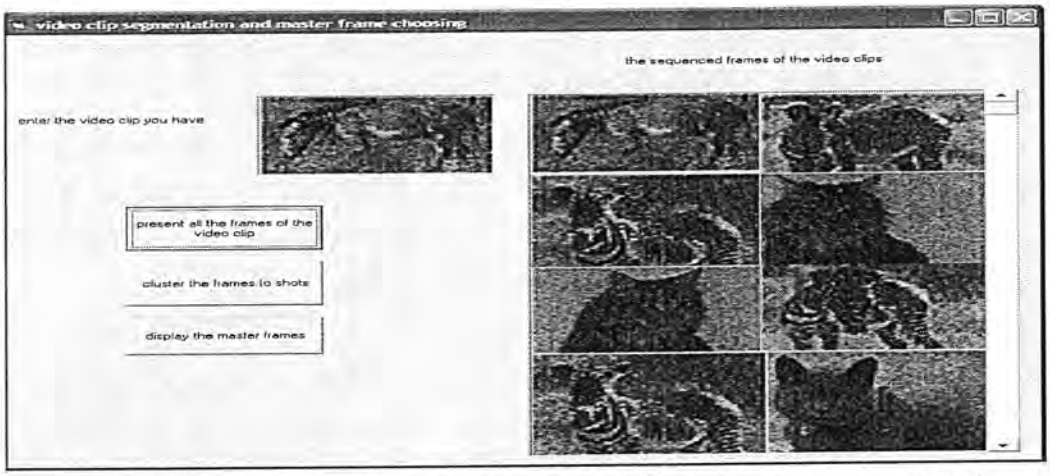

Figure -6 : The main window for introducing the video clip and analyze it.

In figure (6) there are three commands, the first one will be clicked when the administrator present the desired video clip the clicking process will introduce the sequenced frames of the clip. Where clicking the second command will display small window which introduce the results of the clustering algorithm which applied on the sequenced frames to introduce optimized shots, see figure (7).

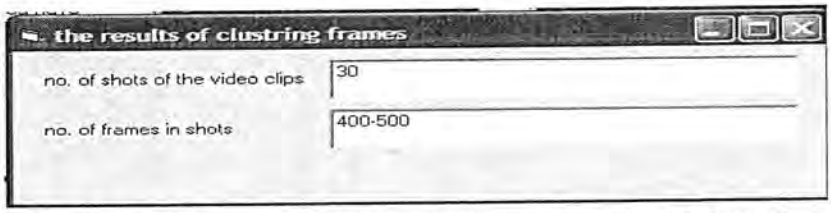

Figure -7 : The window which display the results of clustering.

Finally clicking the third command will display the results of the selecting the master frame from the shot. This window introduce the results of selected frame from shot (according the proposed genetic algorithm) for the two first shot only since all the results already stored in related database, see figure (8).

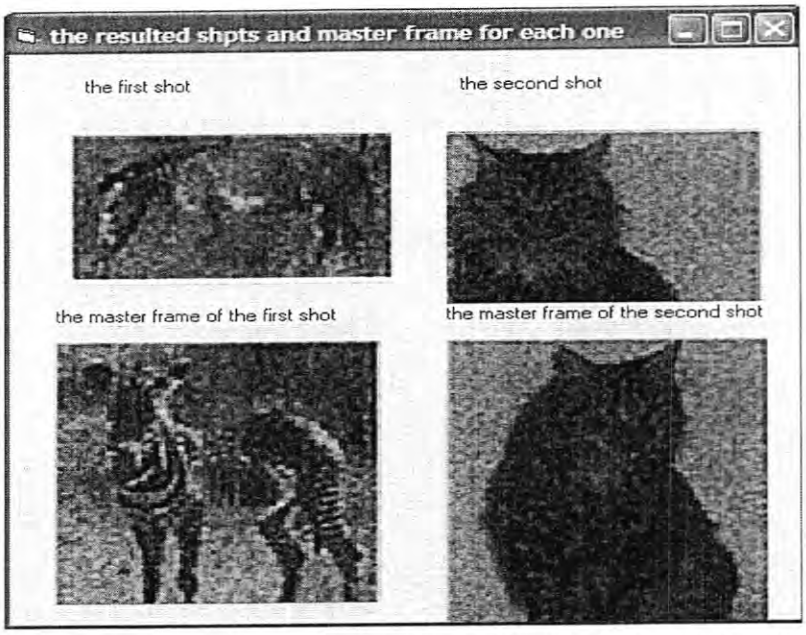

Figure 8 : The window which display the results of selected master frames for the two first shots.

CONCLUSIONS

In context with the results of the present study it can be concluded that:

1. The proposed segmentation of the video clip directly into frames instead of the traditional method (shots then frames and some times senses then shots then frames) will optimize the no. of shots since, the shots will be resulted from applying clustering algorithm on the sequenced frame. This mean we could obtain a shot has the first 200 frame and the last 50 frame that will reduce the no. of shot and reduce the redundancy in different shots.
2. Using the proposed genetic algorithm to get the master frame from each shot will give the optimal result. Since the proposed fitness function deal with each frame as a point and each point represent the overall features contained in the frame so surely the best point will be the best frame.
3. Since GAs are parallel-search procedures that can be implemented on parallel-processing machines for massively speeding up their operations.

REFERENCES

1. Kantardzic M.; *"DM concepts, models, methods and algorithms"*, jhon wiley &Sons, (2003).
2. Vailaya A., Figueiredo A. T., Jain A. K., and Zhang H. J., *"Image Classification for Content-Based Indexing"*, *IEEE Transactions on Image Processing*, Volume: 10 Issue: 1, pp 117 –130, (2001).
3. C. Saraceno and R. Leonardi, " audio as a support to scene change detection and characterization of video sequence", in proceeding of the IGASSP, IEEE computer society press, (1997).
4. Sakurai S., Ichimura Y., Suyama A., and Orihara R.; *"Inductive learning of a knowledge dictionary for a text mining system,"* in Proceedings of 14th International Conference on Industrial and Engineering Applications of Artificial Intelligence and Expert Systems,(2003).
5. Tan K. L., Ooi B.C. and Thiang L. F., *"Retrieving Similar Shapes Effectively and Efficiently"*, *Multimedia Tools and Applications*, Kluwer Academic Publishers, The Netherlands, (2001).
6. Oh J., Bandi B., *"Multimedia Data Mining Framework For Raw Video Sequences"*, Proceedings Third International Workshop on Multimedia Data Mining MDM/KDD', 23rd 2002, Edmonton, Alberta, Canada.
7. K. Minami, A. Akutsu, and H. Hamada, "video handling with music and speech detection", IEEE multimedia, pp: 17-25, (1998).
8. Y. Tonomura, A. Akutsu, Y. Taniguchi, and G. Suzuki, "structured video computing", IEEE multimedia, pp: 34-43, (1994).
9. Gonzalez R. C. and Woods R. E., *"Digital Image Processing"*, Reading, MA: Addison-Wesley,(1993).

Embedding Watermark in Palmprint Images

Amir S. AL-Malab and Methaq T. Kataa
AL-Mustansiriyah University /College of Science Computer Science Dept.

Received 5/9/2007- Accepted 22/10/2007

Keywords: Information Hiding; Watermarking; Biometric; Palmprint

الخلاصة

مع الانتشار الواسع لاستخدام أنظمه التحقق البيولوجية، بات البحث في مجالات التحقق من صحة البيانات البيولوجية نفسها على درجه كبيره من الأهمية. هذا البحث يقترح طريقه جديدة باستخدام الحيز المكاني لزرع بيانات علامة مائية في صوره تمثل راحة اليد دون تشويه صفات الصورة. الطريقة تشمل إدخال بيانات علامة مائية بعد تحديد المناطق التي تظهر فيها الصفات و ذلك من أجل تجنب المناطق التي تستخدم لتميز راحة اليد. بيانات العلامة المائية تزرع وفق شروط معينه. في هذه الطريقة لا توجد حاجه إلى الصورة الأصلية لراحة اليد عند استرجاع العلامة المائية.

ABSTRACT

With the wide spread utilization of biometric identification systems, establishing the authenticity of biometric data itself has emerged as an important research issue. This paper proposes a new spatial method in order to embed watermark data into Palmprint images, without corrupting their features. This method inserts watermark data after determining the features regions to avoid the regions used for Palmprint recognition. Watermark data are embedding according to certain conditions. In this way, the authenticity of the Palmprint image can be established. In process of extracting watermark does not require the original Palmprint image.

INTRODUCTION

Biometrics technology is based on using physiological or behavioral characteristics in personal identification, and can easily differentiate between an authorized person and a fraudulent impostor [1]. While the biometrics techniques offer a reliable method for personal identification, the problem of security and integrity of the biometrics data poses new issues. For example, if a person's biometric data (e.g., his/her Palmprint image) is stolen; it is not possible to replace it as compared to replacing a stolen credit card, ID or password.

A biometrics-based verification system works properly only if the verifier system can guarantee that the biometric data came from the legitimate person at the time of enrollment. In order to promote the wide spread utilization of biometric techniques, an increased level of security of biometric data is necessary [2]. Encryption and watermarking are among the possible techniques to achieve this. Encryption does not provide security once the data is decrypted. On

the other hand, watermarking involves embedding information into the host data itself, so it can provide security even after decryption. Furthermore, encryption can be applied to the watermarked data. However, embedding watermark may change the inherent characteristics of the host image (e.g., locations of feature points in Palmprint). Therefore, the verification performance based on (decoded) watermarked images should not be inferior compared to performance based on non-watermarked images [3]. We present a watermarking method that embeds name of a user in his/her Palmprint images. In this way, the authenticity of the Palmprint can be established.

Watermarking of Palmprint images can be used in applications like: (a) protecting the originality of Palmprint images stored in databases against intentional and unintentional attacks, (b) fraud detection in Palmprint images by means of fragile watermarks (which do not resist to any operations on the data and get lost, thus indicating possible tampering of the data), and (c) guaranteeing secure transmission of acquired Palmprint images from intelligence agencies to a central image database, by watermarking data prior to transmission and checking the watermark at the receiver site [4].

Palmprint System

Palmprint, which has been used as a positive human identifier for more than 100 years, is still considered as one of the most reliable means distinguishing a person from the others due to its stability and uniqueness [5].Palmprint features can be divided into three different categories: a) point features, which include minutiae features from ridges existing in the palm, and delta point features, from delta regions found in the finger-root region; b) line features, which include the three relevant Palmprint principal lines, due to flexing the hand and wrist in the palm, and other wrinkle lines and curves (thin and irregular); and, c) texture features of the skin. The Figure 1 is shown regions of features that listed above [6].

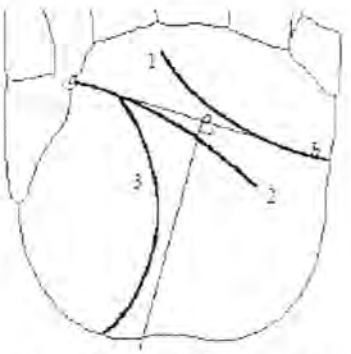

Figure - 1: **Definitions of principal line and datum point in a Palmprint: principal lines (1 heart line, 2 head line and 3 life line) and datum point (*a* and *b* endpoint, *o* the center).**

The Proposed Method

This method inserts the watermark data after determining the regions of features and thus prevents watermarking of regions used for Palmprint classification and recognition. The most commonly used Palmprint features in the Palmprint features extraction methods are principle lines, wrinkles, and ridges which resulted by the thinning process, collectively known as features. Therefore the locations of these features must be avoided in the hiding operation of a watermark. Figure 2 illustrates the flowchart of the proposed method.

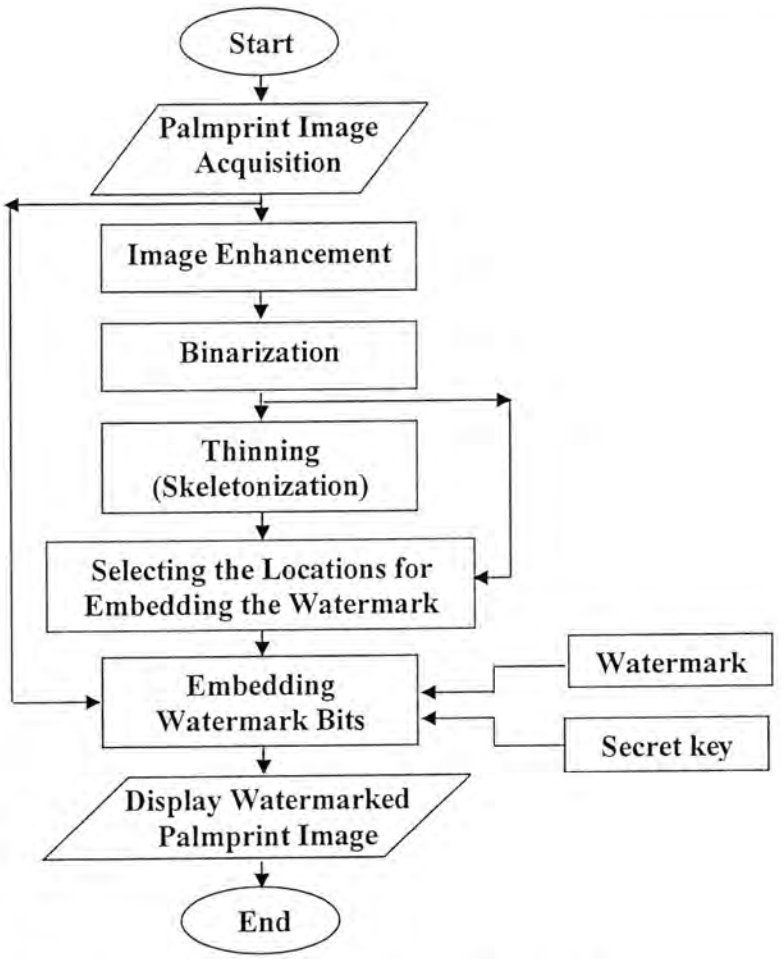

Figure - 2: **The flowchart of the proposed method**

The proposed method consist the following steps:

Image Acquisition: **from plain scanners (or through live-scanners). A digital gray-level image of the Palmprint is captured; the image is shown in Figure 3. This figure is an example of input Palmprint images from scanner.**

Figure - 3:**The Palmprint Image.**

Image Enhancement: **It is usual that during the acquisition step, some noise appears resulting in cutting of the principal lines, ridges, and other undesirable effects. Because of this, a process that improves the quality of the Palmprint is needed in order to improve the clarity of principal lines structures of Palmprint image and to prepare Palmprint image for next step. In this step, the filter which used to remove various types of noise in Palmprint image is Median filter; The median filter has two big advantages compared to convolution filters it removes noise completely without blurring the surrounding neighborhood (if he disturbances are small enough) and it preserves sharp edges. Figure (4A) shows the resulting image after this step is applied.**

Binarization: **In this step, the Palmprint image is transformed from a gray-level image into a binary image. This improves the contrast between the principal lines, ridges and valleys in a Palmprint image, and consequently facilitates the extraction of features. Extract the Principal lines and the ridges from Palmprint image, is the main task from binarization process. One ways of accomplishing this process is by using the edge detection operation and by means of a histogram analysis the optimal threshold is dynamically obtained for each image.**

The Sobel operator is followed by an optimal thresholding operation in which each pixel in the image is assigned a value representing either white or black depending on the magnitude of the gradient at that point as follow:

$$B(x, y) = \begin{cases} 1 \text{ if } EM(x, y) > T \\ 0 \text{ if } EM(x, y) \leq T \end{cases} \quad \ldots (1)$$

EM(x, y) is the edge magnitude value which results from convolution a Sobel operator. The Sobel operator is described in [7], which performs the edge detection operation using horizontal and vertical filters. T is optimal thresholding value that determined based on the analysis of the histogram. Figure (4B) shows the resulting image after this step is applied.

Thinning (Skeletonization): **After the Palmprint image is converted to binary form; it is then submitted to the thinning algorithm which reduces the principal lines and ridge thickness to one pixel wide. The thinning must be performed without modifying the original principal**

lines and ridge. The purpose of thin image which produced from the thinning algorithm is play very important role to determine the hiding locations in which the watermark bits will be stored in the original Palmprint image.

The standard thinning algorithm "Safe Point Thinning Algorithm" (SPTA) is described in [8], which performs the thinning algorithm using two subiterations. This algorithm was selected due to its easy implementation and good performance compared to others. Figure (4C) shows the resulting image after this step is applied.

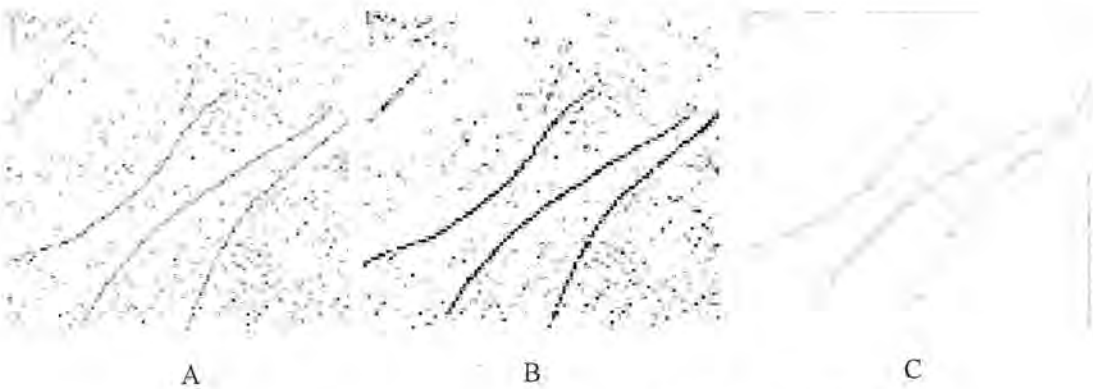

A B C

Figure- 4. (A) Smooth Image (B) Binary Image (C) Thin Image.

Selecting the Locations for Embedding the Watermark: In this step, the watermark will be embed into Palmprint image after determining the locations which are suitable for embedding the watermark where the watermark dose not change the regions of features Palmprint . Watermark data are embed into Palmprint image according to the embedding condition given below:

$$If\ \alpha\ (i, j) = 1 Then\ Insert\ watermark\ bit\ (W)\ in\ I\ (i, j).$$

where $I(i, j)$ are pixel values referring to original pixels at watermark embedding location (i, j). The value of watermark bit is denoted as W, where $W \in [0, 1]$. The α (i, j) term guarantees the pixels (called marked pixels) which will store watermark bit are not belonging to region which used in the features extract process from Palmprint images. Therefore the performance of a method which will be using the watermarked image (e.g., Palmprint verification in the case of watermarked Palmprint images) is unchanging; α (i, j), takes the value 0 if the pixel (i, j) under consideration belongs to a Palmprint feature region; it has value 1 otherwise.

To obtain $\alpha\ (i, j)$, it got the resulted binary image file from the binarization step, and get the resulted thin image file from thinning operation, if binary pixel (i, j) =1and thinning pixel (i, j) =0 then $\alpha\ (i, j)$ =1 otherwise $\alpha\ (i, j)$ =0, this will be used to determine the places in which the watermark bits will be stored in the original Palmprint image, additional to use the secret key. For example Figure 5. Shows three matrices are the binarization results, the thinning results, and the suitable hiding locations selection. These matrices consisting of two values are (zero's and one's). The third matrix plays the main role in determining the hiding locations where each location in third matrix consisting (1) is a suitable hiding location in the original Palmprint image.

1	1	1	1	0	1	0	1
0	1	0	1	0	0	1	0
0	0	0	1	0	1	1	0
0	0	0	1	0	1	0	1
0	1	1	1	1	0	1	1
1	1	0	0	1	0	1	1
0	1	1	1	1	1	1	1
1	1	0	1	1	0	1	1

(A)

1	1	1	0	0	1	0	1
0	0	0	1	0	0	1	0
0	0	0	1	0	0	1	0
0	0	0	1	0	1	0	1
0	0	1	1	1	0	1	0
0	1	0	0	1	0	1	0
0	1	1	1	1	1	1	0
1	0	0	0	0	0	1	0

(B)

0	0	0	1	0	0	0	0
0	1	0	0	0	0	0	0
0	0	0	0	0	1	0	0
0	0	0	0	0	0	0	0
0	1	0	0	0	0	0	1
1	0	0	0	0	0	0	1
0	0	0	0	0	0	0	1
0	1	0	1	1	0	0	1

(C)

Figure – 5:Three matrices :(a) Binarization results, (b) Thinning results, (c) The hiding locations

When the host image is a Palmprint image, additional requirements arise which must be satisfied by the watermarking system. Watermark embedding process must not introduce any changes to the Palmprint image which may alter the features extracted from that image for personal authentication - verification purposes. In the proposed method, this requirement is satisfied. After extracting the principal lines and ridges from the Palmprint image, watermark embedding is done according to condition in above. In this way, since $\alpha\ (i, j)$ term is zero for those feature areas, watermarking does not change original pixel values and the principal lines and ridges of the Palmprint image are preserved. As a result, the Features of Palmprint image are not changed by watermarking. Extracting start with finding the watermark embedding locations on

the watermarked image, via the three steps are Image Enhancement, Binarization, and Thinning (Skeletonization); in additional to secret key used in the step of watermark Embedding .

The algorithm of proposed method is as shown below:

Input: Original Palmprint Image, Binary File, Thin File, and Watermark Data.
Output: Watermarked Palmprint Image.

Begin
Step 1:Get original Palmprint image.
Step 2:Read the watermark data.
Step 3: Convert the watermark data into a bits stream.
Step 4: Get the binary Palmprint image file, this file resulted from Binarization process.
Step 5: Get the thinning Palmprint image file, this file resulted from thinning operation.
Step 6: Compute α (i, j) by using the binary file and thin file to select the locations which use in embedding watermark.
Step 7: Insert watermark bits to original Palmprint image, the Palmprint image pixel values are changed according to the following condition:
If α (i, j) =1Then Insert watermark bit (W) in B (i, j)
Step 8: Save image watermarked.
Step 9: Display the watermarked Palmprint image.
End.

Where *B (i, j)* is pixel in original Palmprint image.

Extracting Watermark:

Watermark data are extracting from Palmprint image according to the extracting condition as follow:

If α (i, j) =1Then Extract watermark bit (W) from $\hat{I}$ (i, j).

where $\hat{I}(i, j)$ are pixel values referring to pixels at watermarked Palmprint image location *(i, j)*.The α *(i, j)* is pixel that stored watermark.

The algorithm of Extracting Watermark is as shown below

Input: Palmprint Image.
Output: The Image Authentic or Unauthentic.

Begin

Step 1: Load the Palmprint image.
Step 2: Apply Image Enhancement operation.
Step 3: Apply Binarization process.
Step 4: Apply Thinning (Skeletonization) process.
Step 5: Compute α (i, j) by using the binary file and thin file to select the locations which use in embedding watermark
Step 7: Extract the watermark bit from the hiding locations in the loaded Palmprint image depending on the following condition:
If α *(i, j) =1 Then Extract watermark bit (W) from* $\hat{I}$ *(i, j).*
Step 8: If watermark bits are found in Palmprint image then
- Collect the extracted bits and convert them to values.
- Display the extracted values on screen; this means the loaded Palmprint image is authentic.

Else
- Display message" the loaded Palmprint image is unauthentic ".

End.

EXPERIMENTAL RESOLT

In order to evaluate the results obtained by proposed watermarking method. Three samples of Palmprint images were selected and the watermark was embedded by using the proposed hiding method in this paper. They are shown in Figure 6. And the features values of each image were calculated before and after the hiding process to ensure the features values of the original Palmprint images and watermarked Palmprint images which must has equal values in the features extraction process, before and after the hiding process. The features values of Palmprint images are calculated according to methods which described in [9], [10]. These methods use the orthogonal moments in the application of Palmprint verification. Moments are the most commonly used technique in character feature extraction. The idea of implementing orthogonal moments as Palmprint feature extractors is prompted by the fact that principal features of both character and Palmprint are based on line structure. These orthogonal moments are able to define statistical and geometrical features containing line structure information about Palmprint. The results are shown in table (1).

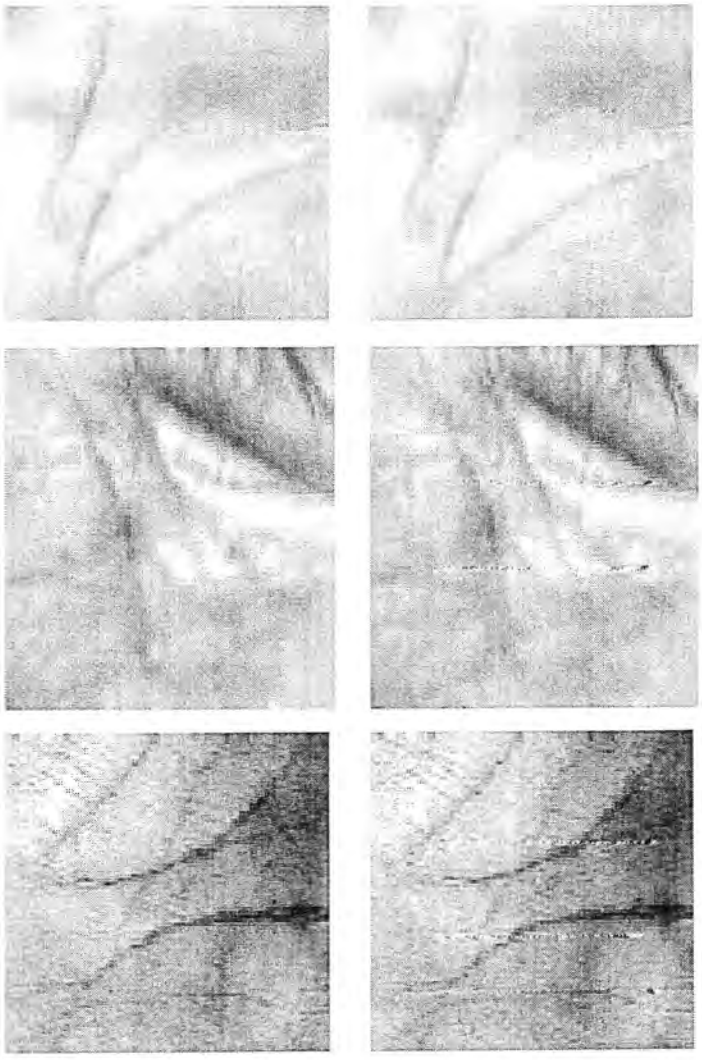

Figure - 6:**the Palmprint Images that used in the experiments. First column are original images. Second column are watermarked Palmprint**

Table - 1: **Testing Results of Features Values for Three Samples before and after the Hiding Process.**

Features Values	*Before the Hiding Process*			*After the Hiding Process*		
	Image1	*Image2*	*Image3*	*Image1*	*Image2*	*Image3*
F1	**0.637186**	**0.674084**	**1.054706**	**0.637186**	**0.674084**	**1.054706**
F2	**1.526736**	**1.874716**	**2.241390**	**1.526736**	**1.874716**	**2.241390**
F3	**2.897601**	**3.399393**	**3.955898**	**2.897601**	**3.399393**	**3.955898**
F4	**2.636246**	**2.956476**	**3.806295**	**2.636246**	**2.956476**	**3.806295**
F5	**5.402831**	**6.127244**	**7.687298**	**5.402831**	**6.127244**	**7.687298**
F6	**3.399420**	**3.891561**	**4.926982**	**3.399420**	**3.891561**	**4.926982**
F7	**3.999775**	**5.390103**	**6.003097**	**3.999775**	**5.390103**	**6.003097**

where F1, F2... F7 are Moments values that represented the extracted features from each the Palmprint image in the process of Palmprint verification.

Moment descriptors (moment invariants) are used in many pattern recognition applications. The idea of using moments in shape recognition gained prominence in 1961, when Hu derived a set of invariants using the theory of algebraic invariants.

The moment invariants are very useful way for extracting features from Two-dimensional images. The moment invariants can be subdivided into skew and true moment invariants, where the skew moment invariants are invariant under change of size, translation, and rotation only but the true moment invariants are invariant under change of size, translation, rotation, and reflection [9].

To determine the amount of distortion watermarking algorithm introduced into the host image. Table (2) shows the PSNR values of all watermarked Palmprint images in the sample above.

Table – 2: PSNR Values for Three Samples.

Images	*PSNR*
Sample 1	42.428
Sample 2	48.179
Sample 3	46.400

The PSNR results of our method are over 42.4 dB (decibel) which is considered as a very acceptable distortion of the original image according to the common practice to measure the quality of the watermarked image.

CONCLUSIONS

The watermark is hidden in such a way that the Palmprint features that are used in matching are not changed during encoding/decoding. As a consequence, the verification accuracy based on decoded watermarked Palmprint images is very similar to that with original Palmprint images.

Because the hiding locations are the edge pixels regions only the proposed method made the changes visibility to the host image are unobserved. Due to the fact that human visual system is relatively less sensitive to changing pixel value in busy image regions and edge image regions.

REFERENCES

1. David Zhang, "*Special Issue on Biometric Systems*", IEEE Transactions On Systems, Man, And Cybernetics—Part C: Applications And Reviews, Vol. 35, No. 3, (2005).
2. Jain A. K. and Uludag Umut, "*Hiding Biometric Data*", IEEE Transactions on Pattern Analysis and Machine Intelligence, Vol. 25, No. 11, (2003).
3. Jain A. K., Umut Uludag and Rein-Lien Hsu, "*Hiding a Face in a Fingerprint Image*", Computer Science and Engineering Department, Michigan State University, USA, (2002).
4. Gunsel Bilge, Uludag Umut, and Ballan Meltem, "*Robust Watermarking of Fingerprint Images*", TUBITAK Marmara Research Center, Information Tech. Research Institute, Turkey, (2003).
5. Jos´e Garc´ıa-Hern´andez and Roberto Paredes"*Biometric Identification Using Palmprint Local Features*", IEEE Transaction on Pattern Analysis and Machine Learning, 25(9):1041–1050, (2003).
6. Xiangqian Wua, David Zhangb, Kuanquan Wanga, Bo Huanga "Palmprint classification using principal lines", 12 February 2004 www.elsevier.com/locate/patcog.
7. Gonzalez, R. and Woods, R., "*Digital Image Processing*" Second Addition, Prentice-Hall Inc., (2002).
8. Naccache Nabil, Shinghal Rajjan, "SPTA: A Proposed Algorithm for Thinning Binary Patterns", IEEE Trans. on Systems, Man and Cybernetics, vol. 14, pp. 409-418, (1984).
9. Ying-Han Pang, Andrew T.B.J, David N.C.L and Hiew F. S., "*Palmprint Verification with Moments*" Journal of WSCG, Vol.12, No.1-3, February 2-6, (2003).
10. Quasy M. J., "*Design and Implementation of a Biometric Authentication System using Palmprint Technique*", M. Sc., Informatics Institute for Postgraduate Studies, (2004), Baghdad, Iraq.

The Role of Rain Drop Size Distribution on Specific Attenuation at Microwave Frequencies

Kais Jamel . Al-Jumaily
Department of Atmospheric Sciences, College of Science, Al-Mustansiriyah University

Received 28/1/2007- Accepted 16/9/2007

الخلاصة

يعتبر التوهين النوعي(التوهين في وحدة المسافة) للموجات الدقيقة بواسطة المطر من العوامل الاساسية في حسابات احصائيات توهين الامطار. وان القانون الاسي للتوهين النوعي للمطر ملائم جدا وشائع الاستخدام في هذا المجال. الهدف من هذا البحث هو دراسة دور التوزيع الحجمي لقطرات المطر على حسابات التوهين النوعي. لقد تم اجراء حسابات التوهين النوعي للمطر عند الترددات من 5 الى 100 كيكاهرتز وللموجات المستقطبة افقيا وشاقوليا ودائريا. ولقد اعتمدت هذه الحسابات على اربعة توزيعات حجمية شائعة الاستخدام.
اظهرت النتائج، ولجميع انواع التساقط المطري، بأن التوهين النوعي للمطر تقريبا لا يعتمد على التوزيع الحجمي لقطرات المطر عند الترددات القليلة التي هي اقل من 30 كيكاهرتز. وعند زيادة التردد لقيم اعلى من هذه القيمة فأن التوهين النوعي للمطر يصبح حساسا للتوزيع الحجمي. وقد بينت النتائج بأن توزيع كاما و توزيع مارشال-بالمر يسببان توهينا اكثر من التوزيعين الاخرين. كما وجد انه في حالة المطر الخفيف يكون توزيع مارشال-بالمر هو التوزيع المسيطر. إن توزيع كاما هو التوزيع الأكثر فعالية في حالة المطر الكثيف وحالة المطر الكثيف جدا.
وقد أوضحت النتائج بأن الموجات المستقطبة أفقيا تتعرض إلى اكبر توهين و الموجات المستقطبة شاقوليا تتعرض الى اقل توهين بينما الموجات المستقطبة دائريا فأنه في وسط الاثنين .

ABSTRACT

A fundamental quantity in the calculation of rain attenuation statistics is the specific attenuation (attenuation per unit distance). The power-law form of rain specific attenuation is very convenient and is commonly used . The aim of this research is to investigate the role of the rain drop size distribution on the computation of the rain specific attenuation. Calculations rain specific attenuation were carried out for the frequency range of 5 to 100 GHz and for horizontally, vertically and circularly polarized waves. These calculations were based on four commonly used rain distributions.

The results showed that for all types of rainfall rate, the rain specific attenuation is almost independent of the rain drop size distribution when the frequency is less than about 30 GHz. As the frequency increases beyond this value, the rain specific attenuation becomes sensitive to the rain drop size distribution. The results also showed that Gamma and Marshall-Palmer distributions cause more attenuation than the other two distributions. It was found that in the case of light rain, Marshall-Palmer rain drop size distribution is the dominant distribution. Gamma distribution is the most effective distribution in heavy to very heavy rainfalls.

The results demonstrated that, horizontal polarized waves are attenuated the most, vertical polarization shows the least attenuation while circular polarization is in the middle of these two.

INTRODUCTION

Rain is one of the most important atmospheric phenomena influencing the attenuation of microwaves. The rain drop size distribution (DSD) and its appropriate parameterization play an

important role in the proper interpretation of the meteorological radar measurement as well as in the estimation of the radiowave attenuation due to rain.

The power-law form of rain specific attenuation is very convenient and has been used in calculating rain attenuation statistics. The term specific attenuation is commonly used, accounting for attenuation per unit distance. It is a fundamental quantity in calculating the rain attenuation. Its power-law form is written as $\gamma = k\ R^{\alpha}$ in dB/km, where R is the rain rate in mm/h, and k and α are power law parameters, which depend on frequency, raindrop size distribution, rain temperature, and polarization.

The DSD has been studied by many researchers, but the most commonly used in the calculation of rain attenuation are: the Gamma rain DSD [1]; the lognormal rain DSD [2] ; the Laws-Parsons rain DSD [3]; and the Marshall-Palmer rain DSD [4] . Zhang and Moayeri (1999) [5] have suggested a power-law parameterization for these four rain DSDs. They presented k and α with polarization dependence a for a rain temperature of 0 °C, over the frequency range of 5 −100 GHz and for rainfall rates from 0 to 150 mm/hr. Ng (1999) [6] has used the power-law formulation for Laws-Parsons rain DSD to predict the 97 GHz signal loss by rain. Fiser (2000) [7] studied the influence of DSD on rain attenuation computation in the 10-150 GHz frequency region. Park et al, (2006) [8] introduced a new model for rain DSD, based on the measurement performed by Park et al, (2004) [9] in Chungnam National University, Korea. They concluded that the lognormal distribution is the most adequate candidate for describing rain DSD than other distribution models.

The aim of this research is to investigate the role of the rain DSD on the computation of the rain specific attenuation using the formulations suggested by Zhang and Moayeri (1999) [5].

THEROY

Electromagnetic waves propagating through rain are attenuated because of the absorption of power in the lossy dielectric medium represented by water. There is also some loss in the direct transmitted wave because of scattering of some energy out of the beam by raindrops [10] . This scattering is usually small, compared to the absorption loss. Scattering is most significant when the wavelength of the electromagnetic radiation is comparable to the dimension of the scattering particles [11].

The rain specific attenuation γ in dB/km is given by [12]:

$$\gamma = 4.343\times10^{3}\int_{D_{min}}^{D_{max}} Q_e(D)N(D)dD \quad (1)$$

Where D_{min} and D_{max} represent the maximum and minimum diameters of raindrops. Q_e (D) is the rain extinction coefficient, and $N(D)$ is the DSD.

The most commonly used rain DSD are:

i. The Gamma rain DSD [1]:

$$N(a) = N_o a^3 \exp(-\Lambda a) \quad (2)$$

where a is the equi-volume radius of raindrops, N_o=1.42×10^{-1} cm^{-4}, and $\Lambda = 1.3R^{-0.13}\times10^{2}$ cm^{-1}.

ii. The Log-Normal rain DSD is given by [2]:

$$N(D) = \frac{N_o}{\sqrt{2\pi}\sigma D}\exp(-\frac{(\ln D-\mu)}{2\sigma^2}) \quad (3)$$

where D is the diameter of the raindrop in millimeters , $N_o = 108R^{0.363}$ m^{-3} , $\mu = -0.195 + 0.199\ln R$, and $\sigma^2 = 0.137 - 0.013\ln R$. R is the rainfall rate in mm/hr and σ is the standard deviation.

iii. The Laws and Parsons rain DSD, according to de Wolf (2001) [13] this distribution was fitted as:

$$N(D) = N_o \exp(-\Lambda R) \quad (4)$$

where D is the raindrop diameter, R is the rainfall rate mm/hr, $N_o = 0.198R^{-0.384}$ cm^{-4}, and

iv. The Marshall-Palmer Rain DSD is given by [4]:

$$N(D) = N_o \exp(-\Lambda R) \quad (5)$$

where D is the raindrop diameter, N_o=0.08 cm^{-4}, $\Lambda = 41R^{-0.21}$, and R is the rainfall rate in mm/hr.

The power–law approach to equation (1) is given by [2]:

$$\gamma = kR^{\alpha} \quad (6)$$

where R is the rainfall rate in mm/hr, and k and α are power-l parameters, which depend on frequency, raindrop size distribution, rain temperature and polarization.

Zhang and Moayeri (1999) [5] tabulated the parameters k and α for linear polarizations (horizontal and vertical). For circular polarization, the parameters can be calculated by the following expressions:

$$k_C = (k_H + k_V)/2 \quad (7)$$

$$\alpha_C = (k_H\alpha_H + k_v\alpha_v)/2k_C \quad (8)$$

where the subscripts H, V, and C refer to the horizontal, vertical, and circular polarizations respectively.

RESULTS AND DISCUSSION

The rain specific attenuation was calculated as a function of the frequency for horizontal, vertical and circular polarizations for the four types of rain DSD. Figure (1) shows the results for light rainfall (1 mm/hr). It is seen that for all the polarizations states, the rain specific attenuation increases sharply with increasing the frequency and that the rain DSD seems to have little effect on the rain specific attenuation for frequencies less than about 30 GHz,. As the frequency increases above the 30 GHz, the rain specific attenuation increases gradually and becomes almost constant at high frequencies (greater than 90 GHz). Also the influence of rain DSD on the rain specific attenuation becomes stronger as the frequency increases. The results of calculations for moderate rainfall (5 mm/hr), heavy rainfall (20 mm/hr), and very heavy rainfall (100 mm/hr) are illustrated in figures (2), (3) and (4) respectively. It is clear that the behavior of the specific attenuation curves for these categories of rainfall are similar to that of the light rainfall case. The results indicated that for higher frequencies, the Gamma and Marshall-Palmer rain DSD's result in relatively higher specific attenuation compared with the other two distributions. For light and moderate rainfall rates the Log-Normal and Laws-Parsons distribution give comparable values of specific attenuation while for heavy and very heavy rainfall rate, the log-normal gives relatively lower values of specific attenuation. These behaviors are attributed to the nature of rainfall rate dependency on the number and size of drops in a specific distribution. It is interesting to note that for light rainfall the Marshall-Palmer distribution gives higher values of attenuation than that caused by rainfall with Gamma distribution. For moderate rainfall these two distributions result in comparable values of attenuation. For heavy and very heavy rainfall, Gamma distribution becomes the dominant distribution.

To illustrate the effect of wave polarization on the rain specific attenuation, calculations were performed for four selected frequencies (5, 35, 65, and 95 GHz) assuming Marshall-Palmer distribution. The results are presented in Figure (5) for the four rainfall categories. It is evident that for light rain the specific attenuation is almost independent of the polarization state of the wave. This is due to the fact that in light rain the raindrops are small and spherical and therefore the differential attenuation is zero. For the other categories of rainfall rates, horizontal polarized waves are attenuated the most, vertical polarization shows the least attenuation while circular polarization is in the middle of these two. This could be explained by the fact high rainfall rates are associated with relatively

larger drops and these drops are oblate spheroids in shape and tend to fall with their major axis parallel to the ground. Therefore, electromagnetic waves attenuate more in the horizontal axis than in the vertical axis. Circularly polarized wave is attenuated more than the vertically and less than the horizontally polarized waves because it is a composite of horizontal and vertical waves of equal amplitudes.

CONCLUSION

This research investigated the role of rain Drop Size Distribution (DSD) on the computation of rain specific attenuation of microwaves. Four different rain DSDs: Gamma; Log-Normal; Laws-Parsons; and Marshall-Palmer rain distributions were considered.

The results indicated that for frequencies less than about 30 GHz the rain specific attenuation is independent of the rain DSD. As the frequency increases beyond this value, the rain specific attenuation becomes sensitive to the rain DSD. This behavior was found for all types of rainfall rates (light, moderate, heavy, and very heavy). The results also showed that Gamma and Marshall-Palmer distributions cause more attenuation than the other two distributions. It was found that in the case of light rain, Marshall-Palmer rain DSD is the dominant distribution. Gamma distribution is the is most effective distribution in heavy to very heavy rainfalls.

The results demonstrated that, horizontal polarized waves are attenuated the most; vertical polarization shows the least attenuation while circular polarization is in the middle of these two.

Future work could be focused on the effect the effect of other hydrometeors drop size distributions, sand , and dust particle size distributions.

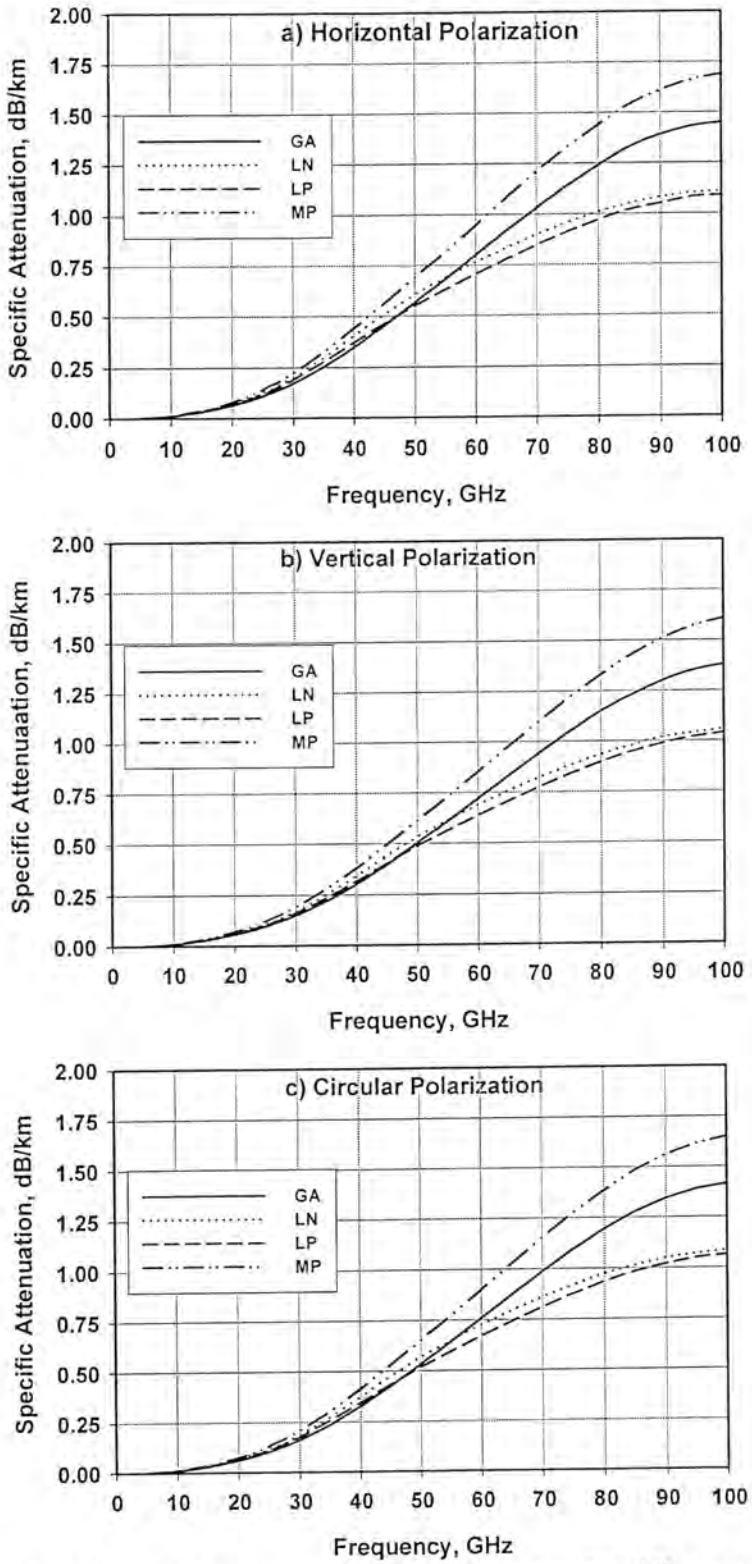

Figure -1: Rain Specific attenuation versus frequency for different rain DSD and polarizations assuming light rainfall (1 mm/hr).

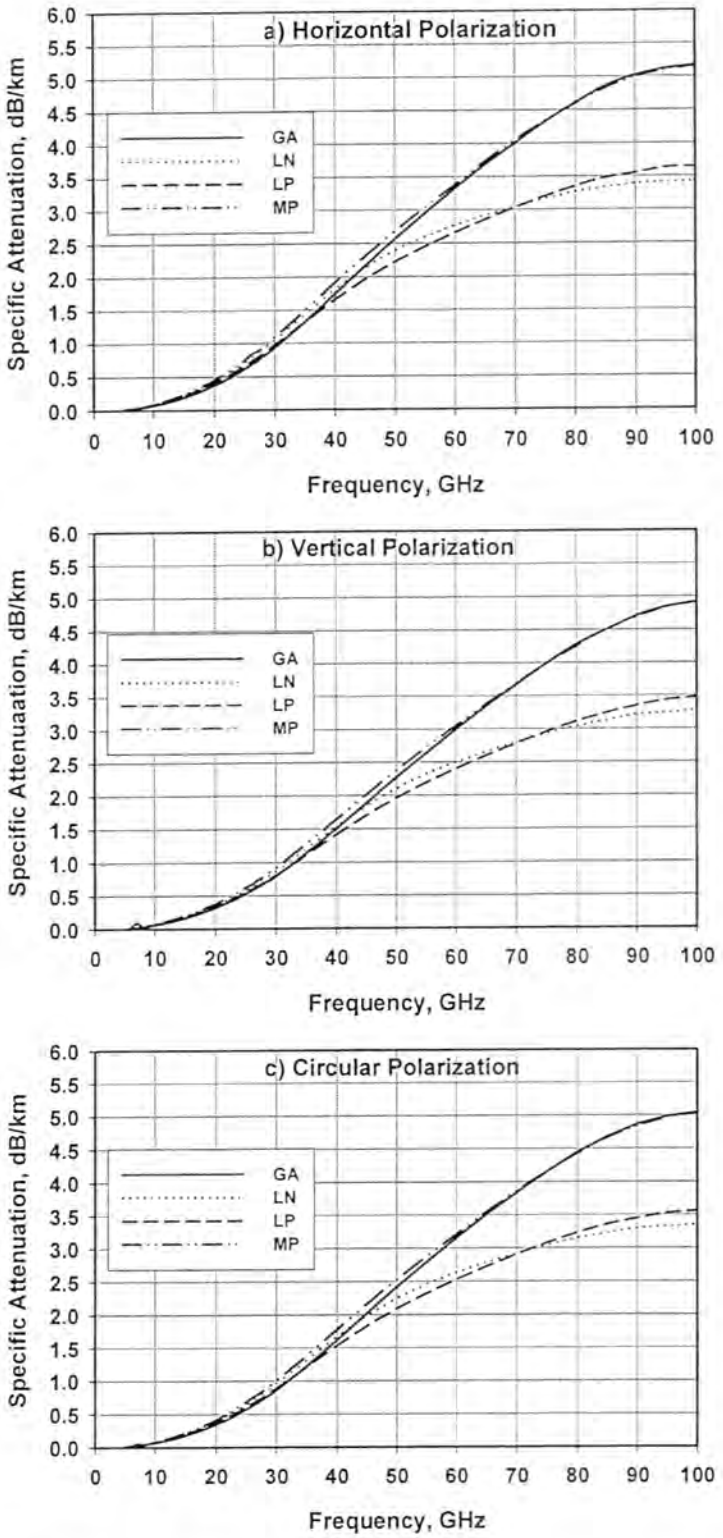

Figure -2: Rain Specific attenuation versus frequency for different rain DSD and polarizations assuming moderate rainfall (5 mm/hr).

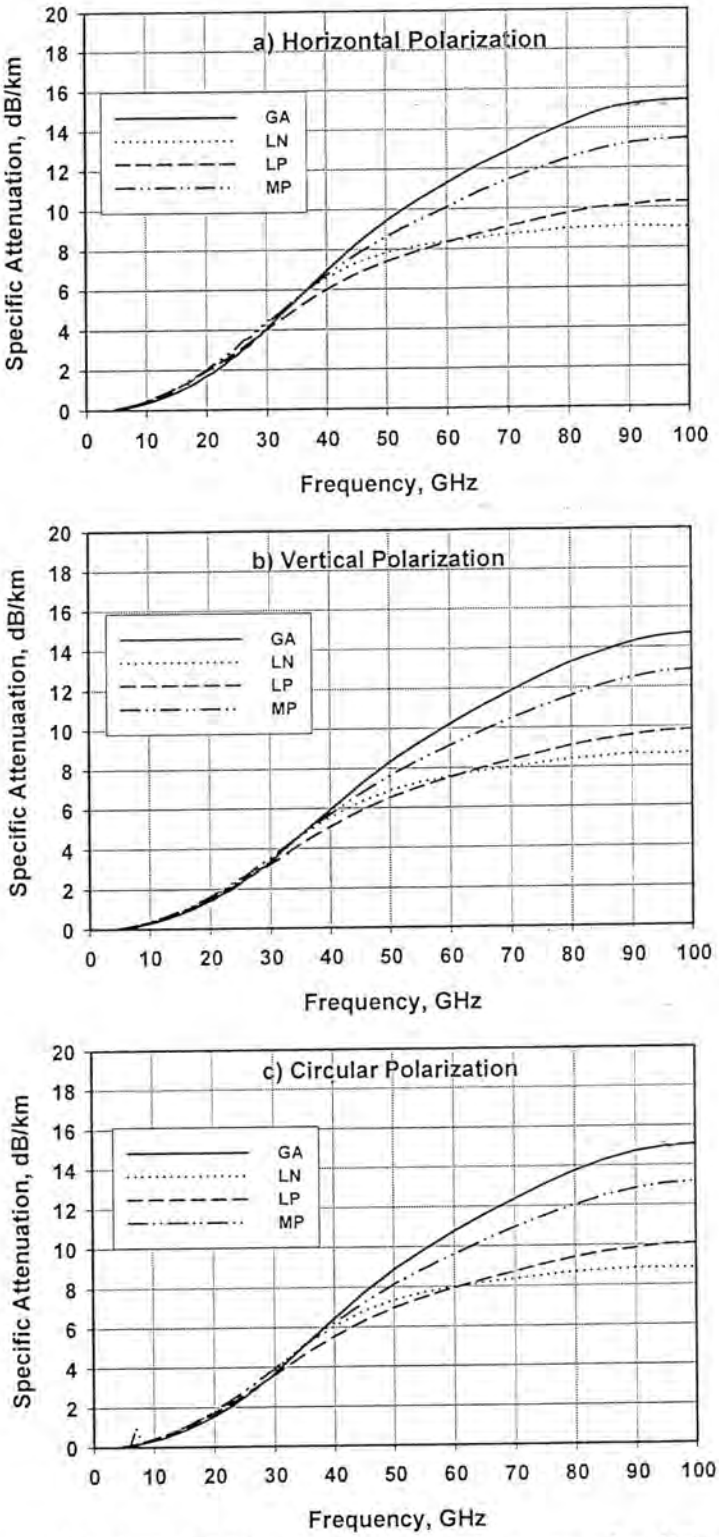

Figure -3: Rain Specific attenuation versus frequency for different rain DSD and polarizations assuming heavy rainfall (25 mm/hr).

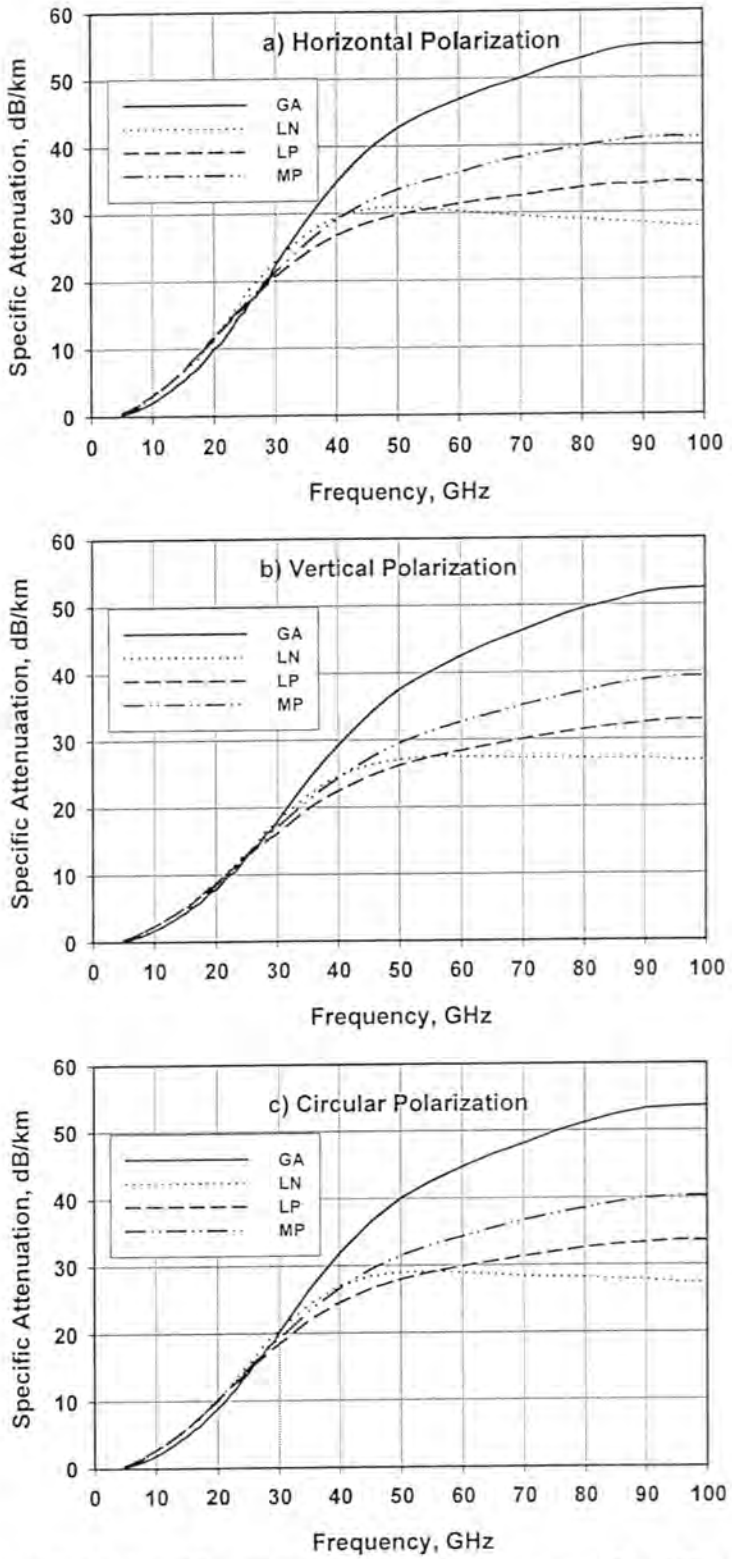

Figure -4: Rain Specific attenuation versus frequency for different rain DSD and polarizations assuming very heavy rainfall (100 mm/hr).

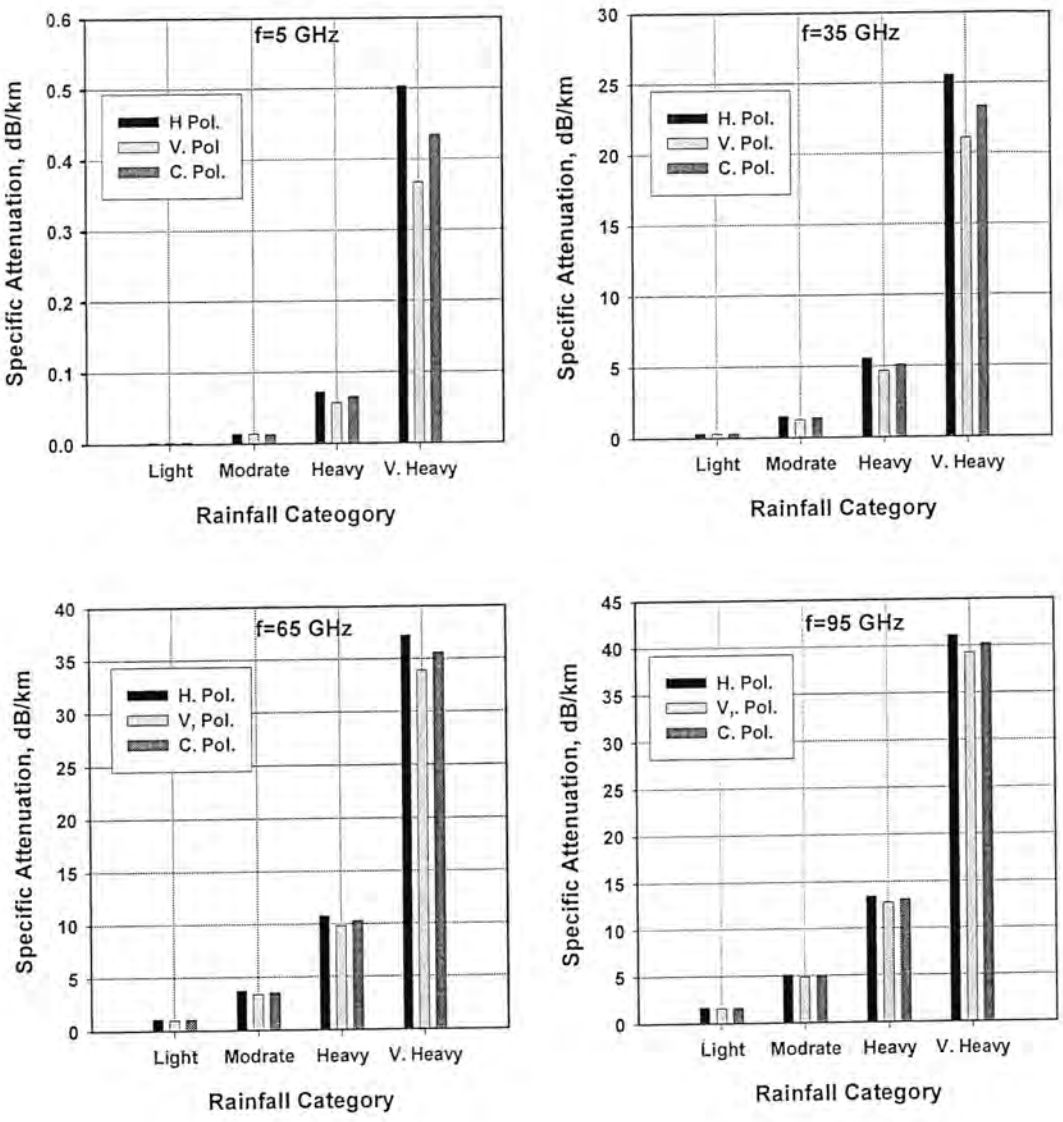

Figure -5: Rain specific attenuation versus rainfall category for different polarizations and for selected frequency bands.

REFERENCES

1. Ulbrich, C.W., "Natural variations in the analytical form of the raindrop size distribution," J. Climate Appl. Meteor., vol. 22, pp. 1764-1775, (1983).
2. Ajayi G.O. and R.L.Olsen, "Modeling of a tropical raindrop size distribution for microwave and millimeter wave applications," Radio Science, vol. 20, pp: 193-202, (1985).
3. Laws J.O. and D. A. Parsons, "The relation of raindrop-size to intensity," Trans. Amer. Geophys. Union, vol. 24, pp: 452-460, (1943).
4. Marshall J.S. and W. McK. Palmer, "The distribution of raindrops with size," J. Meteorol., vol. 5, pp.165-166, (1948).
5. Zhang W. and N. Moayeri,"Power-Law parameters of rain specific attenuation," IEEE 802.16cc-99/24, (1999).
6. Ng S. L., "97 GHz signal path losses prediction ," Thesis, Department of Electrical Engineering, University of Queensland , Australia, (1999).
7. Fiser O., " The role of particular rain drop size classes on specific rain attenuation at various frequencies with Czech data example," roceedings of ERAD, pp 113-116,(2002).
8. Park Y-H, J. H. Lee , N. Jambaljav , and J-ki Pack, " Empirical Study on The Rain Drop-Size Model for Rain Attenuation Calculations," Internet site,(2006).
9. Park Y-H, N. Jambaljav, J-ki Pack, and C-O Ko, "Empirical Study of Raindrop-Size Distribution," Korea-Japan Joint Conference, pp. 331-334, (2004).
10. Collin R.E., "Antenna and Radiowave Propagation," McGraw-Hill Book Company,(1985).
11. Gibbins C.J., " Improved algorithms for the determination of specific attenuation at sea level by dry air and water vapour, in the frequency range 1-350 GHz," Radio Science, vol. 21, No. 6, pp:949-954, (1986).
12. Rogers R.R., "A review of multiparameter radar observationsof precipitation,"Radio Science, vol. 19, pp. 23-36, (1984).
13. de Wolf D.A. "On the Laws-Parsons distribution of raindrop sizes", Radio Science Vol.36, No. 4, pp. 639-642, (2001).

Fractal Image Compression based on New Affine parameters

Jamila H.Al-A'meri
Al-Musenseriyh University, College of Science, Dept. of Computer Science

Received 20/6/2007 – Accepted 16/9/2007
Key Wards: (Fractal, range block, partition, image compression, encoding time).

الخلاصة

الصورة المشفرة في ضغط بيانات الصورة كسوريا يجب ان تقطع الى كتل تسمى المدى. مجموعة من التحويلات المتقلصة تطبق على كتل المدى. هذه التحويلات تنتج صورة تقريبية الى الصورة الاصلية. في تقنية الكسوريات تكون عملية فك الشفرة اسرع من عملية التشفير، عملية التشفير تستغرق وقت طويل نتيجة للعمليات الحسابية التي تجرى على زوج كتل المدى و المدى المقابل. في بحثنا اعتمدنا على طريقة جديدة لتسريع عملية التشفير بالاعتماد على عوامل افينية جديدة غير المتعارف عليها.

ABSTRACT

In fractal image compression, the image to be encoding must be partitioned into blocks called "Range blocks". A set of contractive transformations are applied on the range blocks. These transformations are guaranteed to produce an approximation to the original image where iteratively applied on any initial image. While in raped decoding algorithms exits, the encoding process is extremely time consuming; the large amount of computations needed for optimum mapping between range-domain blocks. We introduced a new method based on new affine parameters to break the long encoding time of the encoding process, which is based on using an unconventional affine parameter.

INTRODUCTION

Fractal image compression (FIC) technique based on the theory of *IFS* and its performance relies on the presence of self-similarity between the regions of an image. Since most images possess high degree of self-similarity, fractal compression contributes an excellent tool for compressing them [1]. Rather than storing an image pixel by pixel, the goal of FIC is to find a loss compression algorithm that takes the advantage of the self-similarities in an image. Barnsley applied his knowledge of fractal and mathematics to image compression, creating optimal forms of image compression [2]. The encoding process of fractal image compression is extremely computationally intensive (long encoding time). This weak aspect makes the fractal compression method, still not widely used as standard compression, although it has the advantage of fast decompression as well as get high values of compression ratios[3]. According to fractal coding algorithm that was suggested by Jacquin, the image is partitioned into non-overlapping blocks (R), where each block will be transformed separately using affine transform. The same image also houses blocks, which are twice the size of the range

blocks and overlap. This collection of all large blocks known as domain block (D), constructs a codebook called domain pool (Ω) [4].

After partitioning a given image into R-blocks, and D-blocks should be found pieces of D_j and a collection of contractive maps $w_1, w_2, ..., w_n$:[5]

$$w_i\begin{bmatrix} x \\ y \\ z \end{bmatrix} = \begin{bmatrix} a_i & b_i & 0 \\ c_i & d_i & 0 \\ 0 & 0 & s_i \end{bmatrix} \cdot \begin{bmatrix} x \\ y \\ z \end{bmatrix} + \begin{bmatrix} e_i \\ f_i \\ o_i \end{bmatrix} \quad \text{....(1)}$$

So that w_i applied to the part of the image over D_j. The crux, then of the encoding image finds contractive maps w_i that minimize the distances between R_i and corresponding D_j, see Fig (1) [6]

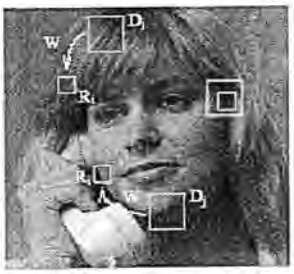

Fig -1: The transform between domain block (D_j) and range block (R_i).

This reason why fractal compression is slow techniques, since each range block must be compared to all domain blocks including eight symmetry orientations (see Fig(2)). This operation allows the best match to be found [7].

Fig -2: The eight spatial orientations (symmetry) of a square block.

In other words, we seek to minimize the quality of distortion over $D \in \Omega$ in equation (2) w.r.t the parameters scale (s) and offset (o)in equations (3)and (4) respectively[8,9]:

$$E(R, D) = \frac{1}{n}\left[\sum_{i=1}^{n} r_i^2 + S\left(S\sum_{i=1}^{n} d_i^2 - 2\sum_{i=1}^{n} d_i r_i + 2O\sum_{i=1}^{n} d_i\right) + O\left(nO - 2\sum_{i=1}^{n} r_i\right)\right] \quad \text{....(2)}$$

Where

$$S = \frac{\left[n\left(\sum_{i=1}^{n} d_i r_i\right) - \left(\sum_{i=1}^{n} d_i\right)\left(\sum_{i=1}^{n} r_i\right)\right]}{\left[n\sum_{i=1}^{n} d_i^2 - \left(\sum_{i=1}^{n} d_i\right)^2\right]} \quad \text{.....(3)}$$

And

$$O = \frac{\left[\sum_{i=1}^{n} r_i \sum_{i=1}^{n} d_i^2 - \sum_{i=1}^{n} d_i \sum_{i=1}^{n} d_i r_i\right]}{\left[n\sum_{i=1}^{n} d_i^2 - \left(\sum_{i=1}^{n} d_i\right)^2\right]} \quad \ldots (4)$$

Fractal Image Compression based on New Affine parameters

Various techniques have been proposed in fractal encoding to overcome the large time consuming during the searching process (matching) between the domain-range pairs. Therefore, in this paper we introduced the transforms of full search problem to a more convenient form by adopting an unconventional affine parameter that has better properties than the conventional offset parameter and we will use a new search algorithm.

As mentioned in the encoding unit, the optimal approximation for every range block must be obtained from equation (2) and with respect to the affine parameters *s* and *o*. In the traditional choice of using the *o* in this equation (2) and many calculations that required to computes this parameter as describe in equation (4) [9], the full search scheme can also be converted to a one-parameter optimization problem. *The question here is: "how does the two parameters problem become a one-parameter optimization, and what is the way to perform the new search operation?* The answer for this question can be illustrated in the following:

The optimal approximation in decoding unit for every range block can be obtained from equation (5).

$$\bar{r} = s\bar{d} + o \quad \ldots\ldots\ldots\ldots (5)$$

Where:

$\bar{r}$ *:* represents the average (mean) for a specific range block.

$\bar{d}$ *:* represents the average (mean) for the mapped domain block for this range block.

It is noted from equation (5) *o* coefficient given by the difference of the range block mean $\bar{r}$ and the scaled domain block mean $\bar{d}$, using this idea to formulate new affine transform equation(6):

$$r_i = s(d_i - \bar{d}) + \bar{r} \ldots \forall i \ldots\ldots\ldots\ldots (6)$$

From equation (6), the fractal parameter is $\bar{r}$, instead of the conventional *o* coefficients. The new affine parameters are $\bar{r}$ is (DC-component) of the range block and is independent of the domain block; *s* is related to the (AC-component) of the range block. Interestingly, the new transformation splits an image into DC and AC, as illustrated in Fig (3).

Clearly, using $\bar{r}$ as one of the affine parameter instead of the o allows de-coupling the optimization of the two affine parameters and thus furthering speed up the search for the best matching domain block.

Moreover, from equation (2), note that s and o are strongly correlated in the traditional transformation. Dependence complicates the quantization to s and o; however, within the new transformation, the new fractal parameters s and $\bar{r}$ are independent, so separable quantization can be done to s and $\bar{r}$.Thus it is more efficient to quantize the $\bar{r}$, especially it has a much smaller dynamic range [0,255] than the o parameter [-255,255]. So, it is more cost effective (in terms of minimizing the quantization error per code) to code the quantization of $\bar{r}$ than to code the o parameter. In the new transformation, $\bar{r}$ uniformly quantized by 6 bits and s is uniformly quantized by 2 bits.

So, from substitute equation (6) in equation (8), the distortion error will be in equations (9) and (10):

$$E(R, D) = \frac{1}{n}\sum_{i=1}^{n}(s.d_i + o - r_i)^2 \quad \text{.....(8)}$$

$$E(R, D) = \frac{1}{n}\sum_{i=1}^{n}(s(d_i - \bar{d}) - (r_i - \bar{r}))^2 \quad \text{...(9)}$$

$$E(R', D') = \frac{1}{n}\sum_{i=1}^{n}(sD' - R')^2 \quad \text{.....(10)}$$

Where:

$R' = r_i - \bar{r}$

$D' = d_i - \bar{d}$

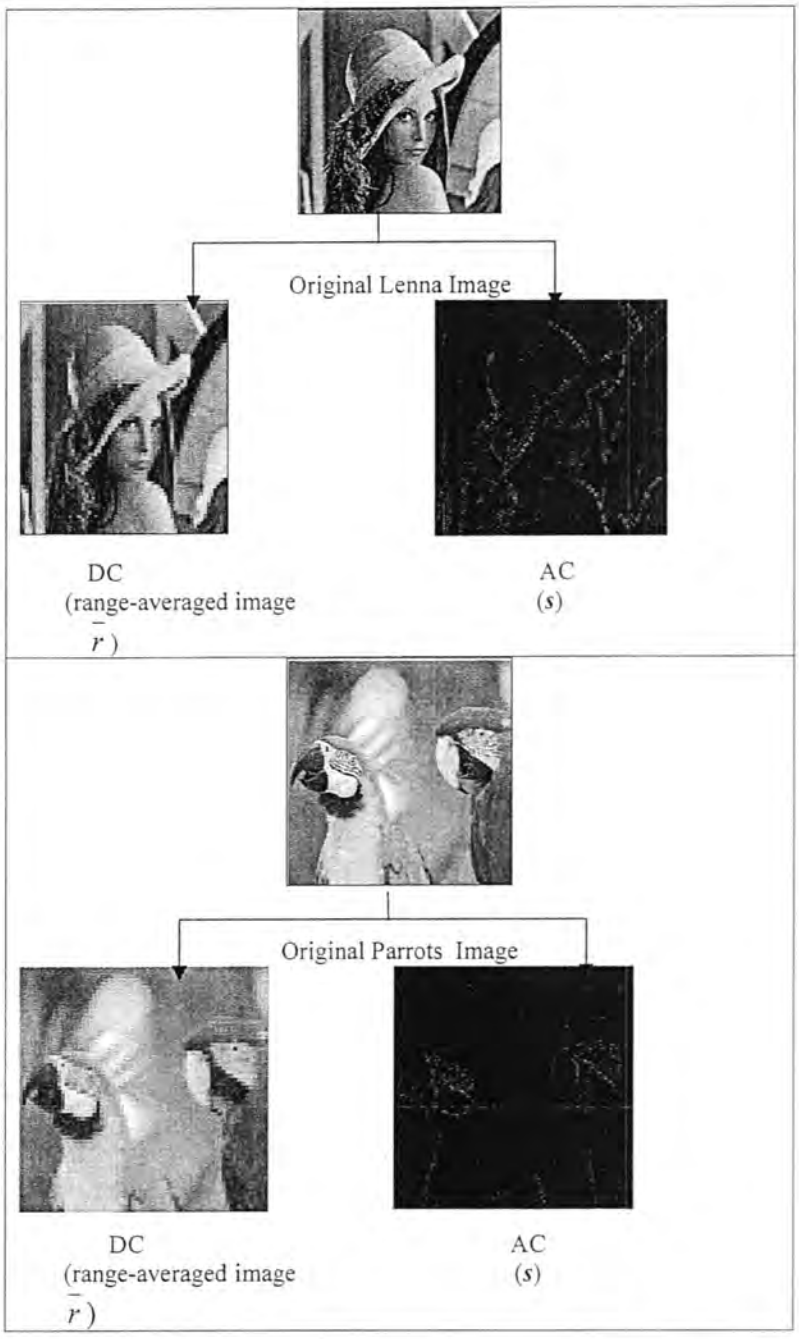

Fig -3: Show the DC and AC-components of the original Lenna and Parrots images.

So, this method will depend on this new distortion's equation and this means the range-domain blocks have been adjusted to a Zero Mean Intensity Level through subtract the mean $(\bar{r},\bar{d})$ from all the range-domain blocks.

Moreover, the $\bar{r}$ can be quantized and coded at the start of the compression to provide a coarse level of compression and hence can be used in a design of progressive fractal compression.

Minimizing equation (10), one can solve for *s*. This can be achieved by taking the derivative of $E(R`,D`)$ with respect to *s* as zero, i.e,

$$\frac{\partial E(R`,D`)}{\partial S}=\frac{-2}{n}\sum(SD_i'-R_i')D_i'=0$$

$$\sum(R_i'D_i')=S\sum D_i'^2$$

$$\therefore S=\frac{\sum R_i'D_i'}{\sum D_i'^2} \quad \ldots\ldots(11)$$

Since, a significant improvement in fidelity can be obtained if only quantized *s* value is used when computing the error $E(R`,D`)$ during encoding and its drawback is that post-quantization to *s* often leads to a poorer result as compared with pre-quantization, the quantity that we actually want to minimize is :

$$E(R',D')=\frac{1}{n}\left[s^2\sum D_i'^2+\sum R_i'^2-2s\sum R_i'D_i'\right] \quad \ldots\ldots(12)$$

The root mean square error is equal to $\sqrt{E(R`,D`)}$.In our method, the search for the best matching domain block only depends on the quantized scaling and the inner product $<R',D'>$, and is independent of the $\bar{r}$. Because the $\bar{r}$ depends only on the range block and thus the parameter can be quantized independent of the search for the best matching domain block. This quantization does not involve searching at all. Thus effectively, two parameters optimization problem becomes a one-parameter optimization, and hence is become much more efficient.

New Encoding Algorithm Based on Proposed Method

To encode an image, we need to select an image partitioning scheme to generate the range blocks. For this purpose, R_i is generated by using fixed block size partitioning, and production of the domain blocks involves the down sampling of the original image by averaging method. Then transformations between domain and range blocks are done. In proposed method we first subtract the mean of range *R* and domain *D* blocks. Secondly we use this new *R`* in search to find the best matching with *D`*.

The overall best matching blocks are then obtained by minimizing the weighted $E(R',D')$ over the quantized level for s_i. Thus equation

(12) leads to the following new encoding algorithm (1) that illustrated new encoding steps

Algorithm (1): Encoding algorithm of proposed method

Input: The original image

Output: The IFS code

Method:

Step1: Load the image into buffer

Step2: Partitioning the image into fixed blocks size with non-overlap $(R_1 \ldots R_n)$

Step3: Generate the domain image from the original image by averaging method

Step4: Build a new domain blocks $(D'_1 \ldots D'_m)$

Step5: For each range block R_i build a new R'_i and do:

i. Quantize $\bar{r}$

ii. Check all the D'_m for the best matching D'_i by:

- Compute the $s = \frac{\sum R'_i D'_i}{\sum D'^2_i}$
- Quantize the *s*;
- Compute $E(R'_i, D'_i; s)$;
- If $E(R'_i, D'_i; s)$ is minimum store the *IFS* –code; else go to the next domain block;

New Decoding Algorithm Based on Proposed Method

New decoding algorithm is based on *new* method which replaces *o* parameter with $\bar{r}$ and assumption that domain block mean $\bar{d}$ could be obtained from the reconstructed image. Since $\bar{d}$ is not a fixed value, but a variable depending on a domain block *D*, it may be difficult to recover in practice. Based on this observation, the transformation *W* can be modified as follows:

$$W(\bar{d}_{ij}) = \bar{r} + s*(d_{ij} - \sum_{m=1}^{B}\sum_{n=1}^{B} d_{mn} \Big/ B^2) \quad (13)$$

Modifying transformation can be written as:

$$W = DC + s(AC) \quad (14)$$

As we see, for the new transformation W, parameter $\bar{r}$ is the DC of the range block and is independent of the domain block; s is related to the AC of the range block and is used to refine the range block iteratively.

At the decoder, the reconstructed image is generated by recursive iterations on the basis of an arbitrary initial image. In the new iteration algorithm, $\bar{d}$ varies as iteration proceeds.

The first decoded image will the range-averaged image (DC) and hence the use of the range-averaged image as an initial image for the next iterations will be cause fast converge to the attractor. As the iterations proceed, the AC components will be added to the DC component, after 2 iterations the reconstructed image becomes stable. Algorithms (2) explain the new decoding algorithm of proposed method.

Algorithm (2): Decoding algorithm of proposed method

Input: The IFS code
Output: The decoded image
Method:
***Step1*: Generate the first domain image arbitrary**
***Step2*: Determine the iterations number**
***Step3*: Load IFS code**
***Step4*: Dequantize the value of scale s_i and range block mean $\bar{r}_k$**
***Step5*: Build a new domains blocks ($D'_1 ... D'_m$)**
***Step6*: Reconstruct the range block: $R_i = s D'_i + \bar{r}$**
***Step7*: Each range block is reconstructed will be located in its position in the decoded image plane**
***Step8*: Down sample the decoded (reconstructed) image into the size of domain image by averaging**
***Step9*: Repeat from step 5 until we reached the attractor state (i.e., decoded image will not be changed as we processed in the iteration)**

RESULTS AND CONCLUSION

In this section we need to discuss the parameters that show significant effect on the results of encoding process of proposed method, and then we see the effect of it on the encoding time, PSNR and compression ratio to evaluate these new results with last results of traditional *FIC*.

1. Quantization Levels of Scale and Range Block Mean

We will show the effects of various quantization levels of the affine parameters s and $\bar{r}$ on the compression results using the uniform quantization. The results are tabulated in table (1).

Table -1: The effects of different quantization levels of s and $\bar{r}$ parameters on the reconstructed Lenna and Parrots images

Images	*Total No.Bits*	*ScaleBits*	$\bar{r}$ *Bits*	*PSNR (dB)*	*C.R*	*E.T. (Sec)*
Lenna (256x256)	8	2	6	31.25	6.09	21
	8	3	5	30.80	6.09	21
	9	3	6	31.72	5.81	21
	9	2	7	31.54	5.81	21
	10	4	6	32.11	5.56	21
	10	3	7	31.95	5.56	21
	11	5	6	32.27	5.33	21
	11	6	5	31.55	5.33	21
	12	5	7	32.49	5.12	21
	12	7	5	31.61	5.12	21
Parrots (256x256)	8	2	6	32.34	6.09	21
	8	3	5	31.57	6.09	21
	9	3	6	32.67	5.81	21
	9	2	7	32.63	5.81	21
	10	4	6	32.99	5.56	21
	10	3	7	32.93	5.56	21
	11	5	6	33.03	5.33	21
	11	6	5	32.18	5.33	21
	12	5	7	33.30	5.12	21
	12	7	5	32.20	5.12	21

From table (1), a limited number of total bits ranging from (8 to 12) has been adopted for s and $\bar{r}$ parameters, from the tests we have found that if we used 8 bits as a total number of bits for s and $\bar{r}$ (i.e., s quantized by 2 bits and $\bar{r}$ is quantized by 6 bits), will still preserve high quality (PSNR) and compression ratio for reconstructed image.

Therefore, our method reduces the number of bits that required representing the affine parameters than the traditional method, while it gets higher values of PSNR and compression ratio. Also it is obvious from the table (1), that the encoding time is reduced here because the computations involved with the mapping search operations of our method are simplified and reduced.

Proposed method shows a considerable increase in the PSNR values than of traditional one, as we see in table (2) and shown in figures (4) and (5). So, we will use *Scale Bits=2* and $\bar{r}$*Bits* =6 for all the rest tests.

Table -2: Comparison between traditional and new *FIC* based on new method using different quantization levels of *s*, *o* and $\bar{r}$

Total No.Bits	Scale Bits	Offset Bits	$\bar{r}$ Bits	Lenna Image	
				PSNR(dB) Trad. FIC	PSNR(dB) New FIC
8	*2*	*6*	*6*	*28.42*	*31.25*
9	*3*	*6*	*6*	*29.44*	*31.72*
10	*4*	*6*	*6*	*29.90*	*32.11*
11	*5*	*6*	*6*	*30.22*	*32.27*
12	*5*	*7*	*7*	*30.30*	*32.49*

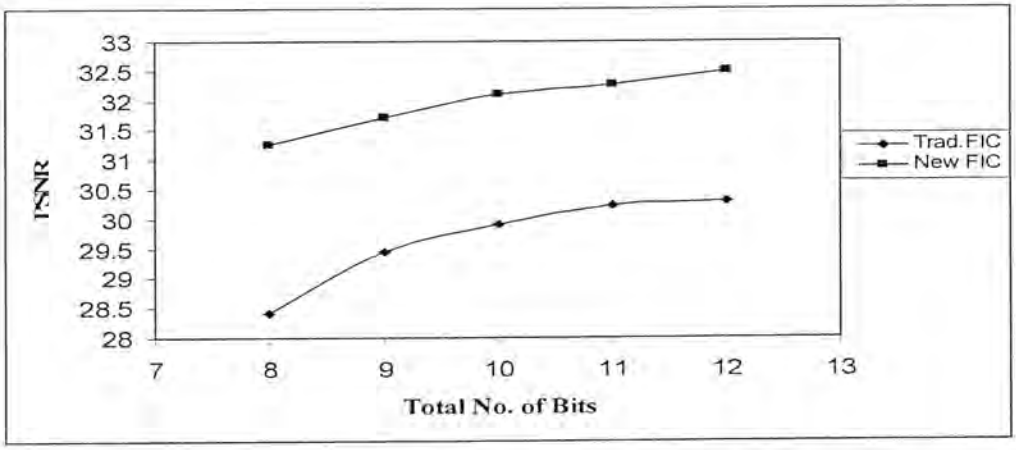

Figure -4: Total number of bits of traditional and new *FIC* parameters versus PSNR for Lenna image.

Traditional FIC	*New (ZMIL) FIC*
	
PSNR=28.42 dB , C.R=6.09 E.T = 29 Sec	PSNR=31.25 dB , C.R=6.09 E.T = 21 Sec

Figure -5: Comparison between traditional and new *FIC* results for Lenna image when ScaleBits =2 and OffsetBits ($\bar{r}$ *Bits*) =6

2. Block Size Effect

Block size parameter effects directly in the encoding time, compression ratio and the quality of reconstructed image (PSNR). If the image is partitioned into small block size (4x4) we have large number of range blocks. These blocks are used in the searching stage, and have effect on the reconstructed values of PSNR and compression ratio. Also, these blocks need many computational processes in the encoding stage. While, if the image is partitioned into big block size (16x16), this means than we are allowed to increase the region with approximately self-similar, used in the searching stage, in this case the number of range blocks will be reduced and this will decrease the encoding time with low PSNR value. Table (3) shows this effect with various partitioning sizes of range block.

Table -3: The effect of different block size on the reconstructed images

Test Images	*Block Size*	*No. of Blocks*	*PSNR(dB)*	*C.R.*	*E.T.(Sec)*
Lenna	4x4	4096	31.25	6.09	21
	8x8	1024	25.15	24.30	11
	16x16	256	21.10	96.22	7
Parrots	4x4	4096	32.34	6.09	21
	8x8	1024	27.35	24.30	11
	16x16	256	24.79	96.22	7

From traditional and new *FIC*, we can see from figure (6) the big block size in traditional method reconstructed bad image quality in the boundary regions like eyes, mouth and hat of Lenna image. But in the proposed method, obviously all the boundary details are reconstructed and in this case the PSNR will be increased.

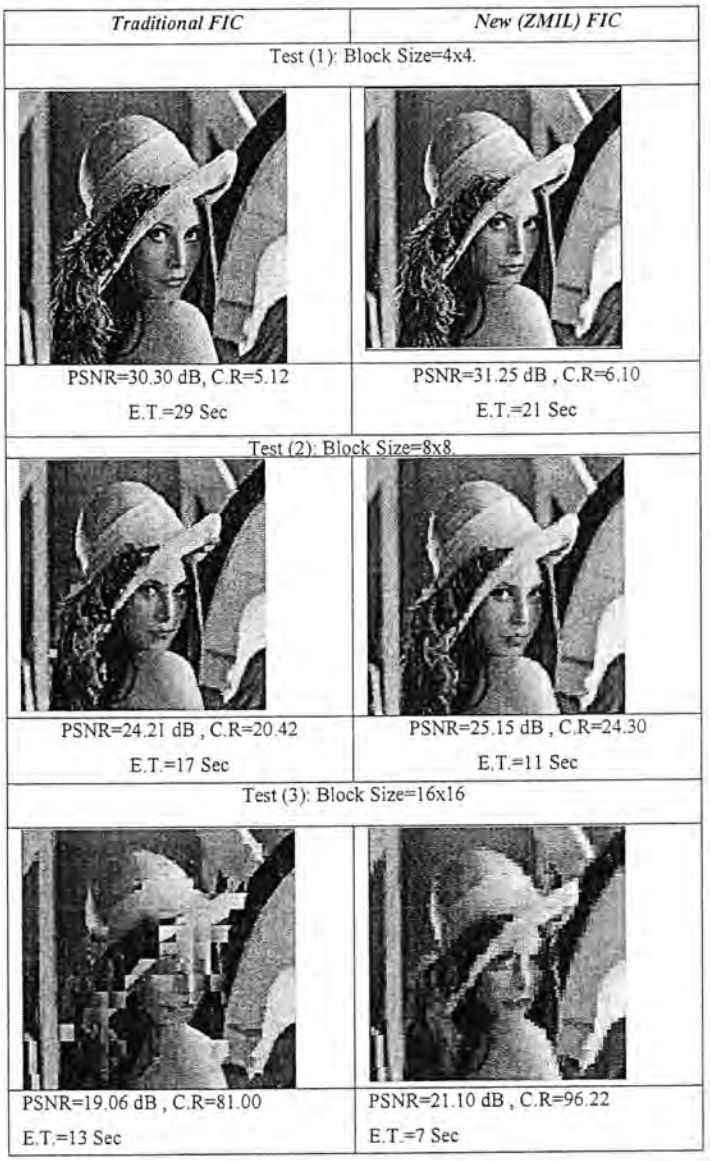

Figure (6): Comparison the results between traditional and new *FIC* based on new method when different bock size are used.

3. Decoding Process of Proposed FIC

The results shown in figure (7) illustrate that from the first iteration; decoded image will be the range-averaged image (DC) and then used the range-averaged image as an initial image for the next

iterations. As the iterations proceeds, the AC components are added to the DC component (i.e., the reconstructed image equals the DC image (the range-averaged image) + AC images.), after 2 iterations the reconstructed image becomes stable. So, as we see from figure (7), the reconstructed image can reach its attractor (fixed point) at the 3rd iteration.

Figure 7a:DC image (range-averaged image)

Figure 7b: The first three iterated AC images.

Figure7c: The first DC+AC (4a+4b from same column) images.

Figure (7): DC+AC components for reconstructed image.

In our method the distance between the original and reconstructed image is very contractive, this means we can use a small value of contractivity factor (MaxScl=0.5) to get high PSNR value. But in the traditional method the contractivity factor (MaxScl=2) get best PSNR value, less than (MaxScl<2) the PSNR

values are decreased. Table (4) shows this effect. Our method is very powerful than the traditional method, because most researchers use high values of MaxScl, Fisher said that the best value lays in MaxScl >1.2, but in this research work it was noticed that this value may reduced to be less than this value (i.e. until when MaxScl=0.5) the quality of the reconstructed image will still good.

Table -4: Show the effect of MaxScl on the PSNR of the reconstructed images in the traditional and new *FIC*.

MaxScl	Traditional FIC Lenna	New FIC Lenna	Traditional FIC Parrots	New FIC Parrots
0.5	21.61	27.99	24.89	*29.39*
1	28.19	31.24	29.73	*32.14*
1.2	29.74	31.26	30.59	*32.12*
1.5	30.14	31.30	30.62	*32.30*
2	30.30	31.25	30.98	*32.25*
2.5	30.24	31.04	30.81	*32.24*

REFERENCES

1. Mahadevaswamy H.R., "New Approaches to Image Compression", Ph.D. thesis, Regional Engineering College, university of Calicut, December, (2000).
2. Lisa A. S., "The Mathematical Foundation of Image Compression", University of North Carolina at Wilmington, May,(2000).
3. Fadhil S., "Adaptive Fractal Image Compression", Ph.D., thesis, Al-Rasheed College of Engineering and Science, Technology University,(2004).
4. Fisher Y., "Fractal Image Compression: Theory and Application", Springier Verlag, New York,(1994).
5. Farhad S., "Fractal Image Compression", MAT 335 Final Project.
6. Kadhim G., "Adaptive Fractal Image Compression", M.Sc. thesis, National computer Center /Higher Education Institute of computer and Informatics,(2001).
7. Robert J., "Combining Fractal Compression with Sampling and Interpolation", Internet paper, January, 10,(2003).
8. Saupe D., and Hamzaoui R., "Optimal Hierarchical Partitions for Fractal Image Compression", IEEE International Conference on Image Processing (ICIP'98), Chicago, (1998).
9. Saupe D., Hamzaoui R., "Fractal Model for Image Synthesis, Encoding and Analysis", SIGGRAPH'96 Course Notes XX, New Orleans, (1996).